AD-A181 298 LASER INDUCED SOLID STATE PLASMA FOR MILLIMETER-WAVE DEVICE APPLICATIONS (U) MARYLAND UNIV COLLEGE PARK DEPT OF ELECTRICAL ENGINEERING C H LEE 31 MAR 87 1/1

UNCLASSIFIED ARO-20100 7-EL DAAG29-83-K-0079 F/G 9/1 NL

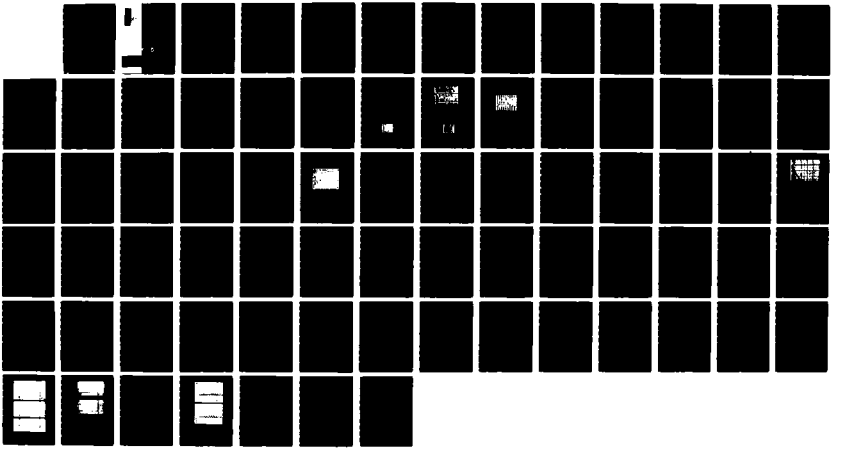

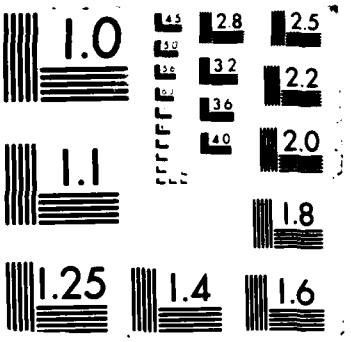
1.0
1.1
1.25
1.4
1.6
1.8
2.0
2.2
2.5
2.8
3.2
3.6
4.0

TECHNICAL RESEARCH REPORT

LASER INDUCED SOLID STATE PLASMA FOR MILLIMETER-WAVE DEVICE APPLICATIONS

FINAL REPORT

March 31, 1987

U.S. ARMY RESEARCH OFFICE

Grant Number: DAAG-29-83-K-0079P00001

by

Chi H. Lee

DEPARTMENT OF ELECTRICAL ENGINEERING

UNIVERSITY OF MARYLAND

COLLEGE PARK, MARYLAND 20742

UNCLASSIFIED
SECURITY CLASSIFICATION OF THIS PAGE

REPORT DOCUMENTATION PAGE

1a. REPORT SECURITY CLASSIFICATION: Unclassified	1b. RESTRICTIVE MARKINGS: AD-A181 298
2a. SECURITY CLASSIFICATION AUTHORITY	3. DISTRIBUTION/AVAILABILITY OF REPORT: Approved for public release; distribution unlimited.
2b. DECLASSIFICATION/DOWNGRADING SCHEDULE	
4. PERFORMING ORGANIZATION REPORT NUMBER(S)	5. MONITORING ORGANIZATION REPORT NUMBER(S): ARO 20100.7-EL
6a. NAME OF PERFORMING ORGANIZATION: University of Maryland; 6b. OFFICE SYMBOL (If applicable)	7a. NAME OF MONITORING ORGANIZATION: U. S. Army Research Office
6c. ADDRESS (City, State, and ZIP Code): Department of Electrical Engineering, College Park, MD 20742	7b. ADDRESS (City, State, and ZIP Code): P. O. Box 12211, Research Triangle Park, NC 27709-2211
8a. NAME OF FUNDING/SPONSORING ORGANIZATION: U. S. Army Research Office; 8b. OFFICE SYMBOL (If applicable)	9. PROCUREMENT INSTRUMENT IDENTIFICATION NUMBER: DAAG29-83-K-0079
8c. ADDRESS (City, State, and ZIP Code): P. O. Box 12211, Research Triangle Park, NC 27709-2211	10. SOURCE OF FUNDING NUMBERS: PROGRAM ELEMENT NO. / PROJECT NO. / TASK NO. / WORK UNIT ACCESSION NO

11. TITLE (Include Security Classification)
Laser Induced Solid State Plasma for Millimeter-Wave Device Applications

12. PERSONAL AUTHOR(S) Dr. Chi H. Lee

13a. TYPE OF REPORT	13b. TIME COVERED	14. DATE OF REPORT (Year, Month, Day)	15. PAGE COUNT
Final	FROM 5/1/83 TO 12/30/86	March 31, 1987	

16. SUPPLEMENTARY NOTATION
The view, opinions and/or findings contained in this report are those of the author(s) and should not be construed as an official Department of the Army position, policy, or decision, unless so designated by other documentation.

17. COSATI CODES			18. SUBJECT TERMS (Continue on reverse if necessary and identify by block number)
FIELD	GROUP	SUB-GROUP	Waveguides, millimeter wave, optical control, phase shifter

19. ABSTRACT (Continue on reverse if necessary and identify by block number)

The results are summary of the investigation of a number of millimeter-wave device concepts based on laser induced solid state plasma in semiconductors. The generation and control of millimeter-wave and microwaves by optoelectronic techniques are reported. Complete time synchronization between RF and optical signals is achieved. Laser controlled phase shifters, switches and modulators at 94 GHz are described.

20. DISTRIBUTION/AVAILABILITY OF ABSTRACT	21. ABSTRACT SECURITY CLASSIFICATION	
☐ UNCLASSIFIED/UNLIMITED ☐ SAME AS RPT ☐ DTIC USERS	Unclassified	
22a. NAME OF RESPONSIBLE INDIVIDUAL	22b. TELEPHONE (Include Area Code)	22c. OFFICE SYMBOL

DD FORM 1473, 84 MAR — 83 APR edition may be used until exhausted. All other editions are obsolete.

SECURITY CLASSIFICATION OF THIS PAGE
UNCLASSIFIED

TABLE OF CONTENTS

I. Introduction

We are currently witnessing a resurgence of interest in millimeter-wave technology. Recent advances in the utilization of optical techniques for the generation and control of millimeter-waves in our laboratory [1]-[2] and elsewhere [3]-[6], make it technologically feasible to build a complete millimeter-wave monolithic phased array system that has the potential to incorporate rapid scan (our goal is to achieve a complete scan in one nanosecond or better), high resolution beam steering and reconfiguration, wideband performance, reduced susceptibility to interference, and a compact lightweight design specifically for phase scanning or multiple-beam applications.

At present, there are a number of phased array concepts which involve some kind of optical feeding [7]-[10], using either fiber coupling [8], or space-fed illumination [11]. The central issue of these systems is to provide the correct phase and amplitude excitation at each element of the array. For rapid scanning using an optical feed network, the phase and amplitude of the antenna element excitation must be varied at a multi-gigahertz rate. These requirements are beyond the capability of the current technology. Although the system concept seems attractive, many of the key components or subsystems are lacking and await new technology developments. This research project addresses precisely these key issues. These unique array concepts incorporate advanced optical, electronic, millimeter-wave, and antenna technologies. The main concept utilizes optoelectronic beam-forming technologies coupled with a MMIC (monolithic millimeter-wave integrated circuit) active array. We believe that the optical technique offers unique advantages in:

(1) near perfect isolation between controlling and controlled devices,
(2) elimination of RF feeds in a large array system,
(3) immunity from electromagnetic interference,
(4) light weight and compact size,
(5) extremely fast response,
(6) high power handling capability, and
(7) amendability to monlithic integration.

There are many advantages in introducing optical techniques into millimeter-wave technology. With today's mature optical technology, switching, modulating and deflecting of an optical beam can be done easily with picosecond speed capabilities. Optical pulses as short as 10 femtoseconds have been achieved [12]. Integrated and fiber optical devices have advanced to a point that many optical electronic functions can be performed with very small energy requirements and high reliability. Since many device concepts in the millimeter-wave frequency range are analogous to their optical counterparts, there is much to be gained in taking advantage of advanced optical developments.

The most fundamental aspect of interfacing optics and millimeter-waves is to establish time coherence between the two waveforms. There are three concepts: (i) to generate millimeter-wave signals in complete time coherence with an optical pulse, (ii) to modulate optical waves by millimeter-waves, and (iii) to modulate millimeter-waves by optical waves. In this proposal, we propose to investigate all three concepts.

II. Technical Description and Results.

We begin this section by giving a brief introduction to the application of optical techniques for millimeter-wave generation, control, and measurements. Most of our research tasks center

on picosecond optoelectronic techniques. These techniques can be used not only to control the phase and amplitude in a semiconductor waveguide by inducing electron-hole pairs (solid state plasma) [1],[13], but also to generate millimeter-wave signals in complete time coherence with the ultrashort optical pulses [2]. This is the ultimate technique to measure the dynamic change in amplitude and phase of millimeter-wave signals, with a potential time precision of 10 femtoseconds (depending on the stability of the optical delay). The challenge here is to generate millimeter-waves in complete time coherence with the exciting optical pulse. This is usually done by illuminating a picosecond photoconductor with a picosecond laser pulse [14]. Using this technique, we have been able to generate a 10 GHz cw RF-wave by appropriately filtering the pulse train [2]. By using a microstrip filter and time division multiplexing the exciting optical pulse or the electrical signal to ease the stringent filtering requirements, it should be straightforward to extend the RF generation to the millimeter-wave frequency range. One difficulty lies in the accurate measurement of the phase and ampliltude of the cw millimeter-wave signal. We have developed picosecond optoelectronic and/or electro-optical sampling techniques which can be used to coherently detect millimeter-wave signals from 10 to 55 GHz [15]. Optical electronic sampling techniques can be used to coherently measure zero-crossings of the millimeter-wave signal. It should be pointed out that these techniques can be used not only to make accurate measurements of amplitude and phase, but also to perform phase shifting by simply delaying the exciting pulse via an optical fiber of variable length. The coherent millimeter-wave signal thus generated can be amplified by a millimeter-wave FET amplifier. A large phased array system can be realized by incorporating such an active component in each radiating element of the array, as shown in Fig. 1. Since the phase of each radiating element is now precisely controlled by the arrival of the ultrashort optical pulse at each element, an accurately controlled phased array system can be implemented. For example, by using a 10 femtosecond pulse in a 100 GHz system, a phase controlled to better than 0.4 degree is possible. It should be pointed out that in such a phased array system, only DC bias is needed to feed the antenna elements.

Another optoelectronic method to control the amplitude and phase is to optically modulate the electron-hole carrier density in a bulk semiconductor waveguide [1]. Picosecond switching and gating as well as gigahertz modulation of a 94 GHz wave has been demonstrated. A frequency chirped millimeter-wave pulse has also been observed. A dynamic bridge method to measure the phase and ampmlitude simultaneously has been devised with a time resolution of about 1 nanosecond, which is the bandwidth limitation of the oscilloscope. Recently, we have employed a cw mode-locked laser and a phase sensitive detection technique to measure the phase shift and attenuation. We have achieved a time resolution of 25 picoseconds and accuracy of phase measurement down to 0.1°. Many of these electronic functions have been demonstrated with a laser diode. With the 2-D laser diode array to be provided to us by RCA Labs, it will be possible to optically control the phase and amplitude of each individual element in the array by illuminating the 2-D readiation array with the 2-D laser diode array. The optical laser array to millimeter-wave array coupling can be achieved via optical fiber coupling or a space-fed ssystem, eg. holographic illumination.

The limitation of the induced plasma type of phase and amplitude control is that the variables are mutually coupled through the Kramers-Kronig relations. Dynamic loss always accompanies the dynamic phase shift. With precise knowledge of these two parameters, one may still be able to use this technique to control the phased array system by adjusting the laser illumination intensity. The Kramers-Kronig relation suggests that the maximum dynamic loss

occurs at low plasma density where the rate of change of phase with respect to plasma density is at the maximum. At higher plasma density the phase shift saturates at its maximum value while the dynamic loss decreases almost to zero. Therefore an effective means of achieving large phase shift with low loss is to maintain a high plasma density on the surface of the dielectric waveguide. In order to implement these ideas we have used composite dielectric waveguides consisting of thin layers of high purity semiconductor on an index matched insulating substrate, e.g., silicon-on-sapphire, heterojunction semiconductor waveguides fabricated with molecular beam expitaxially grown material, and recently, single crystal silicon on alumina waveguide. These composite dielectric waveguides can prevent carrier diffusion into the bulk material, thereby maintaining high carrier density after the plasma is created. Our recent results indicate that these waveguides can provide the desirable properties required of phase shifters.

II.A A New CW Microwave Source Using an Optical Electronic Technique

The precise generation and control of microwave and millimeter-wave signals using integrated technology is essential for the next generation of high-speed, broadband systems. It is desirable to utilize optoelectronic components where possible for such applications as microwave and millimeter-wave signal processing, receivers/transmitters, and phased array antennas. We now have at our disposal optoelectronic devices that work in the picosecond time domain. The trend is toward a class of devices which integrate optics into electronic functions. We classify this class of devices into the category of picosecond optical electronics, which combines the fields of optics and electronics [14]-[16]. The link for these two fields is picosecond photoconductivity [17].

The picosecond photoconductivity effect is the generation of an ultrashort photo-current signal in a photoconductor when it is illuminated by an ultrashort optical pulse. For example, 8 femtosecond optical pulses have been observed [12]. The unique feature of the picosecond optical device is its ability to generate low-noise electronic pulses synchronized with the optical pulses. For frequencies through Ka-band, a high-speed microelectronic amplifier utilizing HEMT's (High Electron Mobility Transistors) may be integrated with the photoconductor switch. Dispersion in microstrip interconnects will degrade the pulse shape. Therefore, for relatively large distances, it is necessary to convert the electrical signals back into the optical form. Thus, a technology for conversion between optical and electrical waveforms and vice-versa is needed. Electrical pulses can be converted into optical pulses by: (1) electro-optic modulation in an optical channel waveguide, or (2) direct modulation of a laser diode by the pulse current.

The general class of switching devices based on the picosecond photoconductivity effect has received considerable attention recently [14]. The photoconductivity effect is the long wavelength limit of a more general phenomena in which the complex dielectric constant of the semiconducting medium is modified by the introduction of an optically induced electron-hole plasma. When the dimension of the plasma region is much smaller than the wavelength of the electrical signals to be controlled, the plasma region may be regarded as a lumped circuit element. Most semiconductor switches are in this category and they are regarded as conductive mode switches.

Ultrafast optoelectronic switching is an important application for conductive switches. The devices can be categorized into low and high voltage applications. In the low voltage application, the device is used as a high speed optical detector or fast sampler. The important

characteristics are fast rise and decay times for the electrical signal. This generally necessitates a short carrier lifetime, even though this results in the disadvantage of low mobility. In the high voltage application the device is used as a jitter-free switch with extremely fast (a few picoseconds) turn-on time [13]. We have demonstrated the high voltage switching using Cr:GaAs, $CdS_{0.5}Se_{0.5}$ and insulating diamond [13].

The rise time of the photoconductive signal can approach the rise time of the optical pulse, which can be on the order of 10 femtoseconds (terahertz spectral components). The electrical pulse fall time is primarily determined by the carrier lifetime, which can be engineered to be as short as 1 picosecond.

There are a large number of devices which can be based on the picosecond photoconductivity effect. They include switches, gates, samplers, electronic pulse function correlators, A/D converters, optical detectors, DC to RF converters, and coherent microwave/millimeter-wave generators. Such fast photoconductors can handle high power, are scalable (large and/or submicron sizes), have a large dynamic range and can be monolithically integrated with microelectronic devices. These features lend the device to applications such as: high data rate signal processing, high speed detectors, high frequency photomixers, streak camera triggering, millimeter-wave phase shifting and modulating, ultra-short high power pulse generation, microwave and millimeter-wave sources and on-chip picosecond diagnostics. A potentially powerful application for the device when used as a coherent CW source is in a phased array antenna. Optical techniques for feeding arrays have received considerable attention recently [7]-[11]. The central issue is to provide the correct phase and amplitude excitation at each element of the array in a manner which allows rapid scanning. A photoconductive switch with a appropriate filter and amplifier could be placed at each element in the array. The phase of excitation can be controlled optically. Such an array of active elements can be monolithically integrated. The picosecond photoconductor can also be used to realize a Pulse Code Modulator (PCM) by switching a microwave/millimeter-wave signal at appropriate intervals. Such a system permits very high modulation rates.

We have previously demonstrated the generation of 3 GHz CW signals by the pulse excitation of a resonant cavity [18]. The generation of short pulses of microwave signals has been reported [19]-[20]. Also, a 3 GHz CW signal has been generated by using a mode-locked krypton-ion laser with both an avalanche photodiode and an optoelectronic switch [5]. In [6], a technique involving the FM sideband injection locking of a laser diode has been used to generate a 35 GHz CW signal. This was done by beating two longitudinal modes of a diode laser in a high speed PIN detector. This technique requires accurate temperature stabilization of the lasers and provides a signal level of -53 dBm.

This section will elaborate on the realization of a 10 GHz CW microwave source using the photoconductivity effect. An advantage of this technique is that the components required are relatively easy to obtain and use. The technique requires a minimum number of components: a source of short optical pulses (a mode-locked laser), a picosecond optical switch, a microwave filter and an amplifier. Each of these components have the flexibility of being reduced in size so that the entire configuration may be integrated onto a single substrate. This will enhance the overall performance by minimizing the detrimental effects of dispersion, connectors, and cables. The output power and stability of the signal generated by this technique are the most critical factors in determining its applicability. The short term stability of the source is of particular importance and has not previously been considered in detail for this application.

Methods for increasing the power level and improving the amplitude and frequency stability of the output signal are discussed.

Experimental Set-up and Results

The experimental configuration for the generation of CW microwave signals with picosecond photoconductors is shown in Fig. 2. A synchronously pumped Dye laser is used to obtain 3 ps FWHM optical pulses at a repetition rate of 100 MHz. These pulses are applied to a biased photoconductive switch. The spectral components produced at the switch output extend up to tens of gigahertz and are spaced every 100 MHz, corresponding to the harmonics of the pulse train generated. The switch is matched to 50 ohms and fed to a narrowband bandpass filter. The passband of this filter is narrow enough so that only a single spectral component will be present at the output. The low noise amplifier provides this signal with gain so that the signal may be analyzed on a sampling oscilloscope.

The CW microwave signal generated by this technique must satisfy general stability requirements so that it may be used in the applications for phase arrayed system. This set-up is therefore also used to measure the phase stability of the CW signal generated. This is done by measuring the phase noise on the spectral components with the spectrum analyzer. It was found that the noise on the CW signal generated results primarily from the jitter of the optical pulses generated by the mode-locked laser and the picosecond switch introduces negligible jitter in comparison. Both AM and FM noise in the optical pulse train appear as noise sidebands on each spectral component. The large number of spectral components permit the observation of the relative amount of AM and FM noise produced by the laser system as a function of the harmonic number. Each spectral component may be considered as a signal obtained by frequency multiplying the fundamental component by its corresponding harmonic number. The AM noise remains constant with harmonic number but FM noise is proportional to the square of the harmonic number [21]. The AM and FM noise produced by the laser will correspond to amplitude and phase fluctuations in the CW signal generated.

The basic photoconductive switch is shown in Fig. 3. It consists of a microstrip transmission line structure with a small gap which separates the input from the output. When the gap is in the dark state (no optical illumination), the high resistivity of the semi-insulating substrate will provide a path of extremely low conductance. This high impedance state gives the switch excellent noise rejection properties since the dark current generated by the bias voltage is extremely low. When an optical pulse is focused on the switch gap, a temporary electron hole plasma is formed, connecting the input to the output. This action produces an electrical pulse with a rise time approaching the optical pulse rise time and a fall time related primarily to the carrier recombination time. A typical output waveform from a Cr:GaAs switch is shown in Fig. 4, where the interpulse spacing corresponds to the laser cavity round trip time. The power spectrum of this pulse train is shown in the lower trace of Fig. 5, where the spectral components are spaced every 100 MHz, corresponding to the mode spacing of the laser. Under these experimental conditions, we have observed a spectrum extending to 25 GHz.

A single frequency 10 GHz signal may be obtained if a bandpass filter is used to select only the 10 GHz spectral component from the switch output spectrum. The spectrum at the output of this filter is shown in the upper trace of Fig. 5, where in addition to the center frequency at 9.78 GHz, several harmonics are passed by the spurious response of the filter. We used a low pass filter to remove these spurious components.

When the filtered output signal is applied to the amplifier, an extremely clean sinusoid was produced. A sampling oscilloscope display of the 9.78 GHz signal obtained is shown in Fig. 6. This waveform suggests that the jitter of the microwave signal is very small.

Finally the phase stability of the CW signal generated by this technique must be measured. The phase noise of the 9.78 GHz spectral component is shown in Fig. 7. We apply classical frequency stability measurement techniques [21] to obtain a quantitative measure of the signal's short term stability. The short term stability is most easily evaluated by using the frequency domain description of the signal. This is done by representing the signal output as a carrier modulated by AM and FM noise. The discrete noise processes cause discrete spurious noise sidebands while random processes create a continuous noise pedestal. For higher harmonics, the FM noise has a greater contribution than the AM noise. The FM noise to carrier power ratio has a square-law dependence on frequency, as is illustrated by our measured results in Fig. 8. We are particularly interested in measuring the rms time jitter by considering the FM noise.

By integration of the spectrum, we have measured a Δt_{rms} of 1.8 ps from the continuous noise pedestal. The contribution from the deterministic noise processes was computed to be 3.03 ps giving a total rms time jitter of 3.53 ps (for an offset band of 30Hz-5kHz) for a CW signal produced by any of the spectral components. Most of these discrete noise processes could be detected at the output of the RF source driving the Nd:YAG mode-locked unit. These undesired spurious responses may be reduced by utilizing a more stable RF source for the mode-locker. Currently the most effective method of decreasing the time fluctuations in the output of a mode-locked laser is by phase locking the output of the laser to the reference RF source driving the mode-locker unit. Rodwell et. al. [22] have reduced the total time fluctuations of a compressed mode-locked Nd:YAG laser from 2.9 to 0.3 ps rms with this method.

We have described a new technique of producing CW microwave signals which are phase coherent to a mode-locked laser source. Extensive measurements have been made to calculate the frequency stability of the CW signal generated. The total rms time jitter of the 10 GHz signal produced in our experiment is approximately 3.53 ps. This number has been computed by the RF spectrum method from the sideband phase noise power between 30 Hz and 5 KHz. Methods of improving both the AM noise fluctuations and the rms timing jitter have been discussed. It is presently assumed that the jitter in the microwave CW signals generated by this technique is mainly due to laser jitter. We are currently working in a technique that will allow us to measure the small amount of additional jitter contributed by the switch. Stabilization of the YAG laser using a phased locked loop may be necessary for more comprehensive noise evaluations and certain applications.

Higher output power can be obtained by using photoconductor arrays or higher gain amplifiers. Materials with faster switching speeds than Cr:GaAs may also be used, enabling higher power to be obtained at frequencies in the millimeter-wave band. The width of the photoconductive switch gap may be increased to allow for larger bias voltages (increased power handling capabilities). Although 10 GHz operation has been reported thus far, a 100 GHz source is feasible, as a femtosecond laser and photoconductors with picosecond carrier lifetime are currently available. The filtering operation becomes more demanding at the higher frequencies. It is therefore desirable to increase the effective repetition rate of the laser. This can be done by using optical or electrical delays. With the optical technique, the repetition

rate can be multipled by 8 or 16 without difficulty [5]. The integrated filter currently being studied will be necessary for higher frequency operation. The ultimate goal is to integrate the laser, photoconductive switch, filter and amplifier. This will result in a compact, robust, high performance system which can be employed for many high frequency source, high speed data processing and antenna applications.

II.B Optically Controllable Dielectric Millimeter Waveguide

One of the important parts of microwave and/or millimeter wave systems is the waveguide. Traditionally, metal waveguides have been commonly used. For integrated systems, waveguides such as microstrip or dielectric waveguide are attractive. Both of these structures can be fabricated by integrated circuit techniques. Complex millimeter-wave integrated circuit elements can be easily formed from dielectric materials by employing batch fabrication techniques using sandblasting, machining, laser cutting, etc. Microstrip transmission lines are used up to 30 GHz. For frequencies greater than 30 GHz, the losses in microstrip structures are high, higher-order modes may be a problem, and fabrication techniques become more difficult due to the small stripwidth and substrate thickness. Dielectric rectangular waveguides become, then, an important alternative to the expensive metal waveguides. The use of high purity semiconductor materials as dielectric waveguides is particularly important, since active devices such as oscillators, Gunn or Impatt diodes, mixers/detectors, and modulators can all be fabricated 'in situ' into the semiconducting waveguides.

One important aspect of millimeter-wave devices is the control of phase and amplitude of a wave propagating through the waveguide. Such types of devices with a reasonable speed and acceptable bandwidth are not available yet in the millimeter-wave region. The use of semiconductor bulk phenomena in implementing microwave control components has been discussed [1]. The principal phenomena explored have been the dielectric and conductive properties of the plasma states. A frequency-scanning millimeter-wave antenna utilizing periodic metallic stripe perturbations on a silicon waveguide has been demonstrated [23]. Millimeter-wave dielectric image-guide integrated devices have been developed [24]. In the optical region, there are a whole variety of controllable waveguide devices which have not found their counterparts in the millimeter wave region.

Phase shifting is a fundamental control operation. A general approach to this operation, used extensively at both optical and microwave frequencies, is to alter the phase velocity along a fixed interval of a guiding medium. We have studied in our laboratory a method to control the phase and amplitude of the millimeter-wave signal propagating in a semiconductor waveguide by optically injecting a thin, but high density, plasma with above bandgap optical radiation. Our research has resulted in several important findings, leading to the demonstration of a laser controlled millimeter-wave phase shifter with a phase shift of up to 1400 °/cm observed. More importantly, our current work has enabled us to better understand the physics of these type of devices, particularly regarding the loss mechanism [1].

In this section, we shall first review the concept of optically controllable millimeter-wave devices based on semiconductor waveguides. Highlights of current results will also be presented at the end of this section. The detail of this aspect of research is included in appendix I which has been published in Infrared and Millimeter Waves, Vol. 15, K. Button, edited, by Academic Press.

(1) Concept of optically controllable millimeter-wave propagation.

Shown in Fig. 9 is a schematic of the optically controllable phase shifter. It consists of a rectangular semiconductor waveguide with tapered ends to allow efficient transition to and from a conventional metal waveguide. Optical control is realized when the broad wall of the semiconductor guide is illuminated by light generated by either a proximal source or one removed by a suitable optical guiding medium. The width a and height b of the guide are selected so that it supports an E_{11}^y mode. The initial depth of the plasma injection is controlled by selecting an appropriate combination of optical radiation wavelength and semiconductor absorption properties.

At sufficiently small injection depths, the final thickness of the plasma is determined primarily by processes of carrier diffusion and recombination. The effect of the plasma occupied volume is to introduce a layer whose index at the millimeter-wave frequency is larger than the remaining volume of the waveguide. From Drude theory, the index of refraction can be written as

$$(\eta - jk)^2 = \epsilon_r - \frac{w_p^2}{w^2 + \nu^2} - j\frac{\nu}{w}\frac{w_p^2}{w^2 + \nu^2} \tag{1}$$

Here, ϵ_r is the dielectric function of the host lattice, w_p is the plasma frequency, ν is the carrier collision frequency, η and k are the real and imaginary part of refractive index respectively, and w is the angular frequency of the electromagnetic field. The plasma frequency is defined as $w_p^2 = \frac{ne^2}{\epsilon_0 m^*}$. Since n, the carrier density, is directly proportional to the laser intensity, one can use the laser to control the refractive index of the plasma region in the dielectric waveguide. From simple physical arguments one would expect this effect to become strong as one approaches and then exceeds the plasma density at which the value of the plasma frequency equals the frequency of the guided millimeter-wave signal. At sufficiently high plasma densities, the millimeter-wave signal is totally screened from the occupied volume and one would expect that the phase shift per unit length would saturate as a function of plasma density. At extremely high densities the plasma layer becomes metallic and the dielectric waveguide becomes approximately an image guide. As the optical illumination intensity increases from a low value, a significant phase shift will not appear until the plasma frequency exceeds the frequency of the guided millimeter-wave signal, after which it will rapidly rise and eventually saturate. However, the form and magnitude of the phase shift versus the intensity of illumination, and hence the plasma density, depends on the material and geometrical factors that characterize the optically perturbed guiding structure and their determination requires a detailed solution of the corresponding boundary value problem. The optically induced phase shift $\Delta\phi$ for a given section of waveguide of length l is determined by computing the propagation constant in the z direction, first in the absence of the injected plasma k_z and then with the plasma k_z', thus

$$\Delta\phi = (k_z' - k_z)l \tag{2}$$

We have developed a complete theory and performed a computer calculation of the boundary value problem and have measured the phase shift as a function of laser intensity to test our model. Details of the experimental technique and numerical calculations are given in appendix I. In general, there are overall good agreements between the experimental observations and theoretical predictions. We feel very confident that we have a good understanding of this problem.

With slight variations of the phase shifting technique we have also demonstrated opto-electronic switching, gating and modulation of millimeter-wave at 94 GHz by an optically induced plasma in a silicon, GaAs, silicon-on-sapphire (SOS), InP, and a composite waveguide consisting of thin layer of single crystal silicon on alumina. A millimeter-wave pulse width as short as 100 picoseconds and variable to tens of nanoseconds can readily be obtained by this technique. We conclude from these studies that the optical injection of a plasma is superior to electrical injection because of the near perfect isolation between the controlling and controlled devices. The geometry and nature of the injected plasma column is amenable to theoretical analysis. Excellent agreement between experiment and theory encourages further study and a search for a better experimental configuration to realize a new class of devices with high efficiency. Of particular interest is the development of an electronically steerable phased array antenna.

As mentioned above, the key to the realization of optically controlled millimeter-wave device in a semiconductor waveguide is to have a complete understanding of the physics of the interaction of the millimeter-wave signal with the induced plasma layer on the surface of the waveguide. We began our study by theoretically analyzing the boundary value problem assuming that a uniform layer of plasma is created at the surface. We have calculated the phase shift and attenuation of a 94 GHz signal in such a waveguide as a function of plasma density for various plasma layer thicknesses. The data for a $2.4 \times 1mm^2$ silicon waveguide is shown in Figs. 10 and 11. It is clear from these figures that in the ideal case the phase shift will saturate at a plasma density larger than $10^{18}/cm^3$, where the attenuation is also very small. This is due to plasma screening of the millimeter-wave signal. As the plasma density descreases via recombination or other means, the millimeter-wave signal begins to penetrate into the plasma region, causing loss. The maximum attenuation occurs when the skin depth at 94 GHz is roughly equal to the thickness of the plasma layer. This means that the carrier diffusion process may result in large loss for two reasons: (1) carrier diffusion causes the plasma layer to become thicker, and (2) at the same time the plasma density will further decrease because of diffusion. According to Fig. 11 the attenuation will quickly increase.

In order to explore the dynamics of carrier and wave interaction, we have to devise a way to measure the attenuation and phase shift of the propagating millimeter-wave signal as a function of time. In many semiconductors, the carrier recombination lifetime and transport dynamics can take place in nanoseconds (or less). However, there is no commercial vector network analyzer at 94 GHz with a time resolution in this time range. We therefore have to invent our own vector network analyzer. This work has recently been published in IEEE Transactions on Microwave Theory and Techniques, entitled, "Measurements of time-varying millimeter-wave vectors by a dynamic bridge method" [25]. This method employs a millimeter-wave bridge in which a plasma-controlled waveguide is placed in one arm of the bridge and a precision phase shifter and a precision attenuator are placed in the other arm [1]. A schematic of the millimeter-wave bridge is shown in Fig. 12. The millimeter-wave bridge is initially (with no plasma generation) balanced by adjusting the variable attenuator A and the phase shifter ϕ in arm b so that there is no signal at the output. When a plasma is generated in the semiconductor waveguide by electronic or optical means, a phase shifted and/or amplitude modulated millimeter-wave signal appears at the output of the bridge. Usually the signal thus generated is of transient nature with a characteristic decay time. The temporal variation of the signal depends upon the carrier transport dynamics.

A dynamic bridge technique has been developed to determine the values of the plasma-induced phase and attenuation. This method exploits the fact that the temporal profile of the output of the bridge depends sensitively upon the initial phase angle between the electric fields in the two arms as well as the dynamics of the phase shift and attenuation due to the induced electron-hole plasma. This method has a large dynamic range: it is possible to follow the decay of the plasma density over four orders of magnitude. A detailed description of the dynamic bridge method can be found in reference [25]. (See also appendix I for details.)

We have applied the dynamic bridge method to measure the variation in amplitude and phase of a millimeter-wave signal as a function of time after a silicon waveguide is illuminated by a single 30 ps laser pulse. A comparison of the theoretical model and the experimental results obtained by using the dynamic bridge method alone is shown in Fig. 13. Here, the recombination time was fitted at 20 μs and the ambipolar diffusion coefficient was held at a constant $18 cm^2/sec$. The initial plasma density was fitted at $10^{18} cm^{-3}$, an order of magnitude less than the plasma density inferred from measurements of the laser energy. One reason for this discrepency is that the complete theoretical model assumes an abrupt junction between the plasma layer and the rest of the waveguide. From the steady state model [1], it can be seen that the millimeter-wave signals begin to interact with the plasma in the density range from 10^{14} to $10^{16} cm^{-3}$, depending upon the plasma depth. The plasma layer model chooses an average plasma depth and density which is spatially abrupt. This model ignores the plasma in the tail of the distribution, which for large total plasma densities may be significant. These smaller plasma densities at larger plasma depths interact with millimeter-wave signals producing larger attenuations than those predicted by the abrupt junction model. The large peak in the theoretical attenuation curve in Fig. 13 is probably due to the fact that the model of the waveguide used [9] predicts a cutoff waveguide size for the lowest order semiconductor waveguide mode. This "cutoff" never occurs in reality. In the theoretical model, as the plasma is diffusing into the semiconductor waveguide, the waveguide is becoming pinched off. The predicted attenuation in the near pinch-off case is probably too high due to the model predicting an actual cutoff condition.

These results suggest that the new measurement technique developed in our laboratory is an important tool to accurately characterize the plasma-wave interaction. These observations suggest that in order to reduce dynamic loss one has to confine the carriers to a thin layer at the surface. The ideal waveguide for a low-loss phase shifter should be able to sustain a surface plasma at a high density for a sufficiently long enough time (preferrably a few microseconds).

Recently, we have focussed our attention to search for such an ideal waveguide. We have studied the silicon-on-sapphire (SOS) as a possible candidate. By assuming that the epitaxial silicon layer on the sapphire substrate has as good a quality as a single crystal silicon, we have calculated the phase shift and attenuation at 94 GHz in such a waveguide as a function of time. The calculated results are shown in Figs. 14 and 15, where the carrier lifetime and mobility in the epitaxial layer are assumed to be the same as those in the bulk. These calculated results indicate that SOS is indeed a good waveguide material since it can maintain a large phase shift with low dynamic loss for several microseconds. However, our experimental data indicates otherwise. Using the dynamic bridge method, we have measured the attenuation and phase shift of a 94 GHz signal as a function of plasma density for the SOS waveguide. The measured data is compared with the theoretical values in Figs. 16 and 17. These results are disappointing since it shows large attenuation which sets in within one nanosecond after

the optical illumination. Fortunately, these results can be explained by the poor quality of the silicon epi-layer: 1.5 ns lifetime and $\mu_e = 500 cm^2/v.s$. These studies clearly point out the requirements of the ideal waveguides. Recently we have fabricated a composite waveguide consisting of a single crystal thin silicon layer attached to an alumina substrate. Since the silicon layer is made of high quality bulk material (10 μm thick), it has a high mobility and a long lifetime. In addition, the surface recombination is also small and the preliminary results are very encouraging. We have observed for the first time that a high density plasma state can be maintained for a few microseconds, resulting in a low dynamic loss (Fig. 18). Another important waveguide structure may be an MBE-grown heterojunction material, such as AlGaAs and GaAs. The larger bandgap AlGaAs region can be used to prevent carrier diffusion from the GaAs surface layer. The two dimensional electron gas system simulates a high density state with extremely high mobility. We have also started to investigate these materials both theoretically and experimentally.

II.C Highlights of current results

1. We have succeeded for the first time in generating a CW microwave signal at 10 GHz by a picosecond optical electronic technique. The phase noise is found to be very small, leading to the possibility of using this technique for an optically fed phased array antenna which requires D.C. bias as the only electrical feed network.
2. We have conceived and demonstrated the concept of an optically controllable millimeter-wave phase shifter at 94 GHz in a semiconductor dielectric waveguide. Phase shifts as large as 1500 °/cm have been observed.
3. A dynamic bridge technique has been developed which has lead to the development of a vector network analyzer at 94 GHz with a time resolution better than one nanosecond.
4. With the use of a CW mode-locked laser and a lock-in amplifier, the dynamic bridge method time resolution has been improved to 25 picoseconds and phase variation of less than 0.1° can be measured.
5. A complete theory and computer code to tackle various boundary value problems has been developed. Currently a multi-layer dielectric waveguide is being analyzed.
6. Demonstrations of ultrafast millimeter-wave switching, gating, and modulating. The generation of a millimeter-wave "chirp" pulse has been observed for the first time.
7. Development of a composite dielectric waveguide which is capable of yielding large phase shifts with small dynamic losses.
8. An ultrafast photomixer with 10 picosecond time resolution has been fabricated and successfully tested. This device will mix a two mode laser signal to generate an I.F. in the millimeter-wave spectral range.
9. Generation of an ultrashort millimeter-wave pulse by optical modulation of an InP waveguide.
10. Demonstration of optical control using laser diodes.

REFERENCES

[1] A.M. Yurek, C.D. Striffler and Chi. H. Lee, "Optoelectronics devices for millimeter-waves", Chap. 4 in Infrared and millimeter-waves, vol. 14, Millimeter Wave Components and Techniques, K.J. Button, editor, Academic Press, pp. 249-290, (1985).

[2] C.J. Clark, E.A. Chauchard, K.J. Webb, K. Zaki, Chi H. Lee, P. Polak-Dingles, H-L. A. Hung and Ho C. Huang, "Investigation of a new optoelectronic CW microwave source", accepted for publication in the IEEE Transaction on MTT-S, 1987.

[3] R. Kunath and K. Bhasin, "Opitically-controlled phased array antenna concepts using GaAs MMIC's", Symposium Digest of APS International Symposium, June 8-13, pp. 353-356, (1986).

[4] N. Jesperson, P. Herczfeld, A. Rosen and P. Stabile, "Optically-controlled beamforming for phase array antennas", Symposium Digest of APS International Symposium, ibid., pp. 357-360, (1986).

[5] A. Mooradian, "Use of spatial time-division repetition rate multiplication of mode-locked laser pulses to generate microwave radiation from optoelectronic switches", Appl. Phys. Lett., Vol. 45, pp. 494-496, (1984).

[6] L. Goldberg, A.M. Yurek, H.F. Taylor and J.F. Weller, "35 GHz signal generation with an injection locked laser diode," Elect. Lett., Vol. 21, pp. 814-815, (1985).

[7] G.A. Koepf, "Optical processor for phased array antenna beam formation", *Optical Technology for Microwave Applications*, S. K. Yao, Ed., Proc. SPIE, 477, pp. 75-81, 1984.

[8] P.G. Sheehan and J.R. Forrest, "The use of optical techniques for beamforming in phased arrays", ibid., pp. 82-89.

[9] P.D. Stilwell and W.C. Collins, "Fiber optically fed phased arrays," presented in *Optical Technology for Microwave Applications II*, SPIE's Technical Symposium East, 1985.

[10] R. Foreer, H.W. Yen and R.A. Peters, "Opto-electronic switch arrays for microwave networks", ibid.

[11] A. Mooradin, "Picosecond pulses for millimeter-wave generation," ibid.

[12] E.P. Ippen and J.G. Fujimoto, "Applications of femtosecond optics", paper TuE1 at *CLEO*, 1985, Baltimore, MD.

[13] C.H. Lee, "Picosecond optoelectronic devices based on optically injected electron-hole plasmas", Picosecond Optoelectronic Devices, C.H. Lee, Ed., Academic Press, Orlando FL, 1984.

[14] C.H. Lee Ed., Picosecond Optoelectronic Devices, Academic Press, Orlando FL, 1984.

[15] D.H. Auston, "Picosecond photoconductors: physical properties and applications", Picosecond Optoelectronics and Applications, C.H. Lee, Ed., Academic Press, Orlando FL, 1984.

[16] C.V. Shank, "The role of ultrashort optical pulses in high-speed electronics", in Picosecond Electronics and Optoelectronics, editors: G.A. Mourou, D.M. Bloom and Chi H. Lee, pp. 18-22, Springer-Verlag, (1985).

[17] S. Jayaraman and Chi H. Lee, "Observation of two-photon conductivity in GaAs with nanosecond and picosecond light pulses", *Appl. Phys. Lett.*, Vol. 20, pp. 392-395, (1972).

[18] M.G. Li, C.H. Lee, A. Caroglanian, E.A. Greene, C.Y. She, P. Polak-Dingles and A. Rosen, Picosecond Electronics and Optoelectronics, G.A. Mourou, D.M. Bloom and C.H. Lee (Eds.), Springer-Verlag, 1985, pp. 216-219.

[19] G. Mourou, C.V. Stancampiano and D. Blumenthal, "Picosecond microwave pulse generation", *Appl. Phys. Lett.*, vol. 38, no. 6, pp. 470-472, 1981.

[20] C.S. Chang, M.J. Rhee, C.H. Lee, A. Rosen and H. Davis, Picosecond Electronics and Optoelectronics, G.A. Mourou, D.M. Bloom and C.H. Lee (eds.), Springer-Verlag, 1985, pp. 220-223.

[21] Frequency Stability: Fundamentals and Measurements, V.F. Kroupa, (Ed.), IEEE Press, New York, 1983.

[22] M.J. Rodwell, K.J. Weingarten, D.M. Bloom, T. Baer and B.H. Kolner, "Reduction of timing fluctuations in a mode-locked Nd:YAG laser by electronic feedback", submitted to *Optics Letters*, May 1986.

[23] K.L. Klohen, R.E. Horn, H. Jacobs and E. Friebergs, "Silicon waveguide frequency scanning linear array antenna", *IEEE Trans. Microwave Theory Tech.*, Vol. MTT-26, pp. 764-773, Oct. 1978.

[24] J.A. Paul and Y.W. Chang, "Millimeter-wave image-guide integrated passive devices", *IEEE Trans. Microwave Theory Tech.*, Vol. MTT-26, pp. 751-754, Oct. 1978.

[25] A. M. Yurek, M.G. Li and Chi H. Lee, "Measurements of time varying millimeter-wave vectors by dynamic bridge method," *IEEE Trans. on MTT*, Vol. MTT-34, pp. 1220-1223, Nov. 1986.

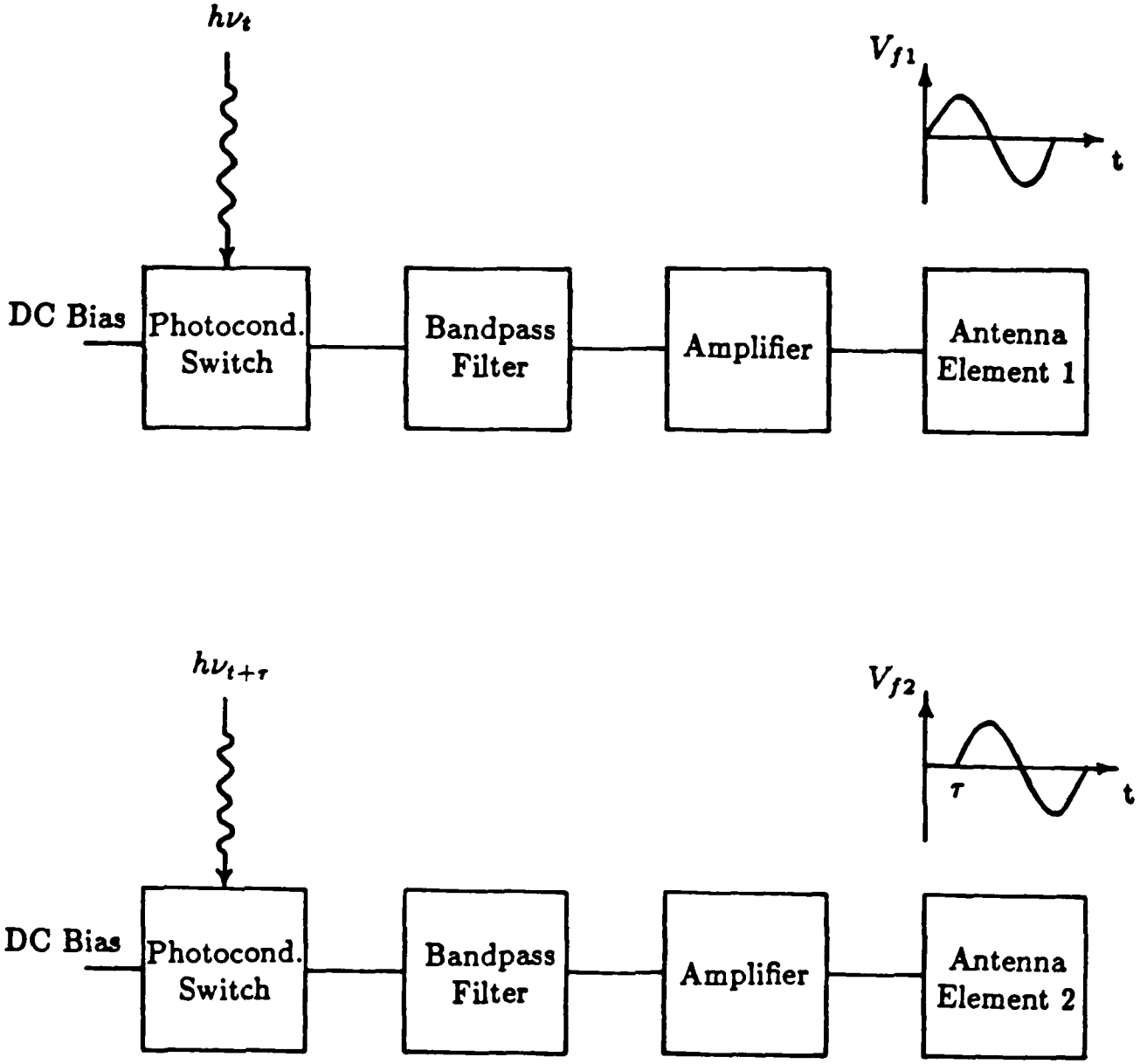

Figure 1. Concept for using picosecond photoconductors in an optically controlled phased array antenna system.

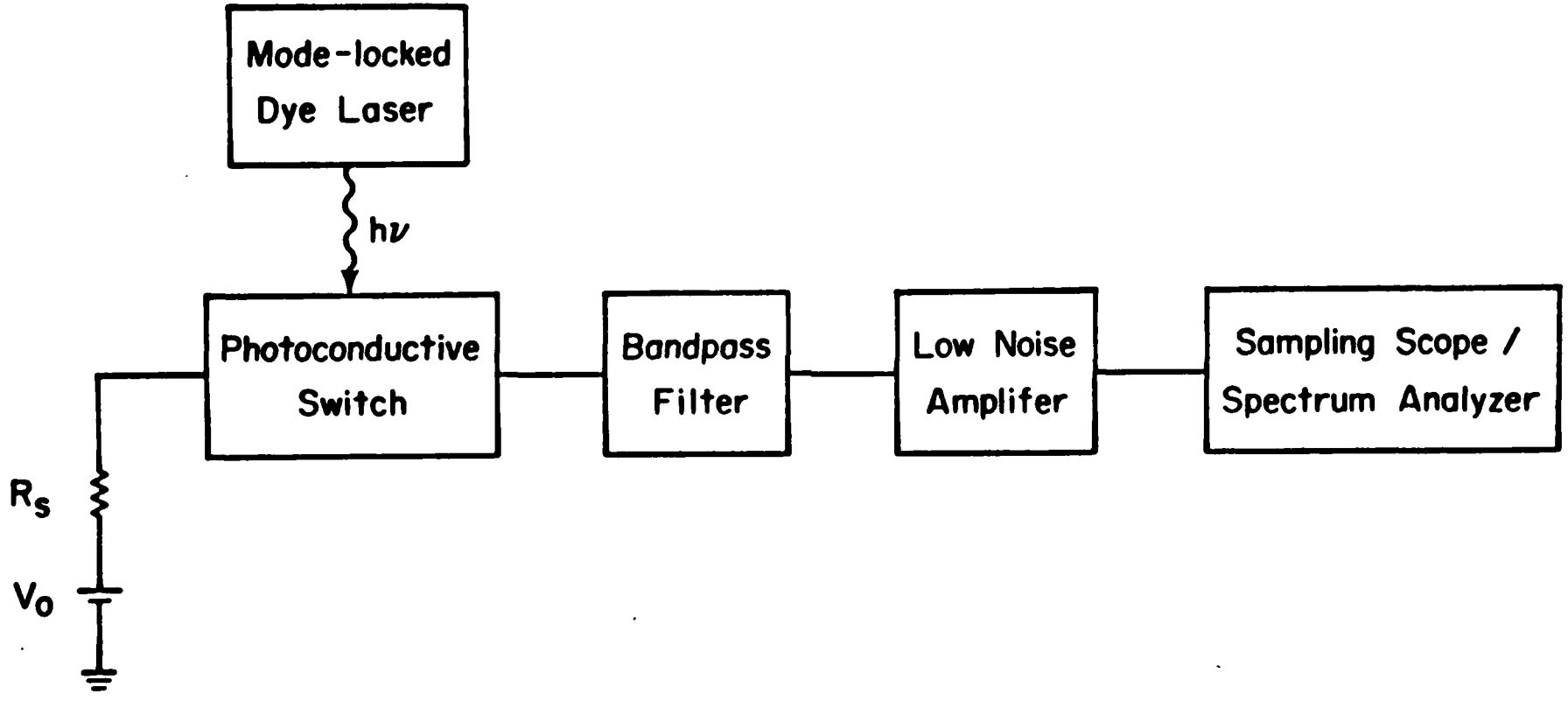

Figure 2. Experimental configuration for a CW microwave source using a picosecond opto-electronic switch.

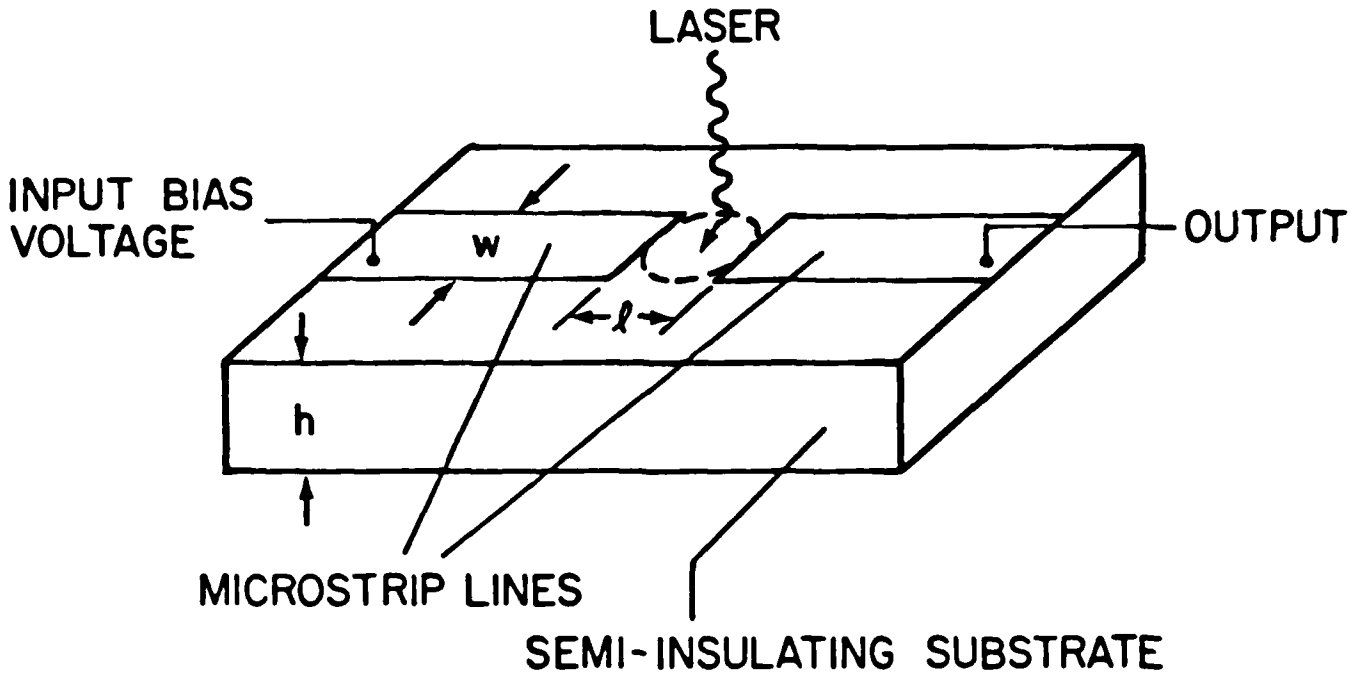

Figure 3. Picosecond photoconductive switch.

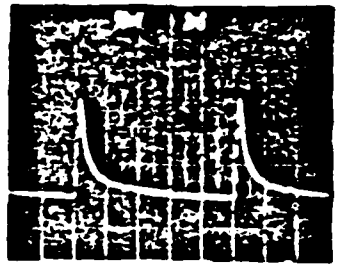

Figure 4. Output electrical waveform from a Cr:GaAs switch with a 100 μm gap and a 15 V bias when illuminated with 6ps FWHM optical pulses with an average power of 280 mW.

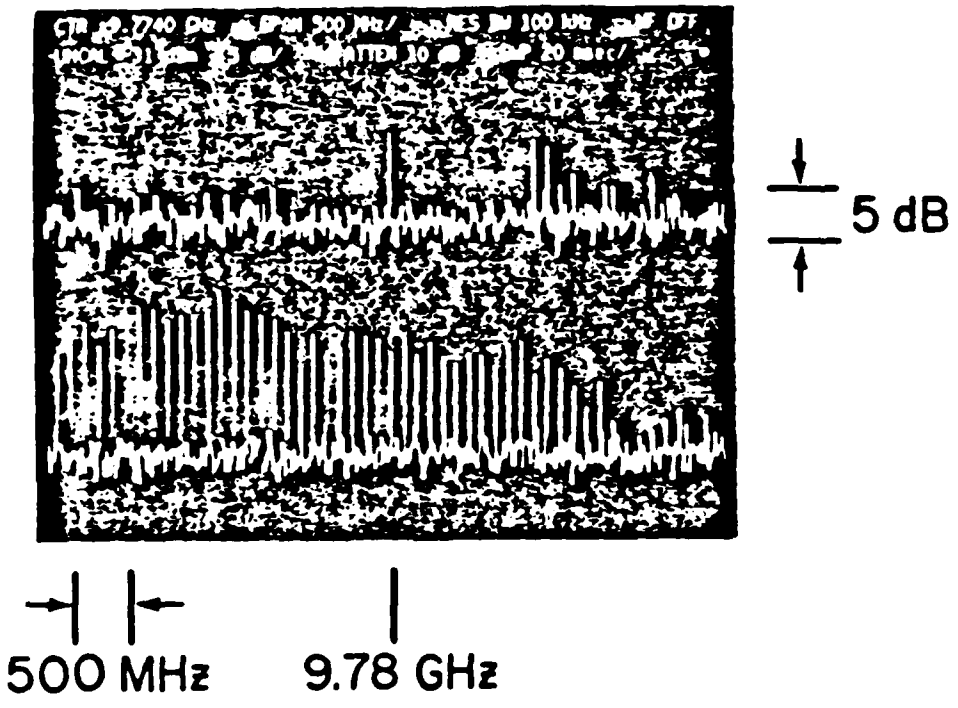

Figure 5. Instantaneous power spectrum of the switch output (bottom trace), and bandpass filter output prior to low-pass filtering (top trace).

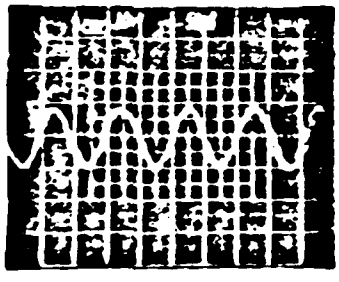

Figure 6. The sampling oscilloscope waveform at the output of the GaAs MESFET amplifier when using both the bandpass and lowpass filters. Vertical scale: 10 mV/larger div, horizontal scale: 50 ps/larger div.

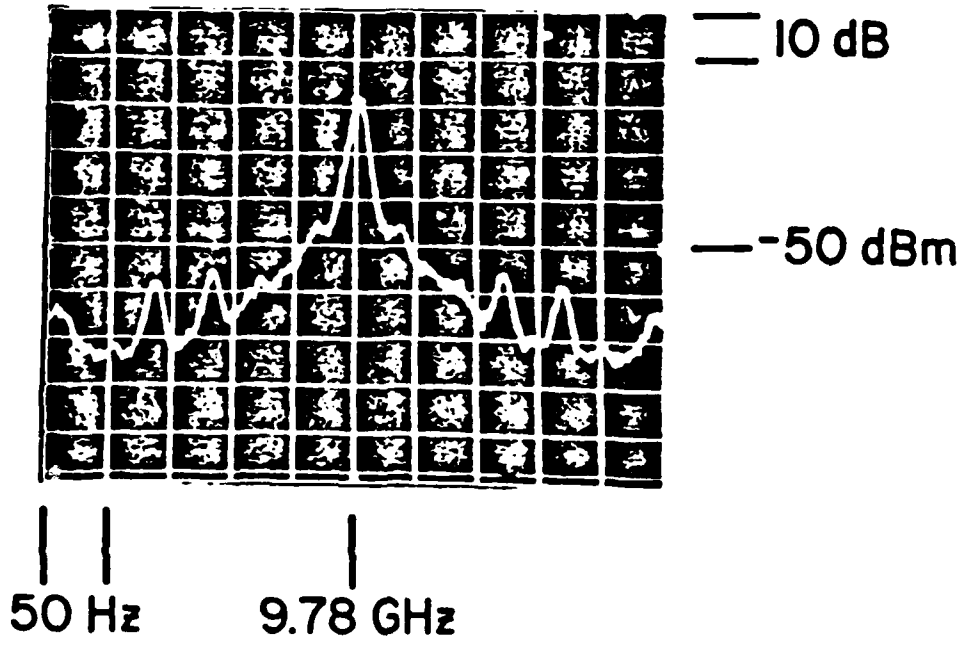

Figure 7. Power spectrum showing close-in phase noise of the 9.78 GHz spectral component. Both continuous and discrete noise processes may be measured.

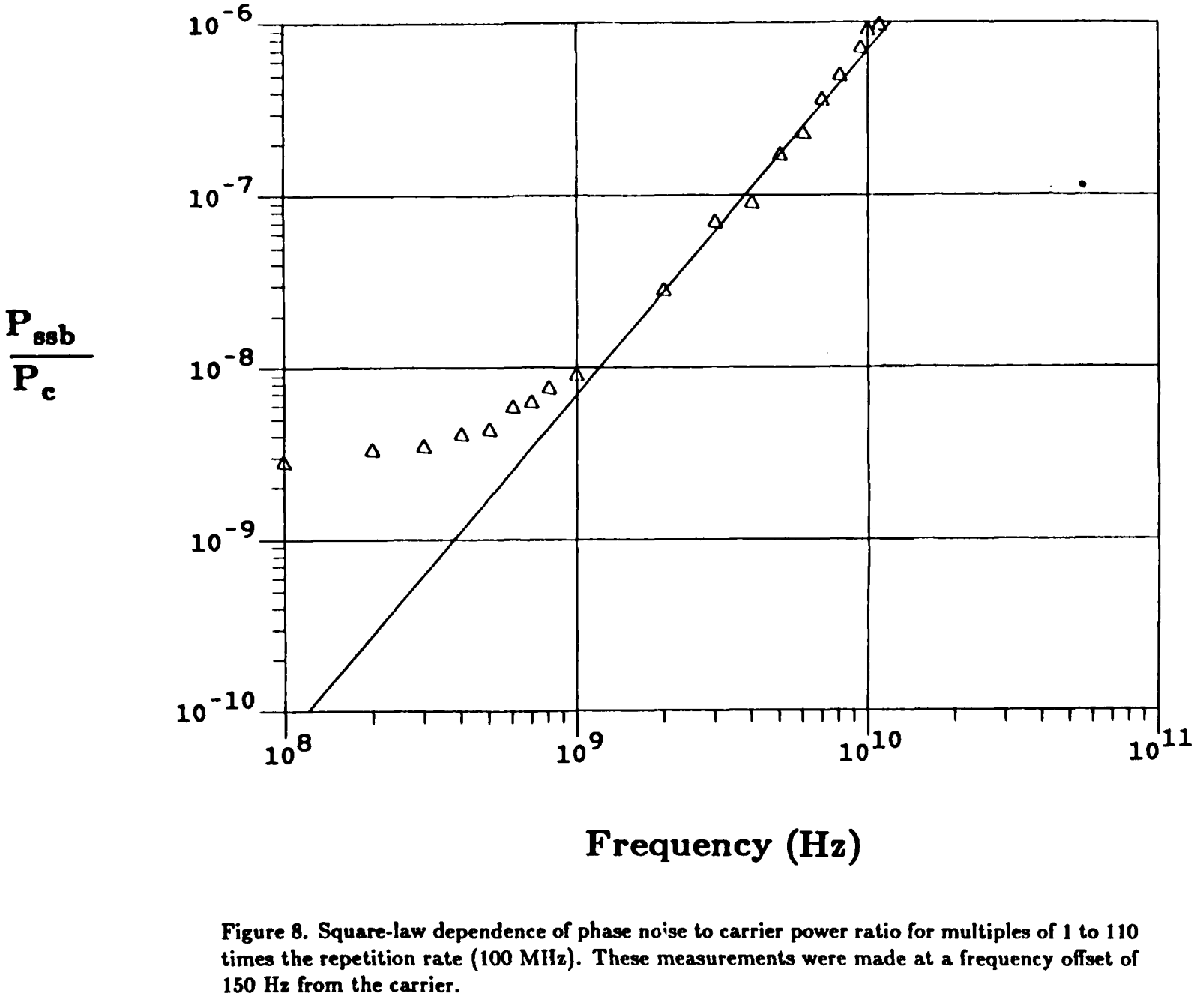

Figure 8. Square-law dependence of phase noise to carrier power ratio for multiples of 1 to 110 times the repetition rate (100 MHz). These measurements were made at a frequency offset of 150 Hz from the carrier.

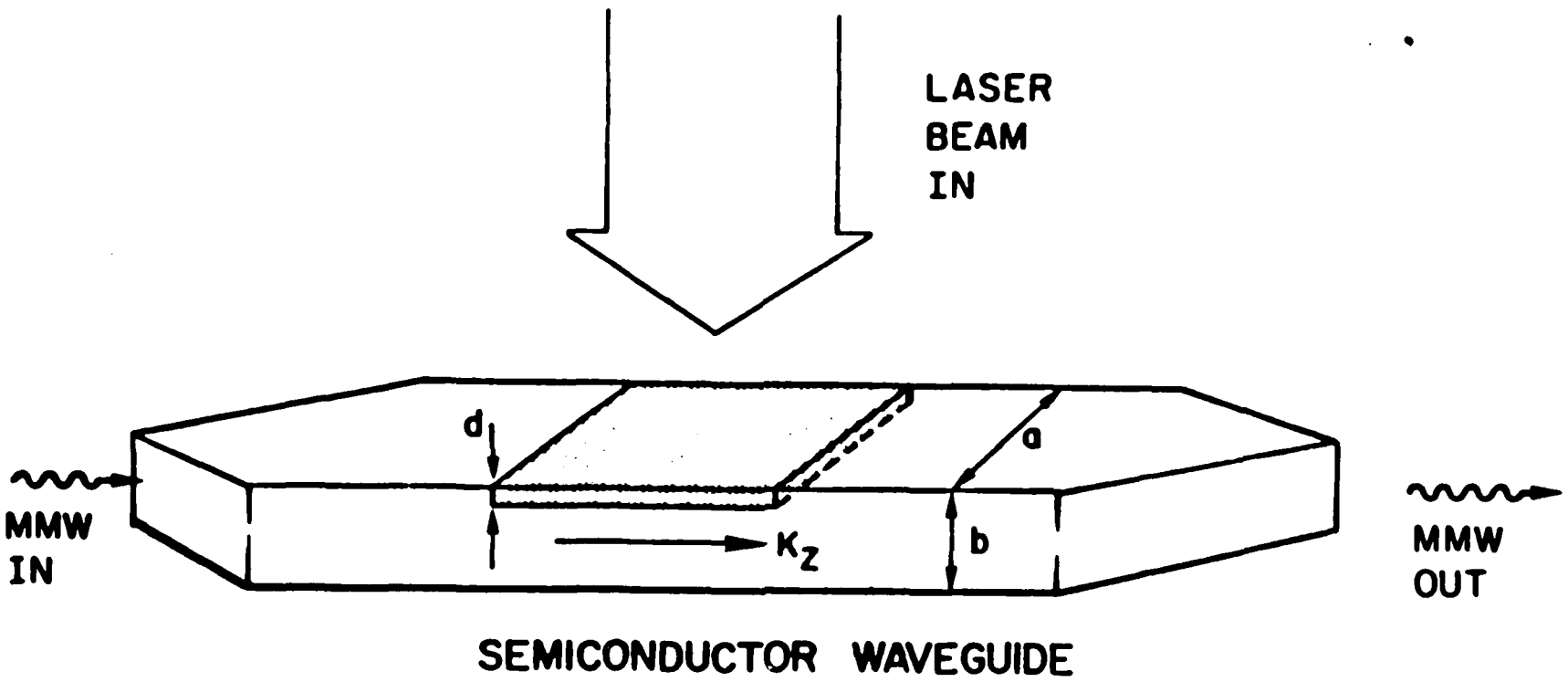

Figure 9. Concept of the optically controlled dielectric waveguide phase shifter.

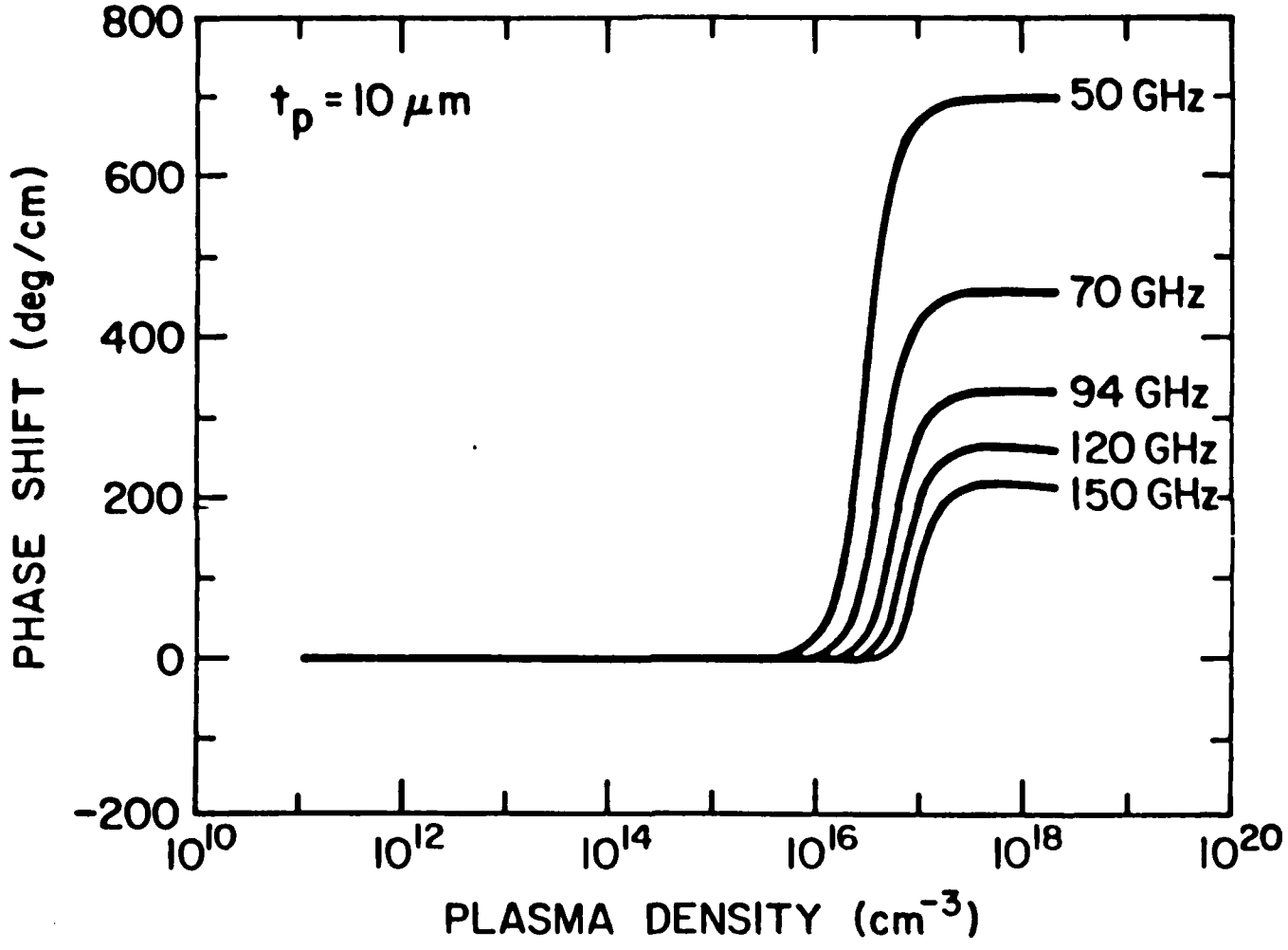

Figure 10. Calculated phase shift as a function of carrier density in Si waveguide. The waveguide has dimensions $2.4 \times 1.0\ mm^2$, the plasma thickness is 10 μm and the E_{11}^y mode is considered.

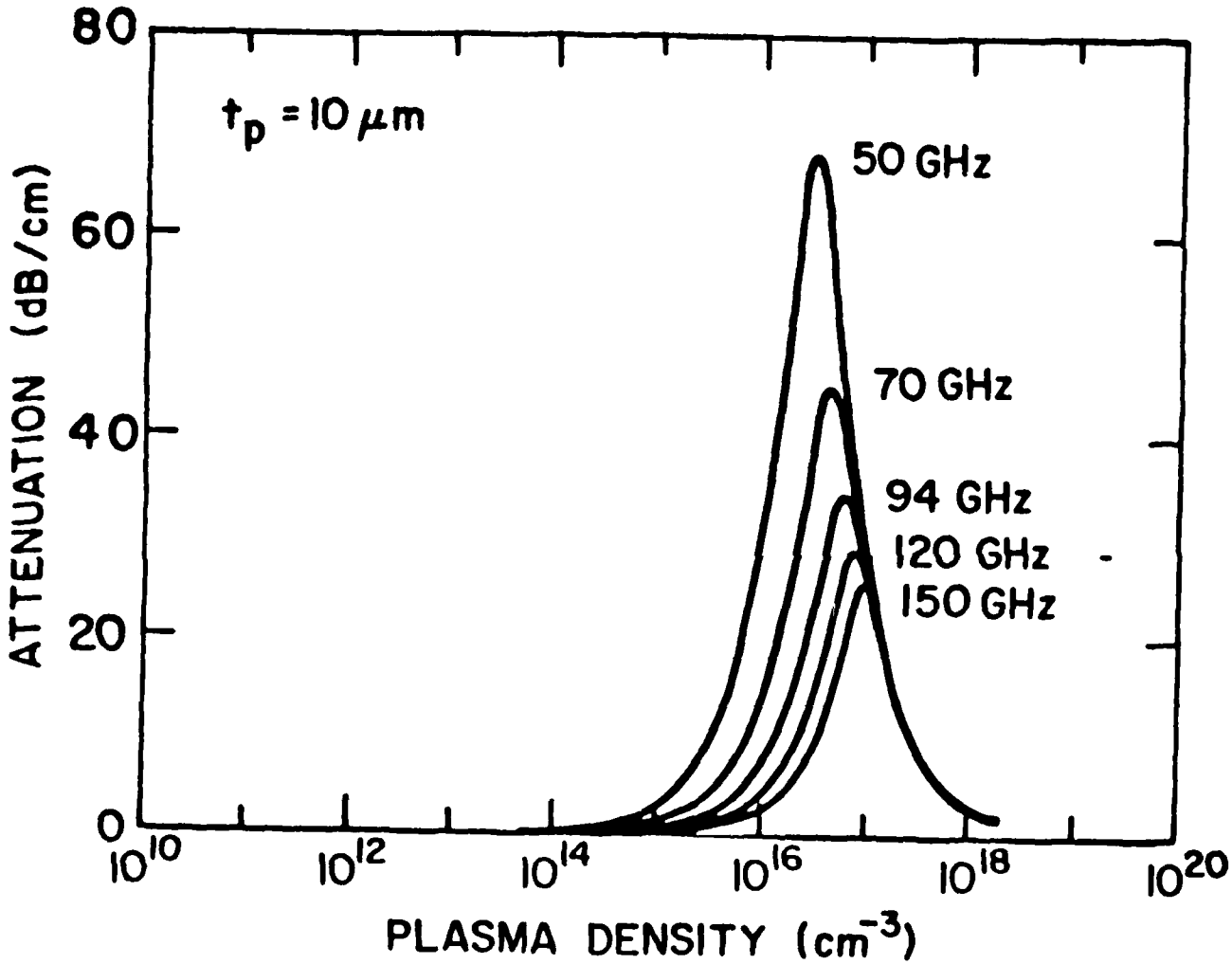

Figure 11. Calculated attenuation as a function of carrier density in Si waveguide. The waveguide has dimensions $2.4 \times 1.0\ mm^2$, the plasma thickness is 10 μm and the E_{11}^y mode is considered.

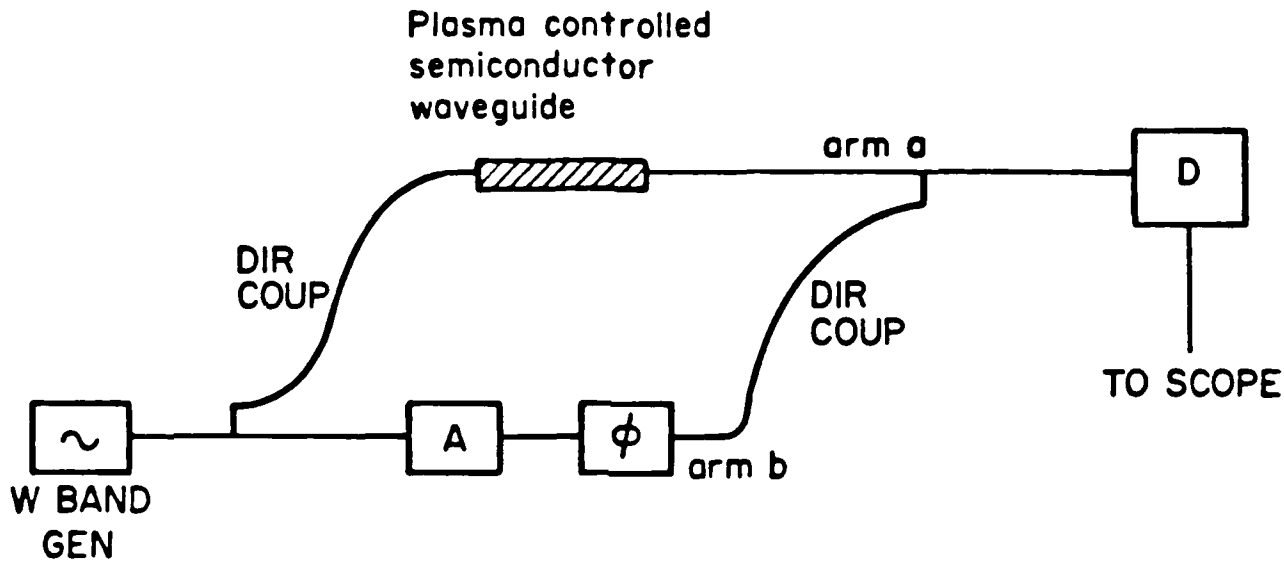

Figure 12. Schematic of the millimeter-wave bridge.

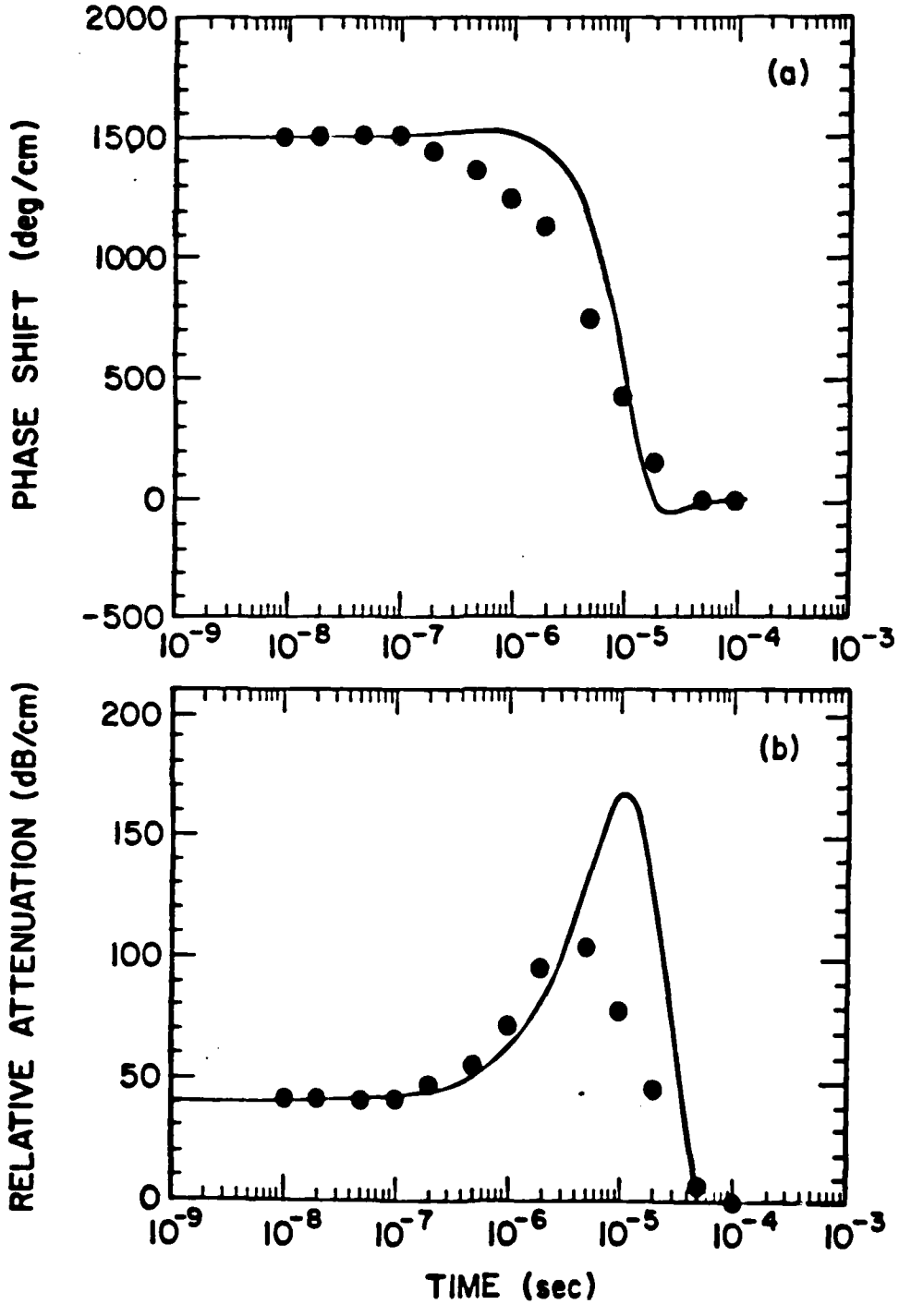

Figure 13. Measured results of phase shift and attenuation as a function of time using the dynamic bridge method. The points represent the experimental results and the solid curve the theory.

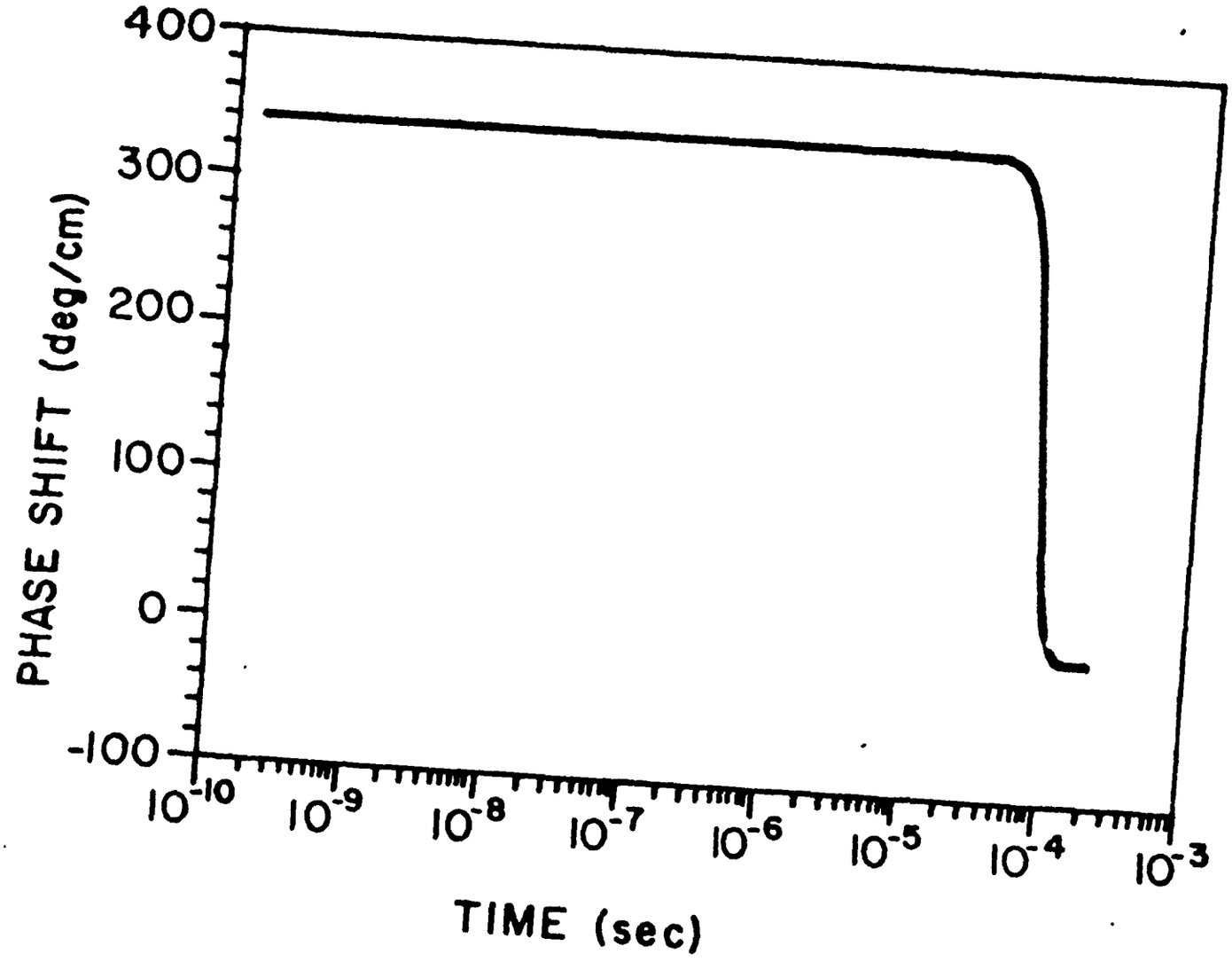

Figure 14. Calculated phase shift of a 94 GHz signal in silicon-on-sapphire (SOS) waveguide as a function of time after illumination by the laser pulse. The carrier lifetime and mobility in the silicon epilayer are assumed to be the same as in the bulk.

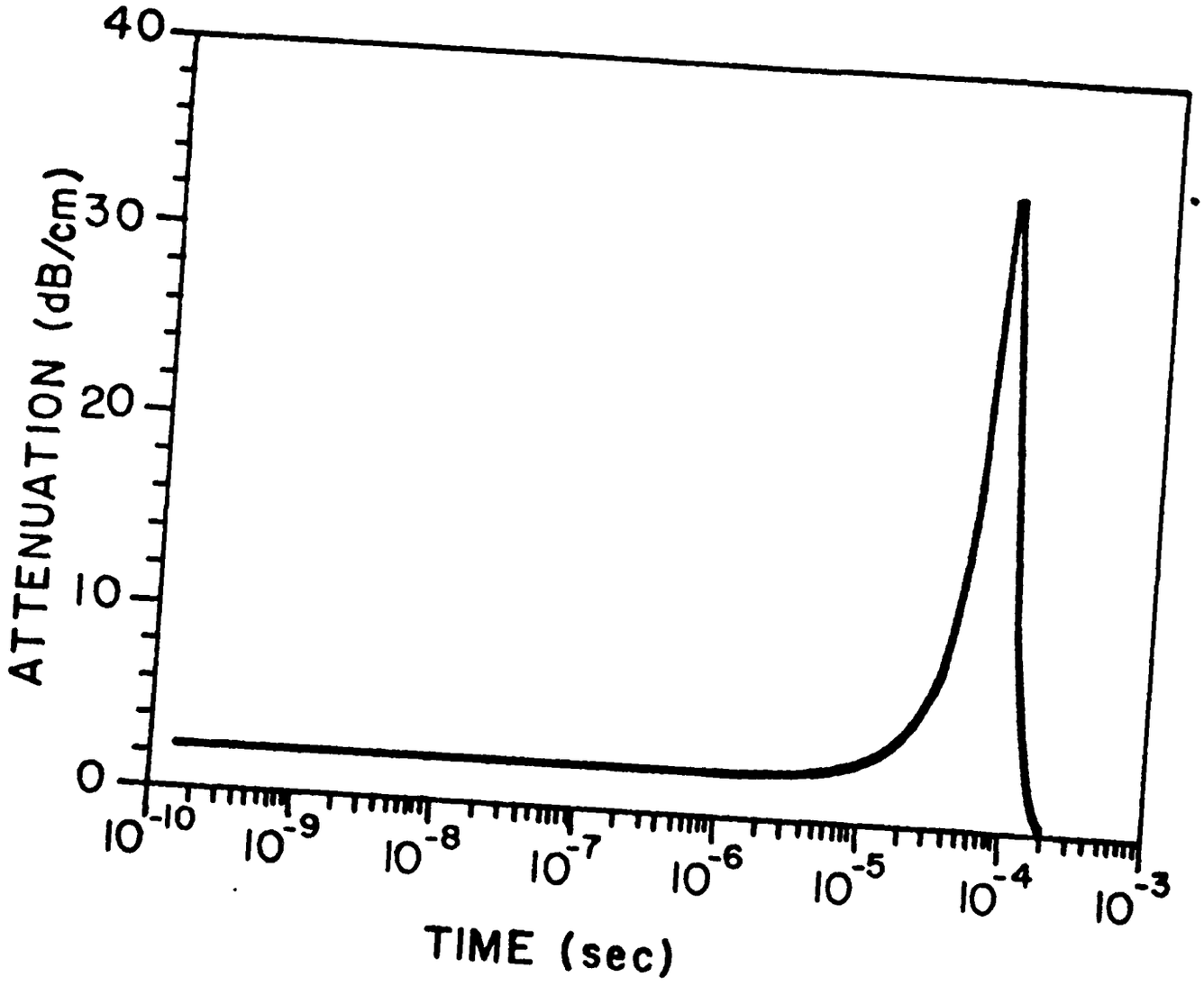

Figure 15. Calculated attenuation as a function of time in the SOS waveguide. The conditions are the same as in Fig. 14.

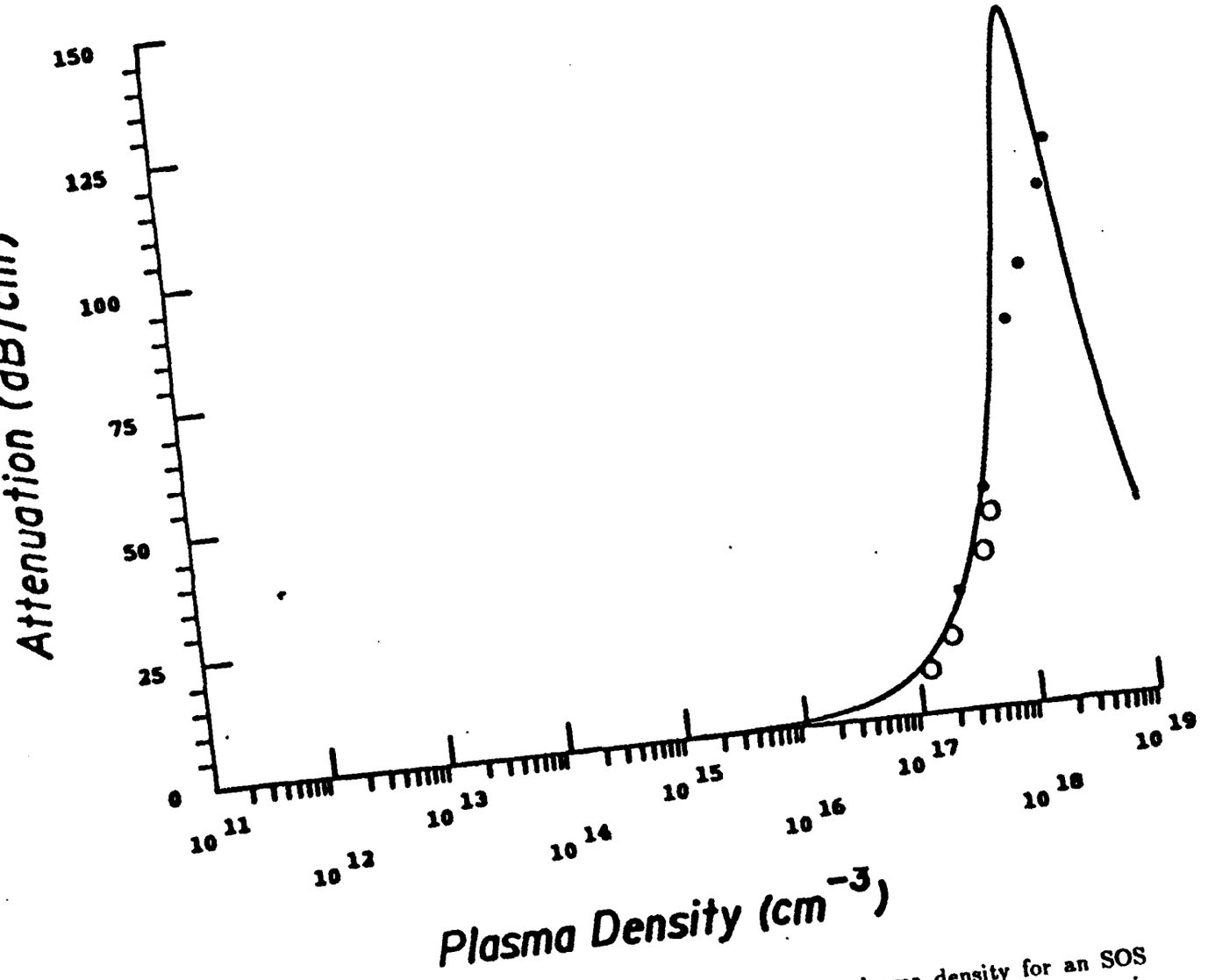

Figure 16. Measured and theoretical values of attenuation vs plasma density for an SOS waveguide 2.4×0.5 mm^2. Low mobilities are used (μ=600 cm^2/Vs) and the plasma layer is 0.5 μm thick (• green, ○ infrared).

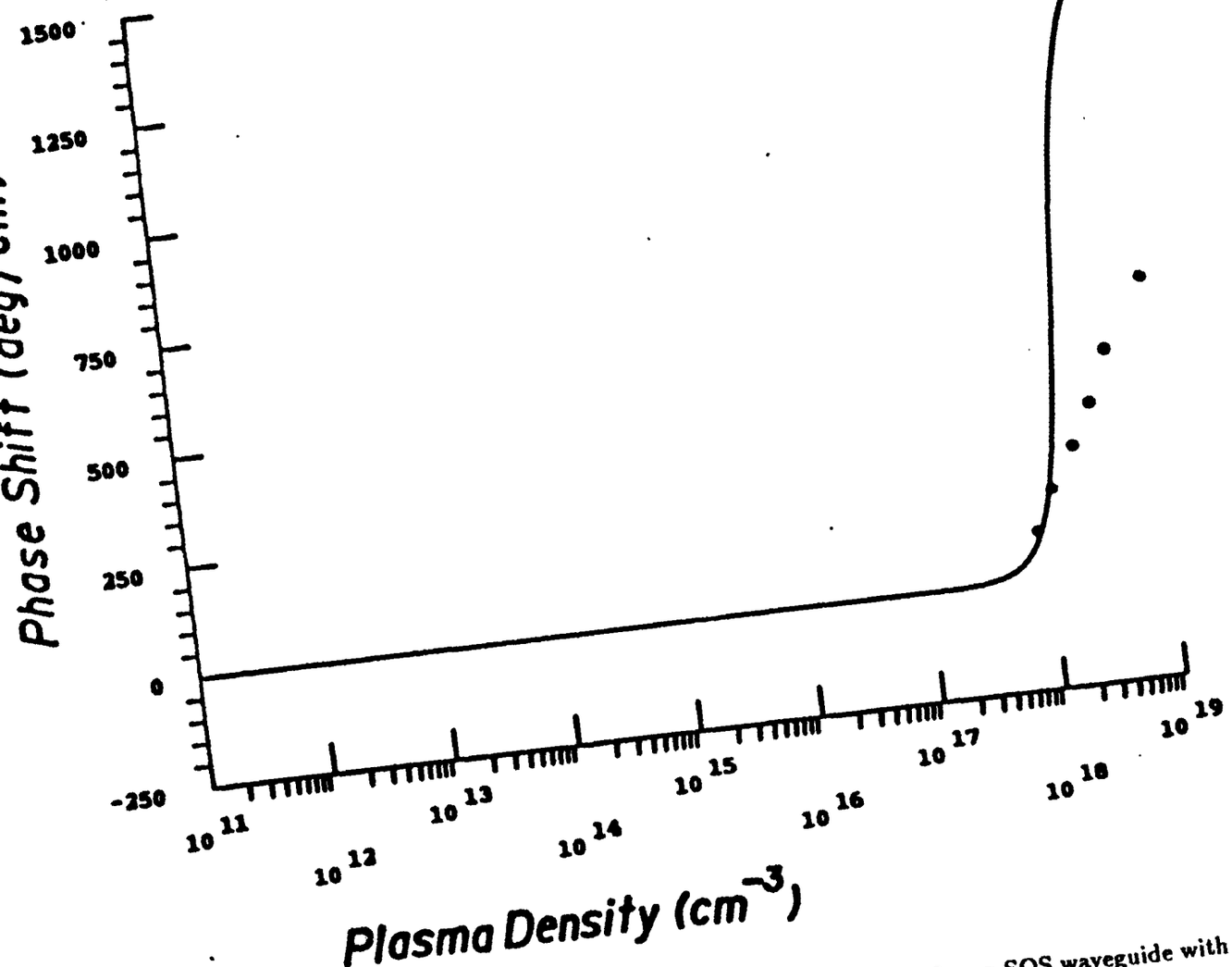

Figure 17. Measured and theoretical phase shift vs plasma density for an SOS waveguide with the same parameters as Fig. 16 (green light used).

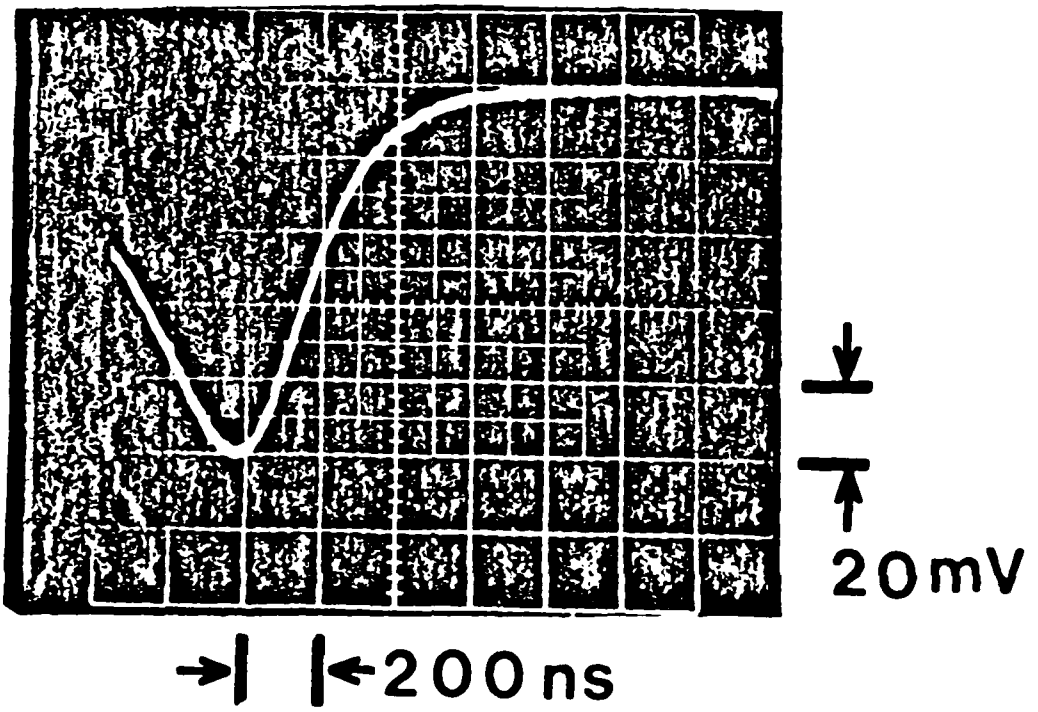

Figure 18. Measured attenuation of a 94 GHz signal as a function of time in a composite waveguide consisting of single crystal silicon-glue-alumina.

INFRARED AND MILLIMETER WAVES, VOL. 14

CHAPTER 4

Optoelectronic Devices for Millimeter Waves

Aileen M. Yurek, Charles D. Striffler, and Chi H. Lee*

Department of Electrical Engineering
University of Maryland
College Park, Maryland

I. Introduction

Recently a great deal of attention has been given to a general class of switching and gating devices based on the photoconductivity effect using picosecond optical pulses (Auston, 1975; Lee and Mathur, 1981; Mourou and Knox, 1979). The photoconductivity effect is the long-wavelength limit of a more general phenomenon in which the complex dielectric constant of the

* Present address: Naval Research Laboratory, Washington, D.C. 20375.

semiconducting medium is modified by the introduction of an optically induced electron-hole plasma. When the dimension of the plasma region is much smaller than the wavelength of the low-frequency (including dc) signals one wishes to control, the plasma region may be regarded as a lumped circuit element. If the wavelength of the rf signal is comparable to or smaller than the dimension of the plasma region, the plasma region must be treated as a distributed circuit element. This is the situation for millimeter-wave propagation in a semiconductor waveguide with a laser or electronically induced electron-hole plasma (Lee *et al.*, 1978, 1980). Here the induced plasma causes a change in both the refractive index and the extinction coefficient, resulting in phase shift and attenuation of the millimeter waves.

Millimeter waves span a frequency region from 30 to 300 GHz. Systems operating in this frequency region are attractive for several reasons. With respect to lower-frequency microwave systems, millimeter-wave devices have larger carrier bandwidths, better spatial resolution, and a more compact technology. Compared to optical systems, millimeter-wave devices offer better atmospheric propagation in selected bands and a technology more amenable to frequency multiplexing (Tomlinson, 1977; Kobayashi and Herui, 1978; Minowa *et al.*, 1979).

Phase shifting and modulation are fundamental control operations. The use of semiconductor bulk phenomena to construct microwave control components has been discussed (Mortenson *et al.*, 1971; Klein, 1983). The dielectric and conductive properties of the plasma state have been used to control millimeter waves (Klohn *et al.*, 1978; Paul and Chang, 1978). An approach to phase shifting used at both optical (Kaminow *et al.*, 1973) and microwave (Garver, 1976) frequencies is to alter the phase velocity along a fixed interval of a guiding medium. The phase shift per unit length is then equal to the change in propagation constant of the guided wave. One method of altering the dispersion of millimeter waves is to introduce an electron-hole plasma into the guiding medium. It has been demonstrated that phase shifts may be generated by injecting plasma with *p-i-n* diodes (Jacobs and Chrepta, 1974; Levin and Wiedener, 1973; Glance, 1979). Electronically induced plasmas have been used to control a semiconductor phase shifter (Novick *et al.*, 1982) and a line-scanning antenna (Horn *et al.*, 1982).

Another method of injecting a controlling electron-hole plasma into a semiconductor waveguide is to illuminate the waveguide with above-bandgap radiation (Lee *et al.*, 1978, 1980). Some of the advantages of optical control are near-perfect isolation between the controlled and controlling devices, low static and dynamic insertion losses in some regimes, fast response, and high power handling capability. IMPATT (Gerlach and Wellman, 1983) and TRAPATT (Kiehl, 1980) diodes have been controlled by optically injected electron-hole plasmas. Optically controlled phase shifters

(Lee *et al.*, 1980; Ogusu, 1983), modulators (Li *et al.*, 1982), and switches (Platte, 1981) have also been demonstrated.

Optically controlled semiconductor waveguides have also been used to generate short millimeter-wave pulses. Gated millimeter-wave pulses of 1- to 10-nsec duration were generated using a silicon waveguide illuminated by single pulses from a mode-locked Nd:YAG laser (Lee *et al.*, 1978). Modulated millimeter-wave pulses of approximately 400-psec duration and with a repetition rate in excess of 1 GHz were obtained using a Cr:GaAs waveguide illuminated by a pulse train from a mode-locked frequency-doubled Nd:YAG laser (Li *et al.*, 1982).

To design such devices more effectively, an understanding of the physical properties of the induced electron-hole plasma is necessary. One way to probe the behavior of an induced electron-hole plasma is to monitor the phase and loss of millimeter waves in a plasma-controlled semiconductor waveguide. This technique is capable of yielding information about the transport properties of plasmas over a range of plasma densities spanning five orders of magnitude.

This chapter analyzes in detail the changes that occur in the propagation characteristics of millimeter waves in an intrinsic semiconductor waveguide when a plasma-dominated region is present. The model and method of analysis are presented in Mak (1979). In that paper, both the experimental and theoretical studies concentrated primarily on the propagation of the dominant lowest-order mode (TM) denoted by $E^y_{1,1}$ for 94-GHz waves in a silicon waveguide. In practice, it has been found that, for waves propagating in an oversized waveguide with a plasma-covered region, the waves will not remain in the fundamental mode. Here the analysis will be extended to include higher-order TM modes $E^y_{p,q}$ and TE modes $E^x_{p,q}$. Calculations have also been carried out at frequencies other than 94 GHz.

Once plasma is injected into a bulk semiconductor waveguide via laser illumination, it begins to diffuse and recombine (Vaucher *et al.*, 1982). Thus, the steady-state model described above is not adequate to explain the variation of the phase and attenuation in the waveguide as a function of time. Since the period of the millimeter waves is much shorter than the characteristic time of such transport properties as diffusion and recombination, a quasi-steady-state model has been developed in which the depth and density of the plasma at any given time are determined by solution of the diffusion equation with appropriate boundary conditions, and the phase shift and attenuation are determined using these parameters as input (Yurek, 1984).

Two methods have been developed to measure the phase shift and attenuation in a semiconductor waveguide as a function of time: a null method and a dynamic bridge method. These methods are an improvement upon previous measurement techniques (Lee *et al.*, 1978, 1980; Mak, 1979) in

that the phase shift and attenuation may be measured simultaneously. For pulsed laser illumination that is repeatable from shot to shot, either the null method or the dynamic bridge method may be used to measure the propagation parameters in the waveguide as a function of time. This is the situation when the laser source is a pulsed GaAs diode laser (Vaucher *et al.*, 1982; Yurek, 1984). When the laser source is not repeatable from shot to shot—for example, a single pulse from a mode-locked frequency-doubled Nd:YAG laser—only the dynamic bridge method is useful for making measurements. Currently, both of these measurement techniques have time resolutions limited by that of the real time, which is about 2 nsec in most cases. This is not a fundamental limitation, however; for repeatable events, with the use of a sampling oscilloscope or a transient waveform analyzer, time resolution down to 30 psec is a possibility.

In Section II the experiments are described and the two measurement techniques are discussed. Section III is a discussion of the theoretical aspects of this work, including a steady-state analysis of the plasma-controlled semiconductor waveguide, an analysis of the spatial and temporal behavior of the optically induced plasma in the waveguide, and a description of the complete theoretical model to predict the relative phase and loss in the waveguide as a function of time after laser illumination. Experimental results are presented in Section IV and compared to the theoretical results of the previous section. Our conclusions are presented in Section V.

II. Description of the Measurement Techniques

The experiment consists of a millimeter-wave bridge with the semiconductor waveguide inserted in one arm (arm a) and a mechanical phase shifter and a mechanical attenuator in the other arm (arm b) (Jacobs and Chrepta, 1974). The bridge is initially (without laser illumination) balanced by adjusting the variable attenuator A and the phase shifter ϕ in arm b so that there is no signal at the output (see Fig. 1). After the null condition is found, an initial phase offset may be chosen if desired. When a pulse from either a mode-locked frequency-doubled Nd:YAG laser (0.53 μm) or a GaAs diode laser (0.9 μm) illuminates the silicon waveguide, an electron-hole plasma is generated at the surface, causing phase shift and attenuation of the millimeter-wave signal as it propagates through the plasma-covered region of the waveguide. The bridge becomes unbalanced and a signal appears at the output. This signal depends strongly upon the laser intensity, which determines how much plasma is generated, and upon the laser wavelength, which determines the initial plasma depth. It also depends upon the carrier transport dynamics, which determine the temporal variation of the signal. The transient signal that appears at the output of the bridge after the laser

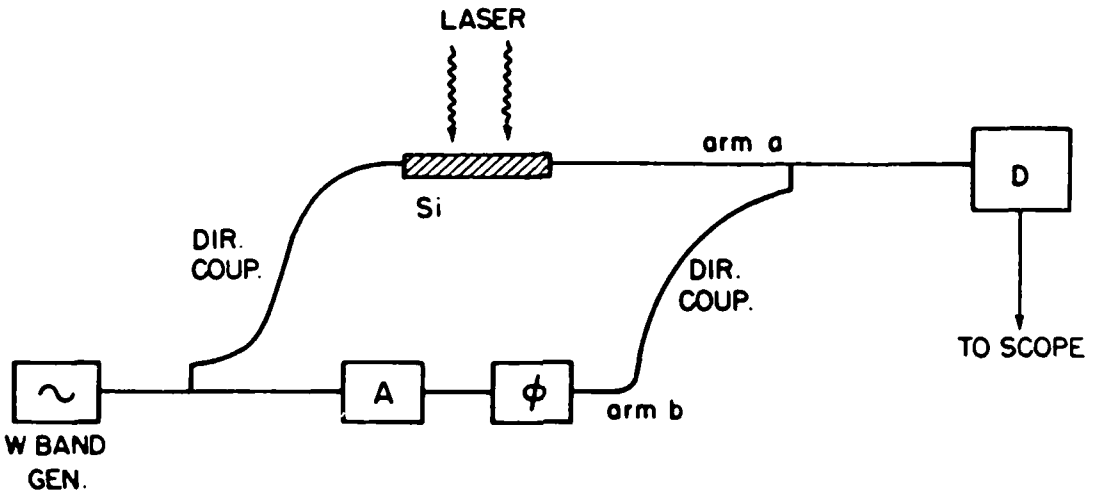

FIG. 1 Experimental arrangement to measure the dynamic evolution of the phase shift and attenuation in a silicon waveguide.

illumination of the semiconductor waveguide persists until the excess carriers recombine. One advantage of this experiment is that the millimeter waves may be used as a probe for relatively small plasma densities (10^{14}-10^{16} cm^{-3}), whereas optical probing techniques are not useful below plasma densities of $\sim 10^{18}$ cm^{-3}.

A. Comparison of the Laser Sources

The two laser sources used in these experiments are a pulsed GaAs diode laser and a mode-locked Nd: YAG laser. The GaAs diode laser is mounted in a box with its power supply and the laser light is emitted through a collimating lens in the side of the box. The pulse energy of the GaAs diode laser is 0.2 μJ, the absorption depth of the radiation is 28.57 μm in silicon, and the amount of plasma generated by a single pulse from this laser is 1.7×10^{16} cm^{-3}. The Nd: YAG laser consists of an oscillator cavity in which the light is both passively and actively mode locked (Kortz, 1983), a switch to extract a single pulse from the mode-locked pulse train, a double-pass Nd: YAG amplifier, and a temperature-tuned CDA frequency-doubling crystal. The frequency-doubled single pulse from the mode-locked Nd: YAG laser has an energy of 42 μJ, an absorption depth in silicon of 1 μm, and generates a plasma of density 5×10^{19} cm^{-3}. The amount of plasma generated by each laser is estimated by measuring the energy of a single pulse from each. In these measurements the reflection loss at the waveguide surface is taken into account. From the total laser energy and the photon energy of each laser, the total number of photons entering the waveguide can be calculated. Assuming a quantum efficiency of 1, each photon generates one electron-hole pair. The illuminated volume is assumed to be a rectangular

parallelepiped with dimensions of the width of the waveguide by the diameter of the laser spot by the absorption depth of the laser radiation. Thus the plasma density is the number of photons divided by the illuminated volume.

Each of the two laser sources has some experimental and theoretical advantages and disadvantages. The GaAs diode laser has a pulse repetition rate of 1 kHz and its laser emission is extremely reproducible in both total energy and temporal energy profile. The repetition rate and reproducibility of this laser make it possible to measure the phase shift and attenuation of the millimeter waves in the irradiated silicon waveguide by both a direct (null) method and an indirect (dynamic bridge) method. These two measurement techniques are discussed in Sections II.C and II.D, respectively. Because both methods could be applied to the case of GaAs diode laser illumination of the silicon waveguide, we were able to test the dynamic bridge method before applying it to the case of the nonreproducible low-repetition-rate Nd: YAG laser illumination. The relatively low energy of the pulsed GaAs diode laser makes it ideal for studies of the case in which the total plasma density injected into the semiconductor waveguide is small. The phase shift and attenuation caused by the GaAs diode laser-induced plasma could be calculated and fitted to the experimental data quite well. This case (small total plasma injection) is the one treated in the theory of Section III. One problem encountered with this laser is its relatively long pulse duration (~ 200 nsec), which caused theoretical problems because the actual laser pulse shape had to be taken into account when calculating the response of the silicon waveguide. Another problem with the GaAs diode laser is that even if the diffusion of the induced plasma is suppressed by some type of composite waveguide structure, the plasma density generated by this laser is not great enough to make the plasma layer sufficiently metallic to produce a large phase shift without large attenuation as well.

The mode-locked Nd: YAG laser has a repetition rate of 1 Hz and a pulse duration of 35 psec. The energy of the laser pulse and hence the density of the induced plasma vary from shot to shot, so that a direct technique such as the null method is not useful for measuring the response of the millimeter-wave system after illumination. The dynamic bridge technique, however, is useful in this case as long as the laser energy is monitored and laser shots are chosen within a narrow energy range. Illumination of the silicon waveguide with a frequency-doubled single pulse from the mode-locked Nd: YAG laser has the theoretical advantage that the duration of the laser pulse is instantaneous compared to the plasma diffusion and recombination mechanisms; the laser pulse may therefore be modeled as an impulse function.

Another advantage of plasma generation in silicon by frequency-doubled (0.53-μm) radiation from a Nd: YAG laser is that the absorption depth is small (1 μm), and the energy of each pulse is large enough so that the surface

plasma layer is metallic and large phase shifts are possible with relatively little attenuation. However, the initial plasma distribution is exponential in depth, and the attenuation measured is generally larger than that predicted theoretically because significant wave-plasma interaction occurs at plasma densities of 10^{15} cm^{-3}. This is to say that the plasma depth predicted theoretically is smaller than that actually encountered by the millimeter wave, and the plasma density predicted theoretically is larger than that encountered by the wave. Another problem with larger initial plasma densities is that fast recombination properties such as surface recombination and Auger recombination, which are not covered in the theory, may be important, causing the silicon waveguide to behave as though the total amount of optically injected plasma were less than expected.

B. The Null Method for Measuring the Relative Phase and Amplitude Response of a Plasma-Controlled Silicon Waveguide

In the experiment where the illumination source is a 900-nm pulsed GaAs diode laser with a repetition rate of 1 kHz, the detected signal from the output of the millimeter-wave bridge of Fig. 1 may be viewed using the sweep mode of a wide-bandwidth oscilloscope. The null method consists of first nulling the bridge without illumination of the silicon waveguide, using the mechanical attenuator and mechanical phase shifter in arm b and noting the initial phase and attenuation from their scales. When the laser is turned on, the 900-nm photons generate an electron-hole plasma in the silicon waveguide, causing phase shift and loss in the millimeter-wave signal as it passes through the plasma-controlled region. The change of phase and loss cause the bridge to become unbalanced, and a signal appears at the output. An oscillograph of the output signal is shown in Fig. 2. Because the signal is repeatable, it may be displayed continuously on the oscilloscope along with a trace of the laser pulse, which initializes the time scale of the experiment. The millimeter-wave signal may be nulled at any time after its initialization by adjusting the mechanical phase shifter and the mechanical attenuator in arm b of the bridge. By subtracting the initial phase and loss noted earlier, the relative phase shift and attenuation may be found. This technique is limited by the accuracy of the scales of the mechnical phase shifter (plus or minus a few degrees) and the mechanical attenuator (error is larger with larger losses). It is also limited by the fact that the null condition is determined by visual inspection of the millimeter-wave signal with respect to the oscilloscope baseline; this gives error in the measured relative phase and attenuation as well as error in the determination of the time response. An improvement to this technique would be to use a digital method of determining the null condition.

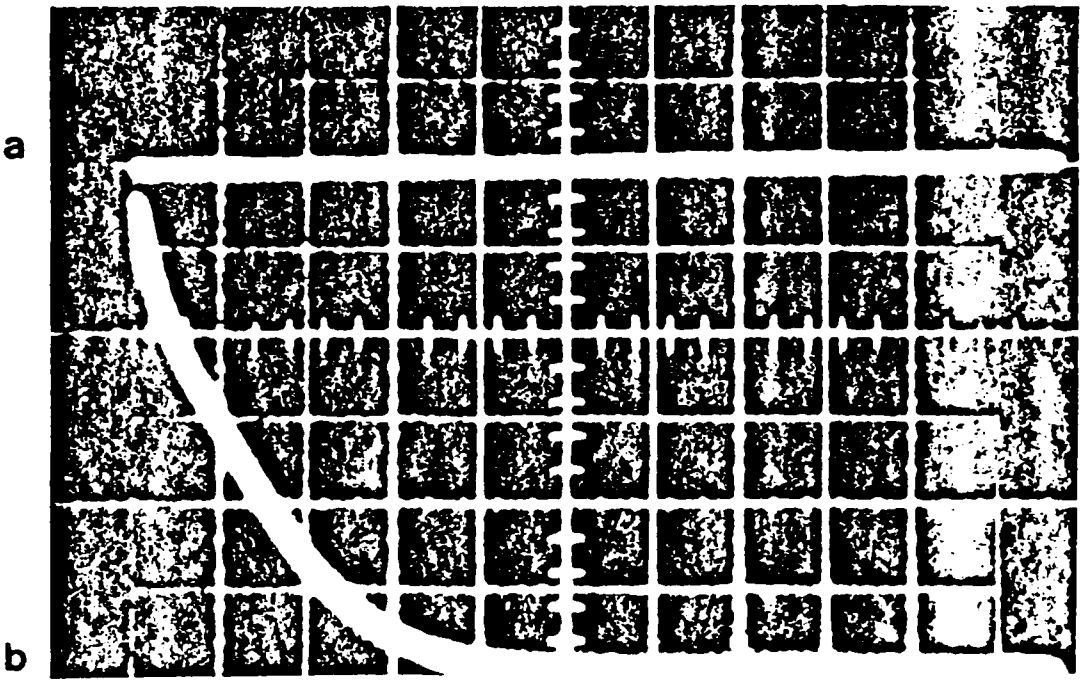

FIG. 2 Oscillograph of the output signal from the initially nulled millimeter-wave bridge after the silicon waveguide has been illuminated by a 200-nsec pulse of 900-nm light from a GaAs diode laser: (a) laser pulse, which appears as a line at this time scale, but is necessary as a trigger signal; (b) output signal from the millimeter-wave bridge. The sweep speed is 10 μsec/div.

C. THE DYNAMIC BRIDGE METHOD FOR MEASURING THE RELATIVE PHASE AND AMPLITUDE RESPONSE OF A PLASMA-CONTROLLED SILICON WAVEGUIDE

In the situation when the laser repetition rate is slow and the laser energy is not the same in every shot, the null method becomes impractical for measuring the change of phase and attenuation in the silicon waveguide after laser illumination. This is the problem encountered when a single pulse from a frequency-doubled Nd:YAG laser is used to generate the electron-hole plasma in the silicon waveguide. A dynamic bridge technique has been developed to determine the values of the laser-induced phase and attenuation (Li and Lee, 1983). This method exploits the fact that the temporal profile of the output of the bridge depends sensitively upon the initial phase angle between the electric fields in the two arms as well as the dynamics of the phase shift and attenuation due to the laser-induced electron-hole plasma. This method has a large dynamic range; it is possible to follow the decay of the plasma density over four orders of magnitude.

To understand the dynamic bridge method, first consider a phasor diagram consisting of two interfering phasors, representing the electric fields in the two arms of the bridge of Fig. 1. Let $\mathbf{E}_a$ represent the electric field in

arm a and $\mathbf{E}_b$ represent the electric field in arm b. The output of the bridge is proportional to the magnitude of the resultant phasor. Since the millimeter waves must propagate in single-mode metal waveguides, they may be considered to be linearly polarized in the same direction. When the bridge is balanced before laser illumination, $\mathbf{E}_a = -\mathbf{E}_b$ and the output is zero. This situation is depicted in Fig. 3. When the bridge is deliberately set to be unbalanced by an angle ϕ, the initial condition is no longer zero but some resultant field $\mathbf{E}_r$, as shown in Fig. 4. The magnitude of $\mathbf{E}_r$ may be calculated to be (assuming $\mathbf{E}_a = \mathbf{E}_b = 1$)

$$|\mathbf{E}_r| = 2\left|\sin\frac{\phi}{2}\right|. \tag{1}$$

If a bridge imbalance is caused by laser illumination, the imbalance angle ϕ varies in time as shown in Fig. 5 due to the buildup and decay of plasma. We will ignore attenuation in this part of the discussion. As ϕ due to the laser decreases, the phasor $\mathbf{E}_a$ rotates from its initial position OA along the circular arc ABCG to its equilibrium position OG. The resultant phasors describing the output of the bridge at different instants in time are given by GB, GC, and so on.

A more realistic situation is shown in Fig. 6. Here the signal in arm a of the bridge follows the trajectory outlined by the points 1-5 of the figure. The magnitude of $\mathbf{E}_a$ is indicated by the length of the vector $\mathbf{E}_a$ (dotted lines), and the phase change is the difference in angle from the initial condition. Figure 6 shows the variation of the resultant phasor $\mathbf{E}_r$ for two different initial phase

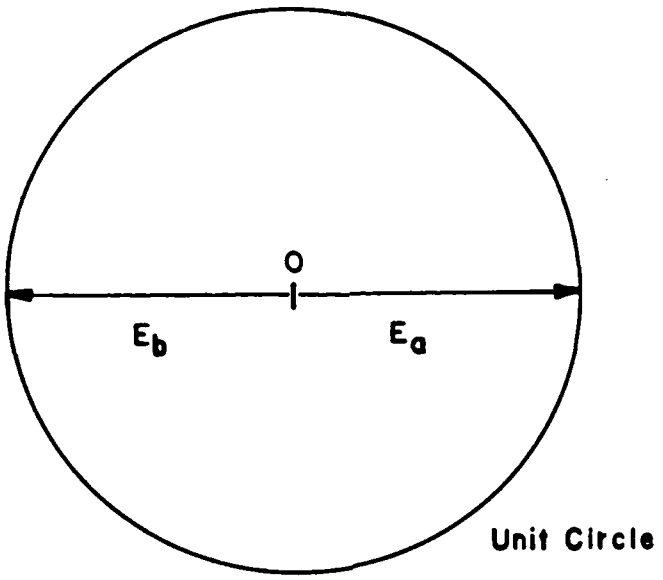

FIG. 3 Phasor diagram for the millimeter-wave bridge in the null condition. $\mathbf{E}_a$ represents the electric field in arm a of the bridge $\mathbf{E}_b$ represents the electric field in arm b of the bridge.

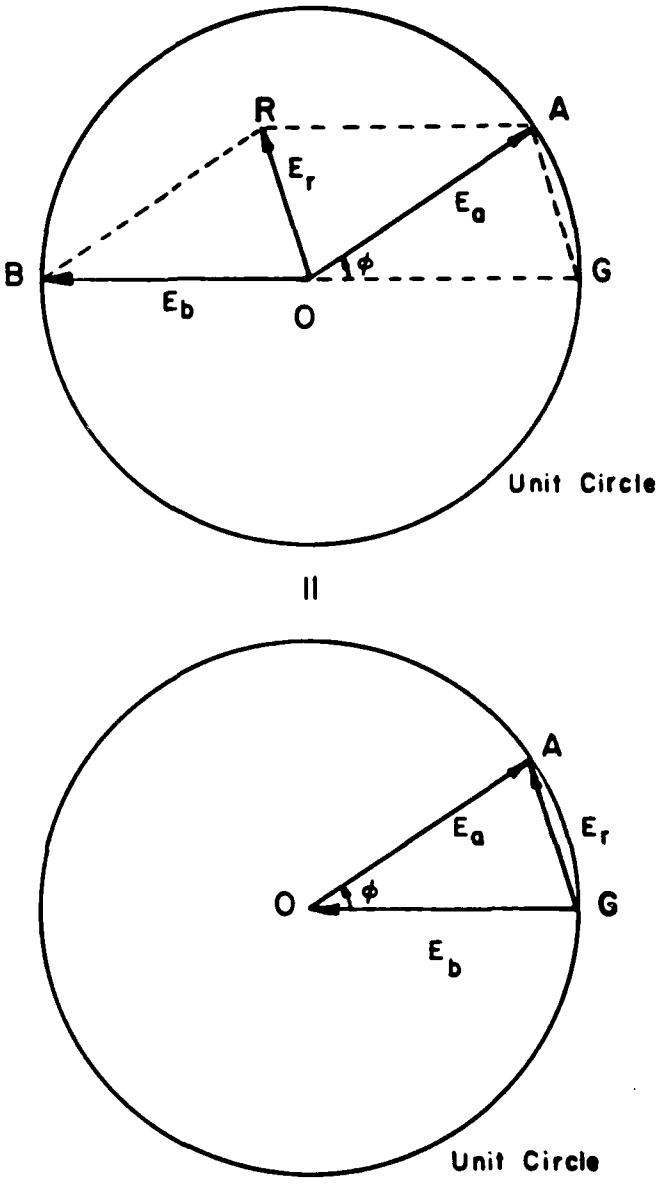

FIG. 4 Phasor diagram for the unbalanced bridge. A simple geometric construction is used to find the resultant phasor $\mathbf{E}_r$.

offsets: (a) shows an initial offset of 0° (the two arms adding) and (b) shows an initial offset of 90°. Note that the variation of $\mathbf{E}_a$ along the trajectory in time is the same for both cases. Also note that experimentally $\mathbf{E}_b$ is fixed, $\mathbf{E}_a$ varies, and $|\mathbf{E}_r|$ is the measurable quantity. If the two initial phase offsets are known, the variation of the magnitude of $\mathbf{E}_r$ may be found from the measured output of the bridge. Figure 7 shows the construction used to find the points of the trajectory taken by $\mathbf{E}_a$ as a function of time. The magnitudes of $\mathbf{E}_{r_0}$ and $\mathbf{E}_{r_{90}}$ are known at any given time after laser illumination. A circular arc is drawn centered at point A with a radius $\mathbf{E}_{r_0}$ and another circular arc is drawn

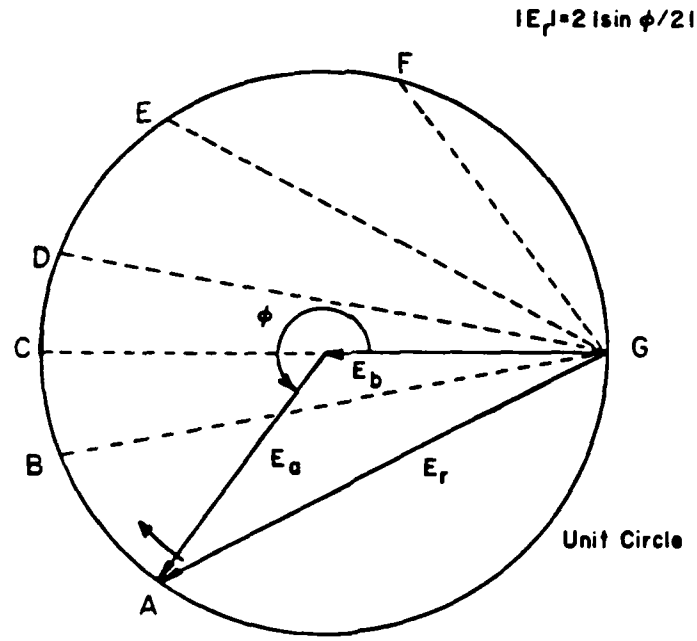

FIG. 5 Phasor diagram showing the variation of the resultant electric field $\mathbf{E}_r$ due to a "laser-induced" phase shift.

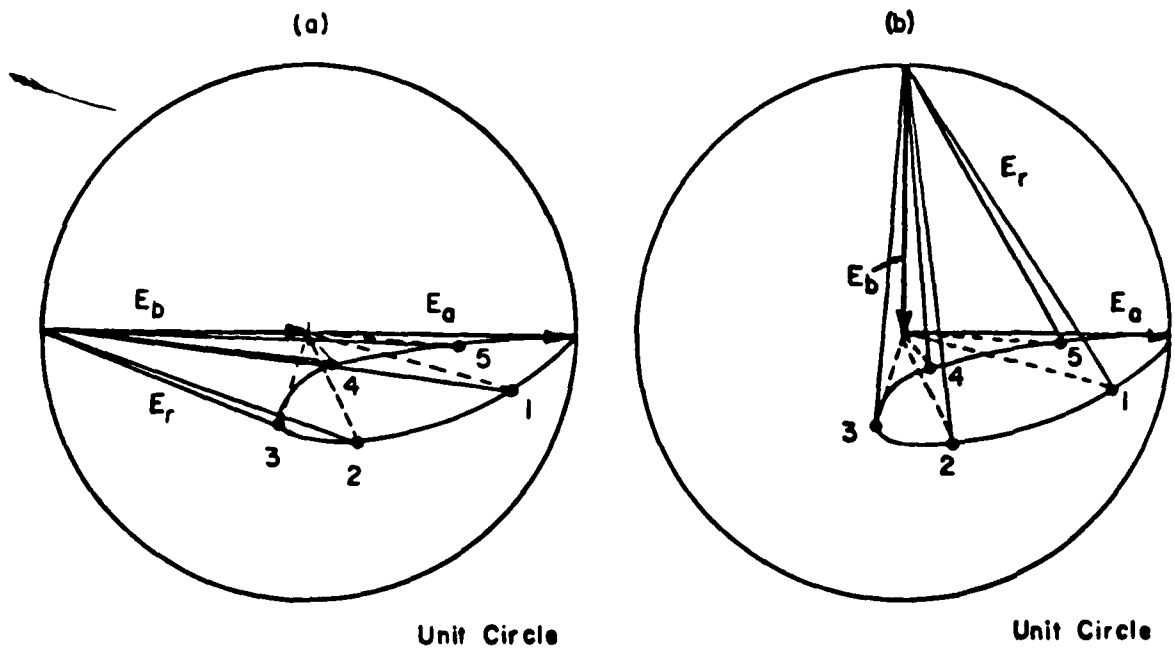

FIG. 6 Phasor diagram representing an actual variation of $\mathbf{E}_a$ and $\mathbf{E}_r$ for two different initial phase offsets: (a) initial offset of 0°; (b) initial offset of 90°.

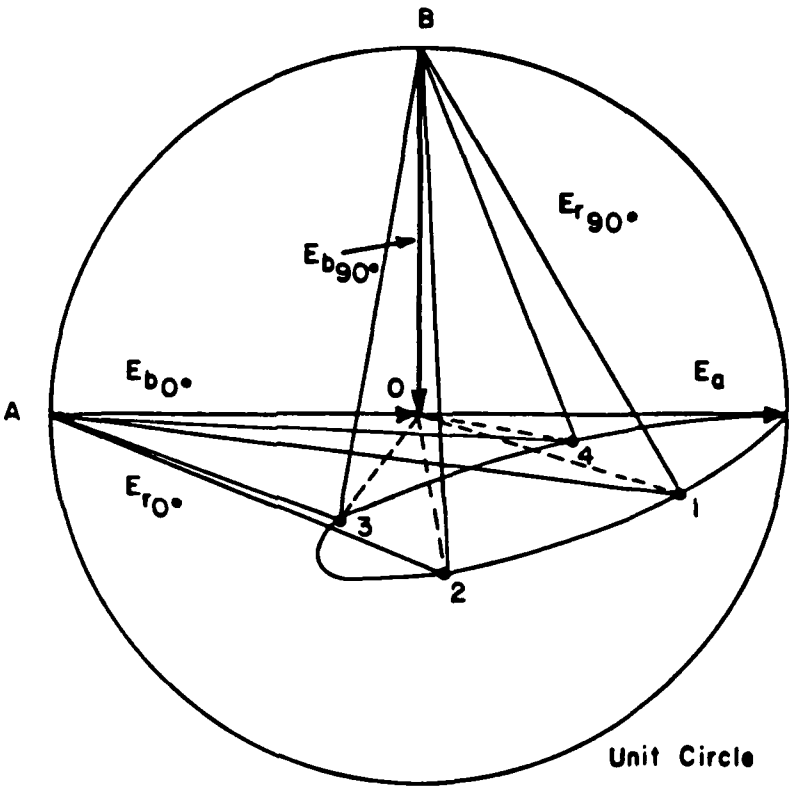

FIG. 7 Construction showing how the magnitude and phase of E_a may be found if the variation of E_r for two initial phase offsets, in this case 0° and 90°, is known.

centered at point B with a radius $E_{r90°}$. The intersection of these two arcs determines a point of the trajectory. The relative attenuation at any time is given by the distance from the corresponding point on the trajectory to the origin, and the relative phase is found in the same manner as in the case for which attenuation was ignored.

The dynamic bridge method is potentially capable of measuring the response of the millimeter-wave system at picosecond time scales. Currently the limitations on this method are due primarily to the response time of the oscilloscope (2.0 nsec).

III. Theoretical Model to Characterize Variations of Phase and Attenuation in Plasma-Controlled Semiconductor Waveguides

Shown in Fig. 8 is a schematic of the optically controllable phase shifter used in the experiments. It consists of a rectangular semiconductor waveguide with tapered ends to allow efficient transition of millimeter waves to and from a conventional metal waveguide. Optical control is realized when the broad wall of the semiconductor guide is illuminated by light generated by either a proximal source or one removed by a suitable optical guiding medium. In most cases, the width *a* and height *b* of the guide are selected so

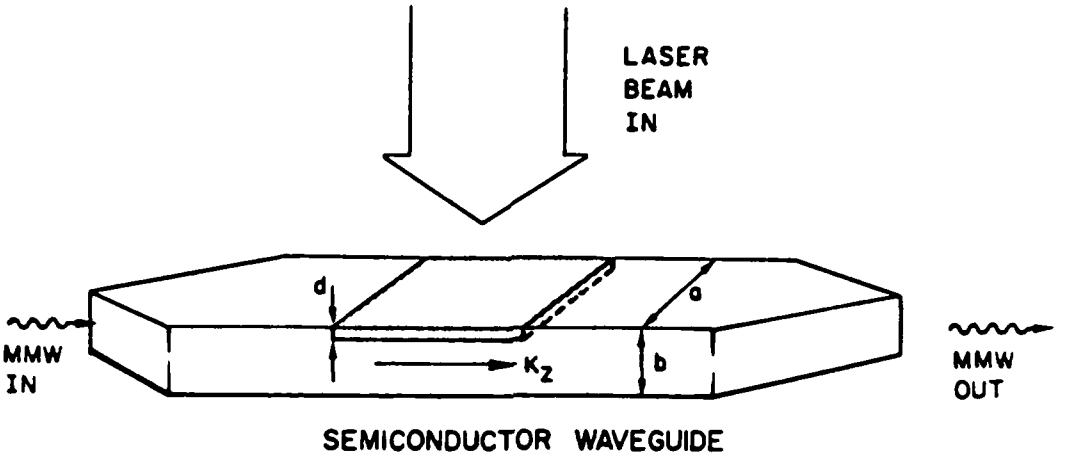

FIG. 8 Schematic diagram of the optically controlled phase shifter. The propagation constant in the guide is k_z, d_p is the depth of the injected plasma layer, a is the width of the guide, and b is the height of the guide.

that it supports only an $E^y_{1,1}$ mode. However, we have run experiments with larger guides that can support many modes. The initial depth of plasma injection is controlled by selecting an appropriate combination of optical radiation wavelength and semiconductor absorption properties. At sufficiently small injection depths, the thickness of the plasma is determined primarily by processes of carrier diffusion and recombination. The effect of the plasma-occupied volume is to introduce a layer whose index of refraction at the millimeter-wave frequency is larger than that of the remaining volume of the waveguide. As the optical illumination intensity increases from a low value, a significant phase shift will not appear until the plasma frequency exceeds the frequency of the guided millimeter wave, after which it will rapidly rise and eventually saturate. However, the form and magnitude of the phase shift versus the intensity of illumination, and hence the plasma density, depend on the material and geometric factors that characterize the optically perturbed guiding structure, and the determination of these quantities requires a detailed solution of the corresponding boundary value problems. The optically induced phase shift $\Delta\phi$ for a given section of waveguide of length l is determined by computing the propagation constant in the z direction, first in the absence of the injected plasma, k_z, and then with the plasma, k'_z; thus $\Delta\phi = (\mathrm{Re}\, k'_z - k_z)l$.

A. Steady-State Analysis of a Plasma-Controlled Semiconductor Waveguide; Phase Shift and Attenuation Due to a Given Plasma Region

The geometry of the rectangular semiconductor-plasma waveguide model is shown in Fig. 9. The guide cross section is in the x-y plane, and the z coordinate represents the direction of propagation. The dimensions of the

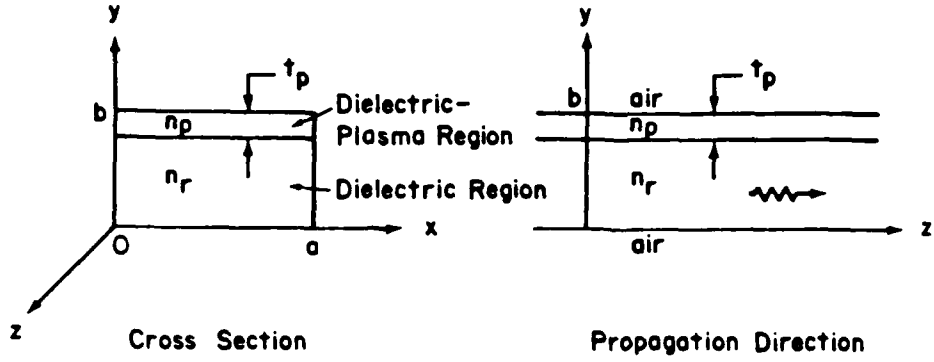

FIG. 9 Geometry of the semiconductor-waveguide model.

guide are denoted by a and b and the plasma region thickness by t_p. The medium surrounding the waveguide is air. The relative dielectric constant and refractive index of the dielectric region ($0 < y < b - t_p$) are ε_r and $n_r = \sqrt{\varepsilon_r}$, respectively, and those of the dielectric-plasma region ($b - t_p < y < b$) are (Lee *et al.*, 1980; Mak, 1979)

$$\varepsilon_p = n_p^2 = \varepsilon_r - \sum_\alpha \left(\frac{\omega_{p\alpha}^2}{\omega^2 + \nu_\alpha^2} \right) - j \sum_\alpha \left(\frac{\omega_{p\alpha}^2}{\omega^2 + \nu_\alpha^2} \frac{\nu_\alpha}{\omega} \right) \equiv (\eta - j\kappa)^2. \qquad (2)$$

The free-charge contribution (plasma) is characterized by a plasma frequency $\omega_{p\alpha} = (q_\alpha^2 N_\alpha / m_\alpha \varepsilon_0)^{1/2}$ of each species of density N_α and an effective collision frequency ν_α. These various species in an optically formed plasma are denoted by thermally ionized and photoinduced holes (light and heavy) and electrons. The values of the various species properties—that is, density, effective mass, and collision frequency—are given in Fig. 10a for Si and Fig. 10b for GaAs. In Fig. 10a, the real part η and imaginary part κ of the refractive index for Si [see Eq. (2)] are plotted as a function of plasma density for a 94-GHz wave (Sze, 1981). Likewise, in Fig. 10b the refractive index in the plasma-dielectric region for GaAs is plotted. At low plasma densities the two summations in Eq. (2) are small compared to ε_r, so in this regime $\eta \approx \sqrt{\varepsilon_r}$, κ is very small, and the plasma region may be considered a nearly perfect dielectric. At very large plasma densities the second summation in Eq. (2) dominates. Then η and κ are approximately equal and increase as $\sqrt{n}$, where n is the induced plasma density. In this regime the plasma-controlled region becomes metallic. The onset of metallic behavior begins at a plasma density of $\approx 10^{16}\,\text{cm}^{-3}$ for silicon and $\approx 10^{15}\,\text{cm}^{-3}$ for gallium arsenide. However, it should be noted that the relation (2) was derived neglecting collisions between electrons and holes; only collisions with the lattice were considered. Therefore, for very large plasma densities (above $10^{18}\,\text{cm}^{-3}$) Eq. (2) does not hold. In this density regime the electron and hole mobilities, and therefore the ν_α's, vary with plasma density.

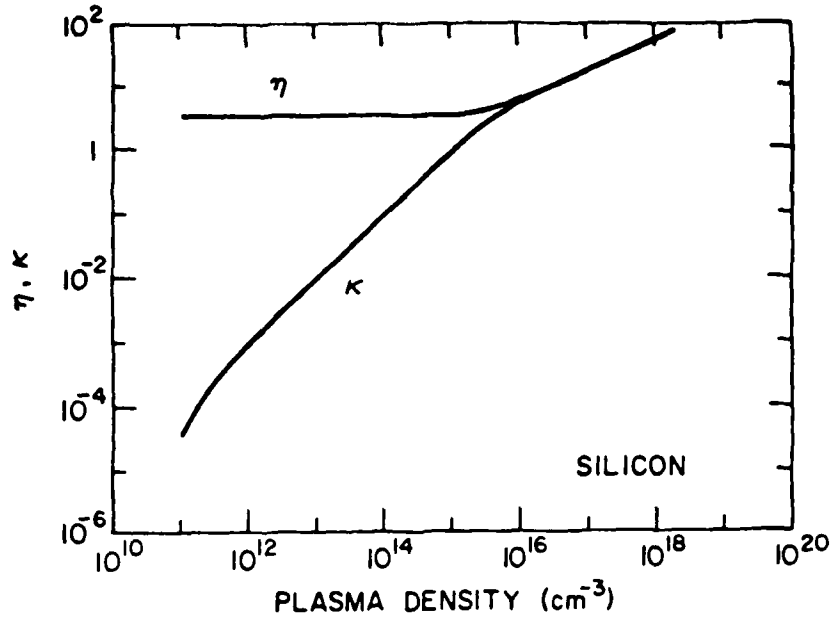

(a)

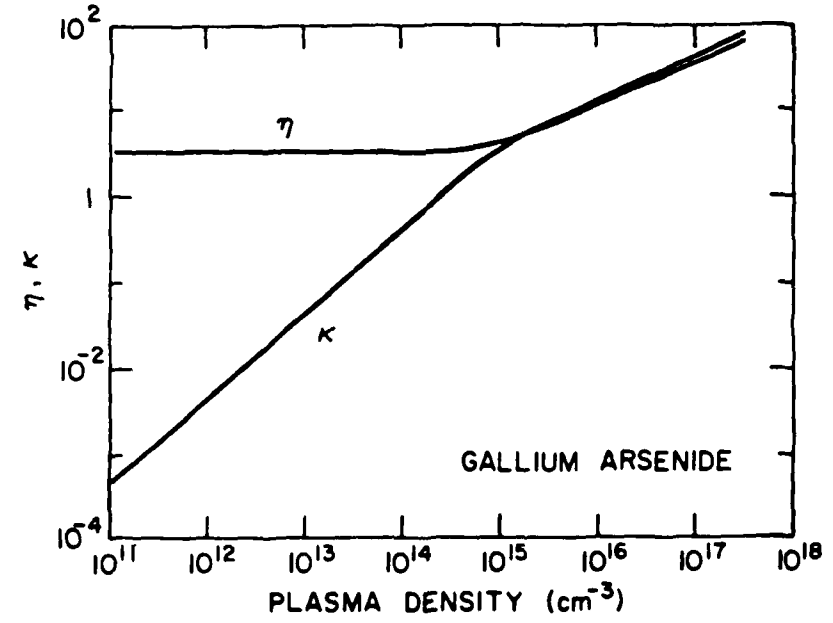

(b)

FIG. 10 (a) Plot of the plasma region refractive index versus plasma density in Si at 94 GHz. Here the relative concentration of light holes $P_L = 0.14N_p$, the relative concentration of heavy holes $P_H = 0.86N_p$, the electron effective mass $m_e^* = 0.259m_0$, the hole effective mass $m_p^* = 0.38m_0$, the light-hole effective mass $m_{P_L}^* = 0.16m_0$, the heavy-hole effective mass $m_{P_H}^* = 0.49m_0$, the electron mobility $\mu_e = 1300\ cm^2/V\ sec$, the electron collision time $\tau_e = 2.2 \times 10^{-13}$ sec, the hole mobility $\mu_h = 600\ cm^2/V\ sec$, the hole collision time $\tau_p = 1.3 \times 10^{-13}$ sec, and the background plasma density $N_{p0} = 10^{11}\ cm^{-3}$. (b) Plot of the plasma region refractive index versus plasma density in GaAs at 94 GHz. Here the relative concentration of light holes $P_L = 0$, the relative concentration of heavy holes $P_H = N_p$, the electron effective mass $m_e^* = 0.06m_0$, the hole effective mass $m_p^* = 0.5m_0$, the heavy-hole effective mass $m_{P_H} = 0.8m_0$, the electron mobility $\mu_e = 8800\ cm^2/V\ sec$, the electron collision time $\tau_e = 3.3 \times 10^{-13}$ sec, the hole mobility $\mu_h = 450\ cm^2/V\ sec$, the hole collision time $\tau_p = 1.28 \times 10^{-13}$ sec, and the background plasma density $N_{p0} = 1.4 \times 10^6\ cm^{-3}$.

For the case of well-guided modes, the analysis is considerably simplified in that the dispersion equation is essentially decoupled between the x and y directions (Marcatili, 1969). That is, if the fields in the dielectric are assumed to vary as $\exp[i(\omega t - k_x x - k_y y - k_z z)]$, we find that the boundary conditions in x determine k_x, those in y determine k_y, and from these one can then determine k_z. With these assumptions, the modes decouple into TM, called $E^y_{p,q}$, and TE, called $E^x_{p,q}$, modes. The propagation constant k_z is computed for the cases with and without the presence of the plasma region, k'_z (complex), k_z (real), respectively, and from these the plasma-induced phase shift $\Delta\phi$ for a given length of waveguide l can be computed by

$$\Delta\phi = (\mathrm{Re}\, k'_z - k_z)l \quad \text{radians} \tag{3}$$

and the attenuation coefficient by

$$\alpha = \mathrm{Im}\, k'_z \quad \mathrm{cm}^{-1}. \tag{4}$$

Specifically, in a waveguide of dimensions a and b and with *no plasma present*, $n_p = n_r(\omega_{pz} = 0)$, k_x and k_y for the $E^y_{p,q}$ mode are approximated by (Marcatili, 1969)

$$k_{x\mathrm{TM}} \approx \frac{p\pi}{a}\left[1 + \frac{1}{\pi a}\frac{\lambda_0}{\sqrt{\varepsilon_r - 1}}\right]^{-1} \tag{5}$$

and

$$k_{y\mathrm{TM}} \approx \frac{q\pi}{b}\left[1 + \frac{1}{\pi\varepsilon_r b}\frac{\lambda_0}{\sqrt{\varepsilon_r - 1}}\right]^{-1}. \tag{6}$$

Here p is the number of extrema in the x direction, q is the number of extrema in the y direction, and λ_0 is the free-space wavelength of the propagating wave. Similarly, for well-guided $E^x_{p,q}$ modes, k_x and k_y are approximated by (Marcatili, 1969)

$$k_{x\mathrm{TE}} \approx \frac{p\pi}{a}\left[1 + \frac{1}{\pi\varepsilon_r a}\frac{\lambda_0}{\sqrt{\varepsilon_r - 1}}\right]^{-1} \tag{7}$$

and

$$k_{y\mathrm{TE}} \approx \frac{q\pi}{b}\left[1 + \frac{1}{\pi b}\frac{\lambda_0}{\sqrt{\varepsilon_r - 1}}\right]^{-1}. \tag{8}$$

With these values of k_x and k_y, we can compute k_z in the guide without the plasma present:

$$k_z = (n_r^2\omega^2/c^2 - k_x^2 - k_y^2)^{1/2}, \tag{9}$$

where k_x and k_y are given by either their TM values [Eqs. (5) and (6)] or their TE values [Eqs. (7) and (8)].

Now consider the case when the *plasma layer is present*, as shown in Fig. 9. Again assuming that the decoupling due to well-guided modes is valid, we note that the solutions for k_x for the $E^y_{p,q}$ and $E^x_{p,q}$ modes are given by Eqs. (5) and (7). In the y direction, the solution for k_y for TM $E^y_{p,q}$ waves is found by solving (Lee *et al.*, 1980; Mak, 1979; Vaucher *et al.*, 1983)

$$\tan^{-1}\left(\frac{K_a\varepsilon_r}{k_r}\right) + \tan^{-1}\left\{\frac{k_p}{k_r}\frac{\varepsilon_r}{\varepsilon_p}\tan\left[\tan^{-1}\left(\frac{K_a\varepsilon_p}{k_p}\right) - k_p t_p\right]\right\} - k_r(b - t_p) + (q-1)\pi = 0 \tag{10}$$

and for TE ($E^x_{p,q}$) waves

$$\tan^{-1}\left[\frac{K_a}{k_r}\right] + \tan^{-1}\left\{\frac{k_p}{k_r}\tan\left[\tan^{-1}\left(\frac{K_a}{k_p}\right) - k_p t_p\right]\right\} - k_r(b - t_p) + (q-1)\pi = 0. \tag{11}$$

In Eqs. (10) and (11) we have defined the various k_y's in each region (Fig. 9) as

$$K_a = \frac{2\pi}{\lambda_0}(n_\omega^2 - 1)^{1/2},$$

$$k_r = \frac{2\pi}{\lambda_0}(n_r^2 - n_\omega^2)^{1/2}, \tag{12}$$

$$k_p = \frac{2\pi}{\lambda_0}(n_p^2 - n_\omega^2)^{1/2},$$

and n_ω is the refractive index of the wave in the decoupled guide. In the plasma layer, the index n_p is complex and depends upon the density of the plasma [see Eq. (2)]. Substituting the k_y's into Eqs. (10) and (11) results in transcendental equations for n_ω. These equations are solved numerically for n_ω, from which k_r is determined. The value of k_r is the value of k_y in the dielectric region in the presence of the plasma layer, and thus k_z' may be found by

$$k_z' = (n_r^2\omega^2/c^2 - k_x^2 - k_r^2)^{1/2}. \tag{13}$$

We can then compute the phase shift $\Delta\phi$ and attenuation α from Eqs. (3) and (4), using Eqs. (9) and (13).

In Lee *et al.* (1980) and Mak (1979), plots of phase shift and attenuation versus plasma density with plasma-region thickness as a parameter were shown for the lowest-order E^y mode; that is, $E^y_{1,1}$. The Si waveguide cross sections for those plots were 2.4 × 1.0 mm and 1.0 × 0.5 mm, and the plasma thickness was varied from 1 μm to half the guide depth. We have extended

this work to include the calculation of $\Delta\phi$ and α as a function of the plasma density for a rectangular Si wavelength of dimensions 2.4 × 1.0 mm for all $E^y_{p,q}$ and $E^x_{p,q}$ modes that can propagate with a plasma region thickness of 10 μm. The results of the calculations are shown in Fig. 11. In Fig. 11a, the phase shift per centimeter is plotted as a function of the plasma density for the $E^y_{1,1}$ through $E^y_{5,1}$ modes, which are the only $E^y_{p,1}$ modes that can propagate in this guide. The corresponding loss in decibels per centimeter is plotted in Fig. 11b. As the plasma density increases from 10^{15} cm^{-3} to 10^{20} cm^{-3}, the skin depth in Si decreases from more than 200 μm to less than 1 μm. When the skin depth is equal to or larger than the plasma layer thickness, the millimeter wave penetrates deeply into the plasma layer, causing loss. The maximum loss occurs when the skin depth is about equal to the layer thickness. The higher-order modes have more loss in this regime than the lower-order modes, because more of the wave power is concentrated in the plasma region when a higher-order mode is propagating in the guide. As the plasma density increases further, the skin depth decreases. When the skin depth is less than the thickness of the plasma layer, the plasma region begins to act as a metallic conductor and the dielectric waveguide becomes an image line. The attenuation then drops off rapidly with increasing plasma density. The maximum phase shift of the higher-order modes is also larger than that of the lower-order modes because the waveguide becomes more dispersive closer to cutoff. The other two TM modes this guide is capable of supporting at 94 GHz are the $E^y_{1,2}$ and $E^y_{2,2}$ modes, both of which are of higher order than the $E^y_{5,1}$ mode. The maximum phase shifts are 1000°/cm and 1450°/cm respectively.

Plots of the phase shift and attenuation curves for the TE modes $E^x_{1,1}$ through $E^x_{4,1}$ in the 2.4 × 1.0-mm guide at 94 GHz are shown in Fig. 12 for a 10-μm plasma layer. The results are similar to those found previously for the $E^y_{p,q}$ modes, except that the magnitude of the maximum phase shift is less and the maximum loss in the guide is less, reflecting the different field distribution requirements of the TE and TM modes.

The effect of varying the frequency of the millimeter waves in the 2.4 × 1.0-mm guide for a 10-μm plasma depth is to shift the attenuation peak and the onset of the phase shift. This is shown in Fig. 13a,b for the $E^y_{1,1}$ wave. This is to be expected since the skin depth is a decreasing function of frequency; therefore, the plasma density at which the greatest amount of interaction between the plasma and the wave occurs increases as the frequency is increased. Also, as the frequency is lowered, the maximum phase shifts and attenuations are larger. This is because the guide operates closer to cutoff at the lower frequencies. For a frequency of 50 GHz, only the mode shown, $E^y_{1,1}$, can propagate in the waveguide.

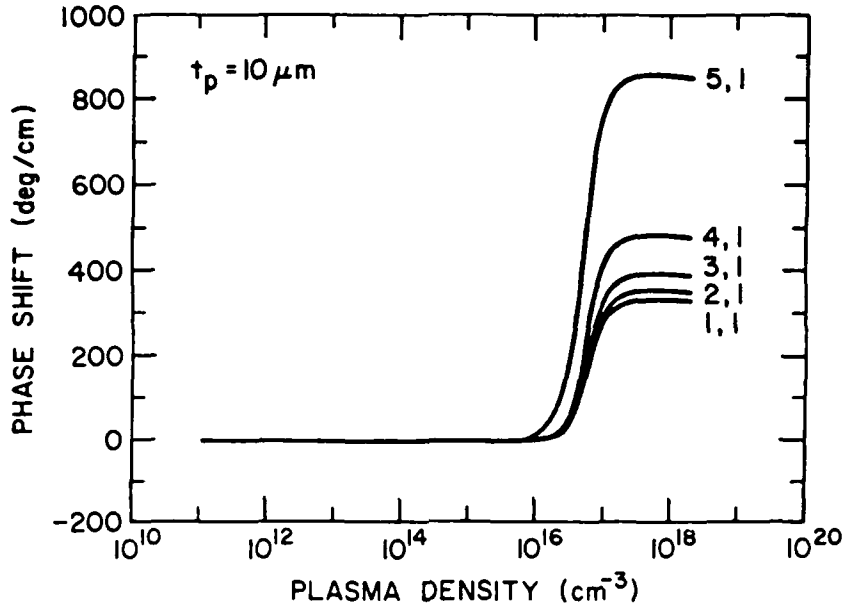

(a)

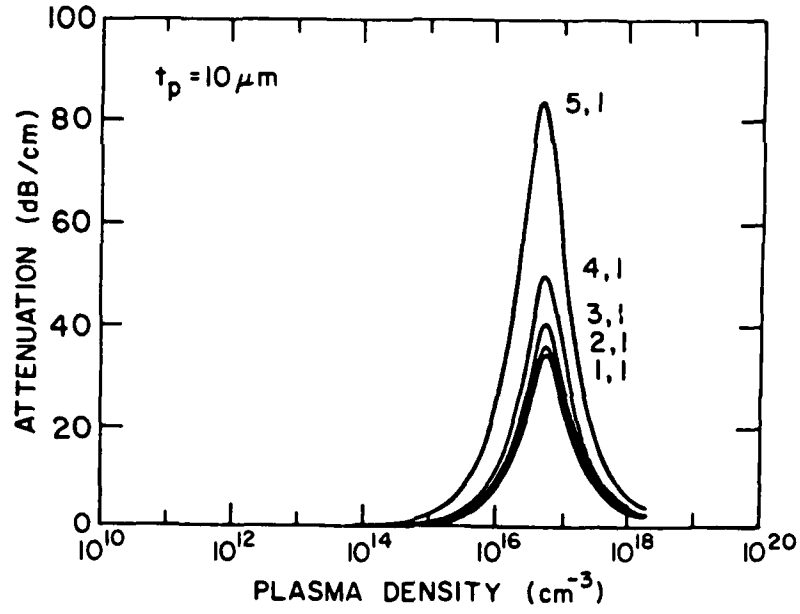

(b)

FIG. 11 (a) Phase shift properties in a 2.4 × 1.0-mm waveguide at 94 GHz with respect to plasma density for a plasma region thickness of 10 μm. Parametric dependence is the TM mode, $E^y_{p,q}$. (b) Attenuation properties in a 2.4 × 1.0-mm Si waveguide at 94 GHz with respect to plasma density for a plasma region thickness of 10 μm. Parametric dependence is the TM mode, $E^y_{p,q}$.

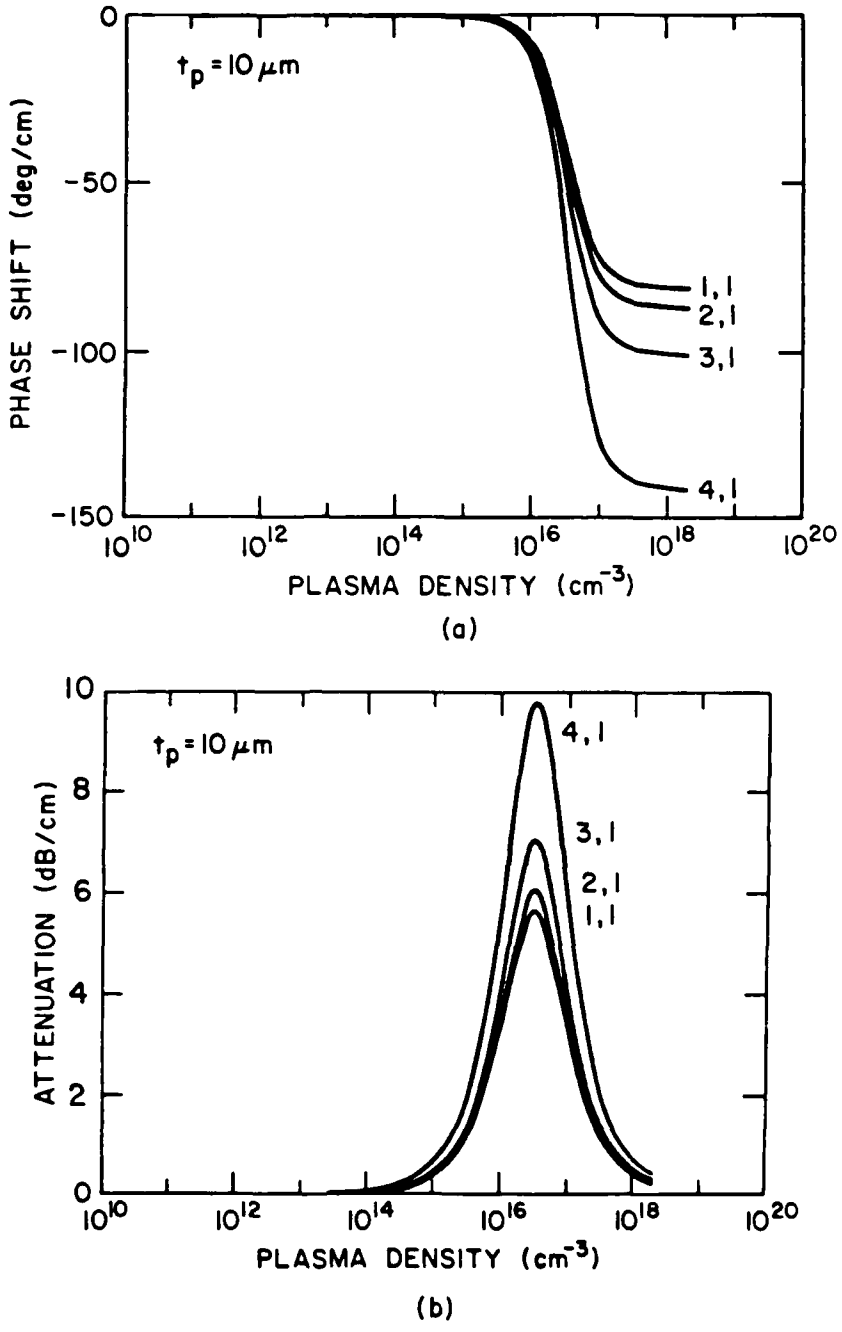

FIG. 12 (a) Phase shift properties in a 2.4 × 1.0-mm Si waveguide at 94 GHz with respect to plasma density for a plasma region thickness of 10 μm. Parametric dependence is the TE mode, $E^x_{p,q}$. (b) Attenuation properties in a 2.4 × 1.0-mm Si waveguide at 94 GHz with respect to plasma density for a plasma region thickness of 10 μm. Parametric dependence is the TE mode, $E^x_{p,q}$.

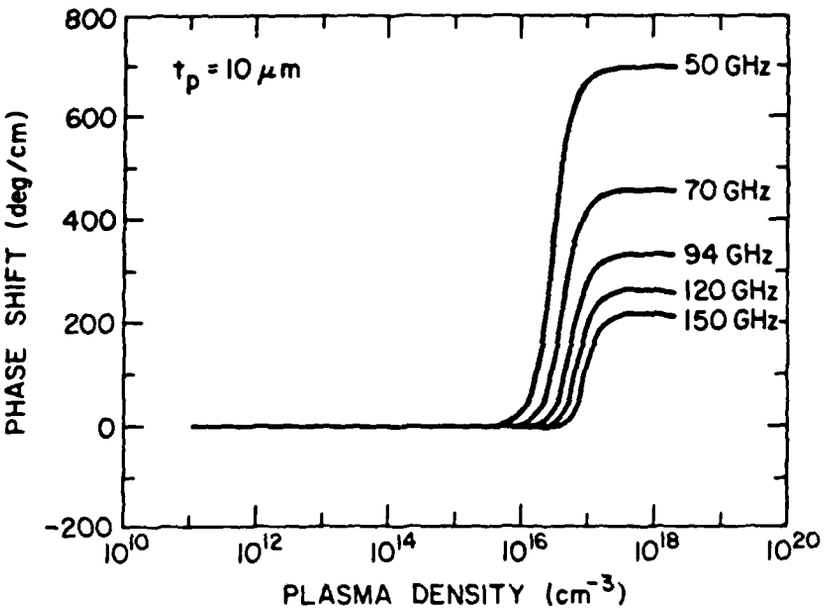

(a)

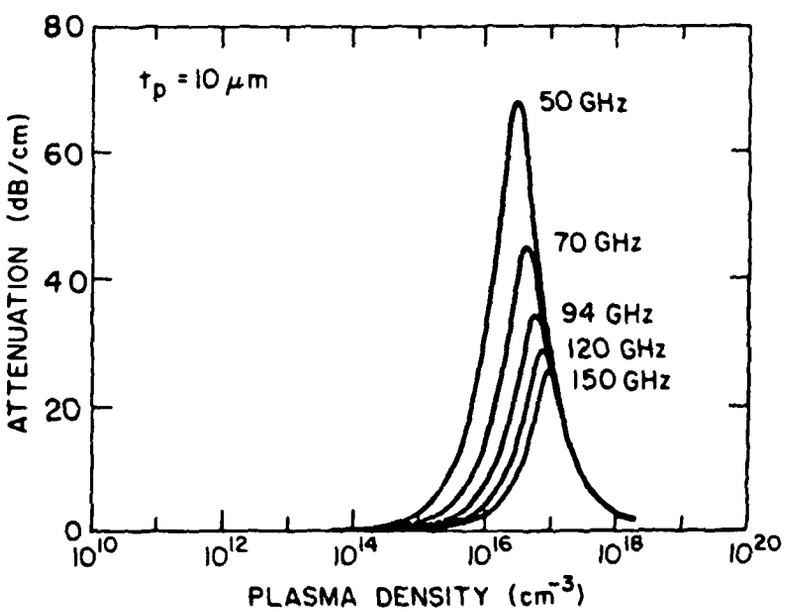

(b)

FIG. 13 (a) Phase shift properties in a 2.4 × 1.0-mm Si waveguide with respect to plasma density for a plasma region thickness of 10 μm and the lowest-order TM mode, $E^z_{1,1}$. Parametric dependence is the frequency of the millimeter wave. (b) Attenuation properties in a 2.4 × 1.0-mm Si waveguide with respect to plasma density for a plasma region thickness of 10 μm and the lowest-order TM mode, $E^z_{1,1}$. Parametric dependence is the frequency of the millimeter wave.

In Fig. 14 we have plotted the results for a 2.4 × 1.0-mm GaAs waveguide. Because the features with respect to multimode and frequency variation are similar to those presented for Si, we have displayed only the lowest-order TM mode, $E^y_{1,1}$, results at 94 GHz with plasma thickness as a parameter. For comparison, the Si guide results are displayed as solid curves. The general features of the GaAs curves are the same as those for Si; however, the curves are shifted toward lower plasma densities consistent with the shift in the dielectric properties of GaAs versus Si shown in Fig. 10.

B. Analysis of the Spatial and Temporal Behavior of an Optically Induced Electron–Hole Plasma in a Semiconductor Waveguide

When a semiconductor waveguide is illuminated with above-bandgap radiation, the initial depth and density of the optically induced plasma are determined by the energy of the radiation and its absorption properties in the semiconductor. At longer time scales, the behavior of the plasma depends primarily upon the processes of diffusion and recombination. These processes may be modeled by the diffusion equation in one dimension:

$$\frac{\partial \Delta N(x,t)}{\partial t} + \frac{\Delta N(x,t)}{\tau_r} - D_a \frac{\partial^2 \Delta N(x,t)}{\partial x^2} = G(x,t). \tag{14}$$

Here ΔN is the number of induced electron-hole pairs, τ_r the recombination time, D_a the ambipolar diffusion coefficient, and G the generation rate of the plasma. In our calculations we choose G to be a product of a function in x with a function in time:

$$G(x,t) = AS_1(x)S_2(t). \tag{15}$$

Equation (14) will be solved subject to the boundary conditions

$$\Delta N(\infty, t) = 0 \tag{16}$$

and

$$\left.\frac{\partial \Delta N}{\partial x}\right|_{x=0} = \frac{S}{D_a} \Delta N(0,t). \tag{17}$$

Here S is the surface recombination velocity. In silicon the surface recombination velocity is very small, ~300 cm/sec, and the processes of diffusion and bulk recombination are dominant; therefore, we will assume that $S = 0$ in the following analysis. We also have the initial condition

$$\Delta N(x,0) = 0. \tag{18}$$

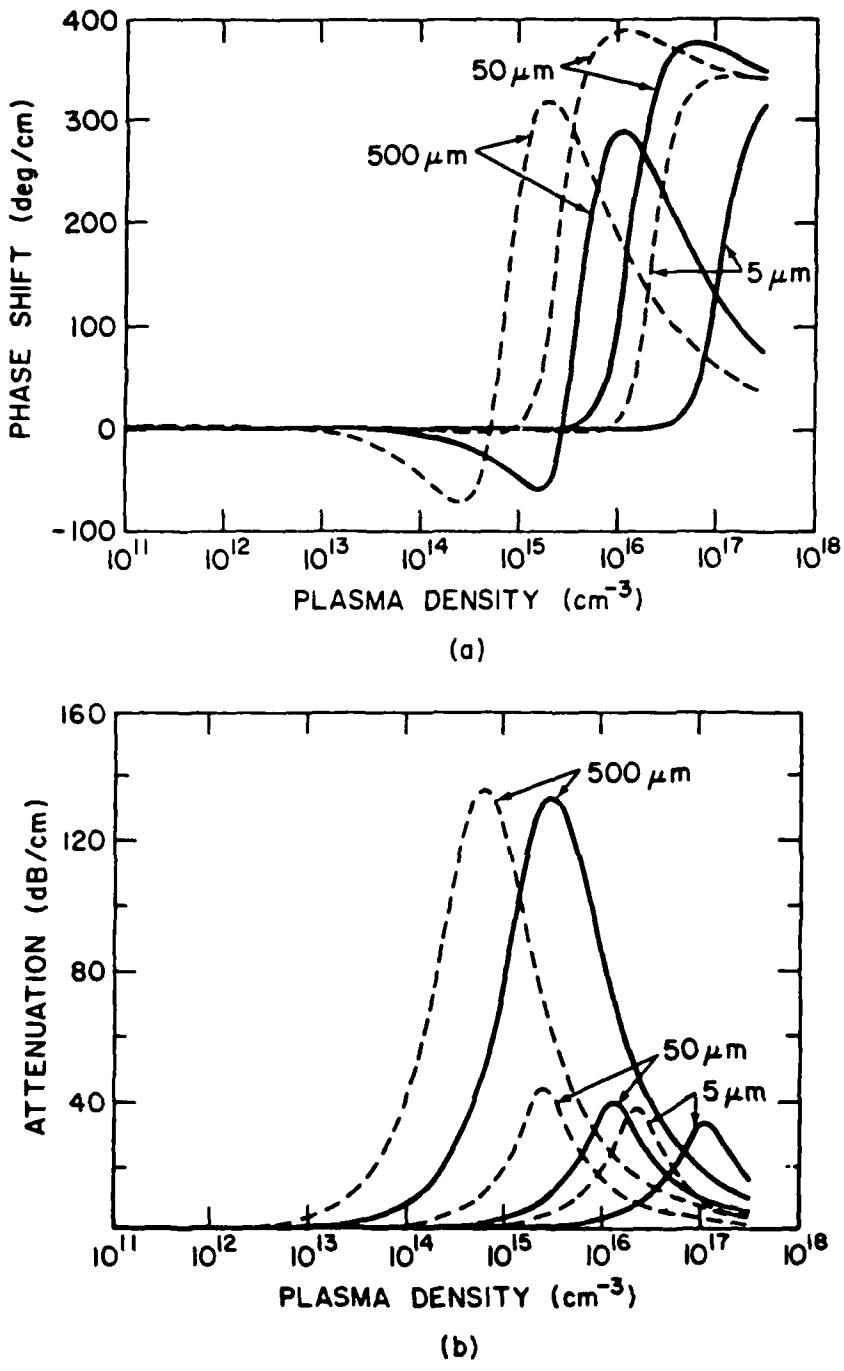

FIG. 14 (a) Comparison of the phase shift characteristics of an $E^y_{1,1}$ mode propagating at 94 GHz in a 2.4 × 1.0-mm waveguide for Si (——) and GaAs (---) plotted with respect to plasma density. The three sets of curves correspond to plasma depths of 500 μm, 50 μm, and 5 μm, respectively. (b) Comparison of the attenuation characteristics of an $E^y_{1,1}$ mode propagating at 94 GHz in a 2.4 × 1.0-mm waveguide for Si (——) and GaAs (---), plotted with respect to plasma density. The three sets of curves correspond to plasma depths of 500 μm, 50 μm, and 5 μm, respectively.

The diffusion equation (14) can be solved by the method of Laplace transform. Taking the Laplace transform of Eq. (14) gives

$$\frac{\partial^2 \mathbf{F}(x, p)}{\partial x^2} - \frac{p + 1/\tau_r}{D_a} \mathbf{F}(x, p) = -A \frac{\mathbf{S}_2(p) S_1(x)}{D_a}, \tag{19}$$

where $\mathbf{F}(x, p)$ is the Laplace transform of $\Delta N(x, t)$ and $\mathbf{S}_2(p)$ is the Laplace transform of $S_2(t)$.

If $S_1(x)$ is chosen to be $\delta(x - x')$, $\mathbf{F}(x, p)$ will become a Green's function $\mathbf{G}(x, x', p)$; or

$$\frac{\partial^2 \mathbf{G}(x, x', p)}{\partial x^2} - \gamma^2 \mathbf{G}(x, x', p) = \xi \delta(x - x'). \tag{20}$$

Here $\gamma^2 = (p + 1/\tau_r)/D_a$, $\xi = -A\mathbf{S}_2(p)/D_a$, and primed coordinates indicate the location of charges. The homogeneous solutions in the regions $0 < x < x'$ and $x > x'$ are

$$\mathbf{G}_1(x, x', p) = \alpha_1 e^{-\gamma(x - x')} + \beta_1 e^{\gamma(x - x')}, \qquad 0 < x < x', \tag{21}$$

$$\mathbf{G}_2(x, x', p) = \alpha_2 e^{-\gamma(x - x')}, \qquad x > x', \tag{22}$$

where boundary condition (16) has been applied to the region $x > x'$. Applying the boundary condition (17) and continuity between the regions gives

$$\mathbf{G}_1(x, x', p) = \frac{-\xi}{\gamma} e^{-\gamma x'} \cosh \gamma x, \qquad 0 < x < x', \tag{23}$$

$$\mathbf{G}_2(x, x', p) = \frac{-\xi}{\gamma} e^{-\gamma x} \cosh \gamma x', \qquad x > x'. \tag{24}$$

Now note that

$$\nabla^2 \mathbf{G}(x, x', p) = \frac{\partial^2 \mathbf{G}(x, x', p)}{\partial x^2} = \eta^2 \mathbf{G}(x, x', p) + \xi \delta(x - x') \tag{25}$$

and

$$\nabla^2 \mathbf{F}(x, p) = \frac{\partial^2 \mathbf{F}(x, p)}{\partial x^2} = \eta^2 \mathbf{F}(x, p) + \xi S_1(x'), \tag{26}$$

and also that Green's theorem number 2 is

$$\int_{\text{volume}} (\mathbf{F} \nabla^2 \mathbf{G} - \mathbf{G} \nabla^2 \mathbf{F}) \, dV' = \int_{\text{surface}} (\mathbf{F} \nabla \mathbf{G} - \mathbf{G} \nabla \mathbf{F}) \cdot d\mathbf{S}'. \tag{27}$$

The right-hand side of Eq. (27) is zero because at $x = 0$, $\nabla\mathbf{G} = \nabla\mathbf{F} = \partial\mathbf{G}/\partial x = \partial\mathbf{F}/\partial x = 0$ by boundary condition (17). Substituting **F** and **G** into Eq. (27) gives

$$\int \mathbf{F}(x', p)\xi\, \delta(x - x')\, dx' = \int \xi\mathbf{G}(x, x', p)S_1(x')\, dx'$$

or

$$\mathbf{F}(x, p) = \int \mathbf{G}(x, x', p)S_1(x')\, dx'. \tag{28}$$

In this work, two different computations were carried out, assuming two different initial carrier profiles $S_1(x')$. One of these was a "rectangular" variation of the plasma density with depth, and the other was an exponential variation of plasma density with depth (Fig. 15). Using Eq. (28), $\mathbf{F}(x, p)$ for the case of a rectangular initial variation of the plasma density with depth is found to be

$$\mathbf{F}(x, p) = -(\xi/2\gamma^2)[2 - e^{-\gamma(x_0 + x)} - e^{-\gamma(x_0 - x)}], \tag{29}$$

and for an exponential initial variation of the plasma density with depth, $\mathbf{F}(x, p)$ is found to be

$$\mathbf{F}(x, p) = \frac{-\xi}{\gamma}\frac{1}{\gamma^2 - 1/x_0^2}\left[\gamma e^{-x/x_0} - \frac{1}{x_0}e^{-\gamma x}\right]. \tag{30}$$

If, in Eqs. (29) and (30), the constants η and ξ are replaced by their values $\eta^2 = (p + 1/\tau_r)/D_a$ and $\xi = -A\mathbf{S}_2(p)/D_a$, both Eq. (29) and Eq. (30) become

$$\mathbf{F}(x, p) = \mathbf{S}_2(p)\mathbf{f}(p, x), \tag{31}$$

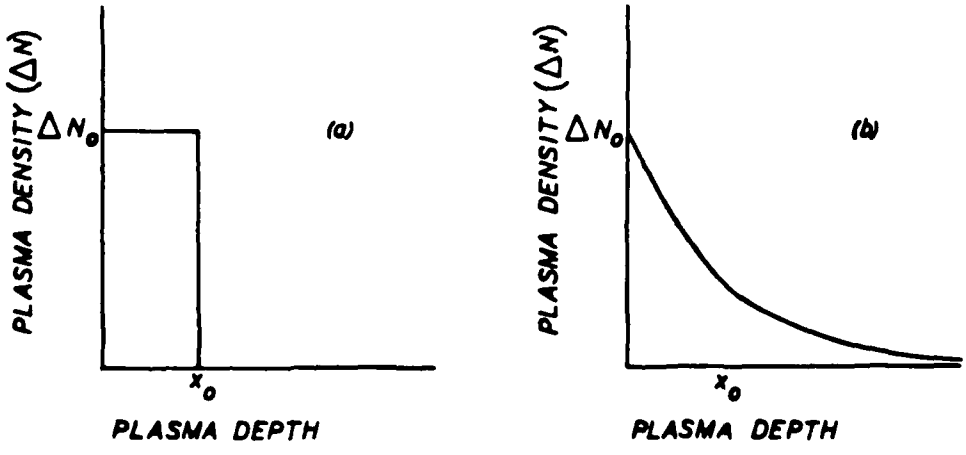

FIG. 15 Plots of the initial carrier profiles used in this work: (a) "rectangular" carrier profile; (b) exponential profile.

where $\mathbf{f}(p, x)$ is different in the two cases. Now a product in the transform (p) space is the same as convolution in time. Therefore

$$\Delta N(x, t) = \mathbf{L}^{-1}[\mathbf{F}(x, p)] = \int_0^t S_2(\tau) f(t - \tau, x)\, d\tau. \tag{32}$$

Here $S_2(\tau) = \mathbf{L}^{-1}[\mathbf{S}_2(p)]$ and $f(t - \tau, x) = \mathbf{L}^{-1}[\mathbf{f}(p, x)]$. If $S_2(\tau)$ is a δ function, then $\Delta N(x, t)$ is equal to $\mathbf{L}^{-1}[\mathbf{f}(x, p)]$ and is simply the impulse response of the system. For more complicated $S_2(\tau)$'s, the integration (32) may be performed analytically (if possible) or numerically. The impulse responses for the two cases are

$$f(x, t) = \frac{N_0}{2} e^{(-t/\tau_r)} \left[\operatorname{erf}\left(\frac{x + x_0}{2\sqrt{D_a t}} \right) + \operatorname{erf}\left(\frac{x_0 - x}{2\sqrt{D_a t}} \right) \right] \tag{33}$$

for the case of rectangular initial variation of the plasma density in x and

$$f(x, t) = \frac{N_0}{2} \exp\left(-\frac{x}{x_0} + \frac{D_a t}{x_0^2} - \frac{t}{\tau_r} \right) \left[1 + \operatorname{erf}\left(\frac{x}{2\sqrt{D_a t}} - \frac{\sqrt{D_a t}}{x_0} \right) \right]$$
$$+ \frac{N_0}{2} \exp\left(\frac{x}{x_0} + \frac{D_a t}{x_0^2} - \frac{t}{\tau_r} \right) \left[1 - \operatorname{erf}\left(\frac{x}{2\sqrt{D_a t}} + \frac{\sqrt{D_a t}}{x_0} \right) \right] \tag{34}$$

for the case of exponential initial variation of the plasma density in x. By convolving the impulse response with the temporal profile of the laser pulse, the plasma density at any given depth at any given time may be computed.

The results of two representative calculations are shown in Figs. 16 and 17. In Fig. 16 the initial plasma depth is chosen to be rectangular with a depth (x_0) of 1 μm. The temporal profile of the laser illumination is chosen to be a δ function. The recombination time and diffusion coefficient are $\tau_r = 20$ μsec and $D_a = 17.93$ cm^2/sec, respectively (Sze, 1981). The plots show the density of plasma with respect to penetration depth at various times after the δ-function illumination pulse. In Fig. 17 the initial plasma distribution is chosen to be exponential with a characteristic length $x_0 = 28.57$ μm. The temporal profile is that of an actual GaAs laser pulse and is depicted schematically in the figure. Once again the plots show the density of plasma with respect to penetration depth at various times during and after the onset of the illumination pulse. In both figures the initial plasma density N_0 was chosen after taking into consideration the actual energies of the two lasers used in the experiments. Figure 16 shows the approximate behavior of the plasma after the waveguide is illuminated with a single pulse from a frequency-doubled mode-locked Nd:YAG laser. In this computation, the duration of the laser pulse was taken to be a delta function and the induced electron-hole plasma was therefore assumed to be generated instantaneously.

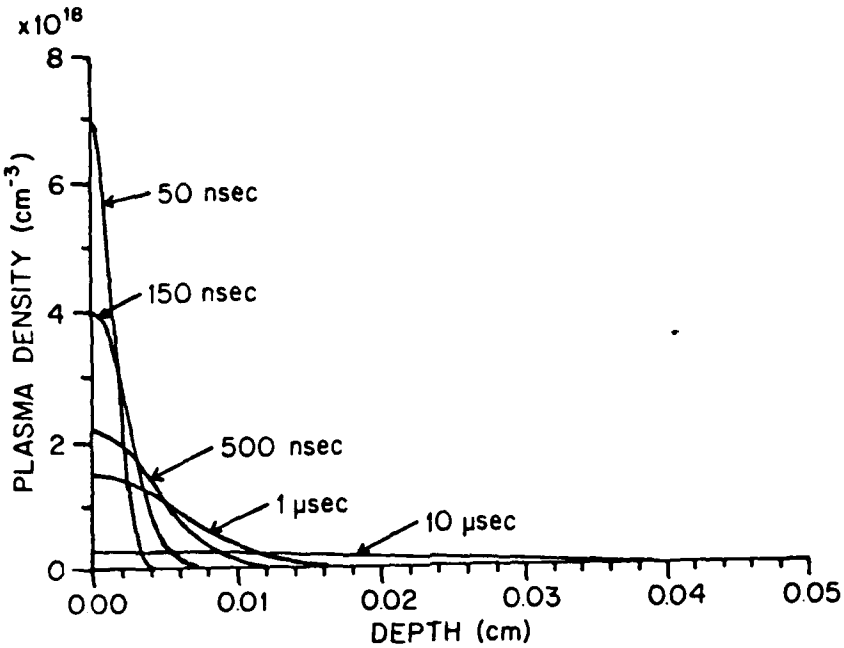

FIG. 16 Plots of the plasma density versus depth in Si, with time as a parameter. The initial plasma distribution is chosen to be "rectangular," of depth $x_0 = 1\ \mu m$, and the temporal distribution of the illumination is taken to be a delta function.

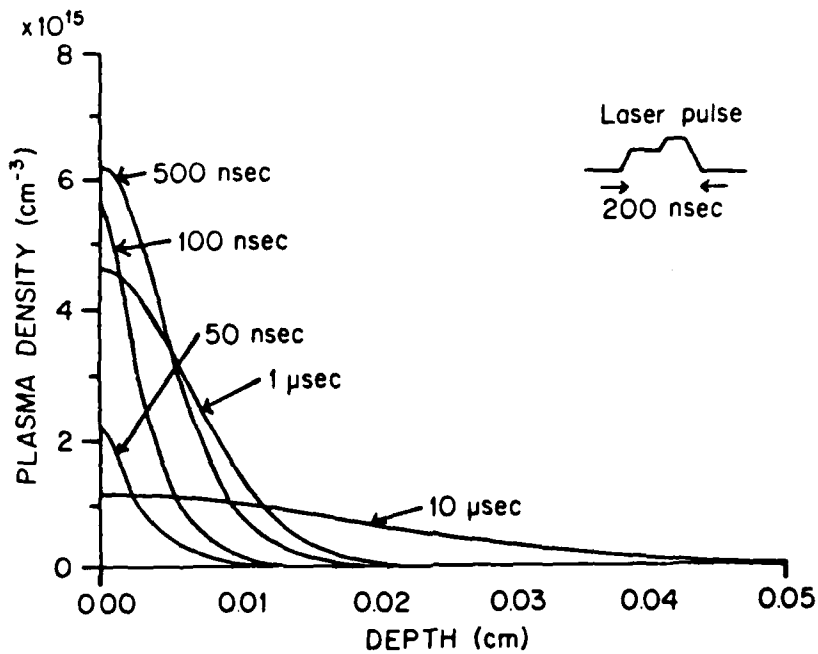

FIG. 17 Plots of the plasma density versus depth in Si, with time as a parameter. The initial distribution is chosen to be exponential, of characteristic length 28.57 μm, and the temporal distribution of the illumination is taken to be the shape of an actual GaAs laser pulse.

This is justified because the duration of the actual laser pulse (≈ 35 psec) is much shorter than the characteristic times of the physical processes that occur after the plasma is generated. The spatial characteristic was arbitrarily taken to be rectangular with an initial depth of 1 μm corresponding to the absorption depth of 530-nm light silicon. From the plots in Fig. 16, it can be seen that at a time of 50 nsec after the laser pulse the plasma has diffused substantially from its initial depth of 1 μm. At longer times the plasma continues to diffuse until it is nearly uniform across the depth of the waveguide. It also recombines in a time assumed here to be 10 μsec. Figure 17 depicts the approximate behavior of the plasma after the waveguide is illuminated with a single pulse from a GaAs diode laser. Here the pulse shape is assumed to correspond closely to the measured shape of the laser intensity. The diffusion and recombination characteristics of the induced electron-hole plasma are determined by the convolution of the impulse response of an exponential initial spatial distribution of the plasma with the actual laser pulse shape. The $1/e$ point of the initial exponential plasma distribution is determined from the initial absorption depth of 900-nm light in silicon, 28.57 μm. At early times the plasma distribution is nearly exponential; as the plasma diffuses, the shape of the plasma density with respect to depth becomes more nearly Gaussian. The plasma density increases until the end of the laser pulse, after which the plasma diffuses and recombines. As in the previous figure, the recombination time here was taken to be 10 μsec.

C. Complete Theoretical Model to Predict the Phase Shift and Attenuation in the Semiconductor Waveguide

The variation of the phase and loss in the semiconductor waveguide may be predicted as a function of time using a quasi-steady-state model that is a combination of the calculations of Sections III.A and III.B. Because the period of the millimeter waves is much shorter than the characteristic times of such transport properties as diffusion and recombination, a quasi-steady-state approach is justified. For a given set of initial conditions (the laser pulse shape and the initial absorption profile of the laser light in the semiconductor) and assuming a quantum efficiency of 1, the plasma depth and density may be determined as functions of time using the method outlined in Section III.B. However, the calculation of Section III.A requires a constant plasma depth and a constant plasma density. So, using the method of Section III.B, the plasma density is calculated as a function of depth at a given time. The plasma depth t_p is chosen as the place where $\Delta N = e^{-1}\Delta N|_{x=0}$, and the plasma density DIF is chosen to be $\Delta N|_{t_p/2}$ (see Fig. 18). Then the phase shift and attenuation are calculated for that particular time using the plasma depth and density chosen as above. These steps are repeated to determine the

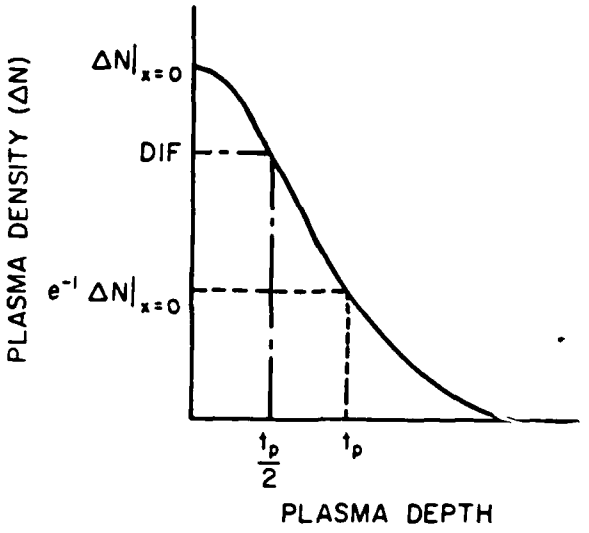

FIG. 18 Illustration of the method used to estimate a constant plasma depth and density from the plasma density profile at a given time after the onset of laser illumination. The plasma depth t_p is chosen as the place where $\Delta N = e^{-1}\Delta N|_{z=0}$ and the plasma density is chosen to be $\Delta N|_{t_p/2}$.

phase shift and attenuation at any desired time after the onset of the laser illumination.

IV. Experimental Results

The variation of the phase and attenuation in a silicon waveguide after plasma generation is measured for the cases of pulsed GaAs diode laser illumination and frequency-doubled single-pulse illumination from a mode-locked Nd:YAG laser. In the case of GaAs diode laser illumination, both the null method (Section II.B) and the dynamic bridge method (Section II.C) were used so that a comparison of these two techniques could be made. In the case of frequency-doubled single-pulse Nd:YAG illumination, only the dynamic bridge technique was applicable. This section discusses first the GaAs diode laser experiments, then the frequency-doubled single-pulse Nd:YAG laser experiments.

A. GaAs Diode Laser Experiments

Using the experimental setup of Fig. 1, the phase and amplitude response of the millimeter-wave system to illumination by a GaAs diode laser was observed. The 900-nm GaAs diode laser illumination was focused to a 1.0-mm-diameter spot on the surface of the silicon waveguide in arm a of the millimeter-wave bridge. The size of the spot was measured by placing a scale on top of the silicon waveguide and observing the laser spot through an infrared viewer. Measurements of the temporal variation of the phase and

loss in the waveguide were measured by both the null method and the dynamic bridge method. In the dynamic bridge measurements, a second calibrated attenuator was placed after the bridge to keep the output signal within the range of the detector calibration at the various phase offsets.

A comparison of the theoretical model and the experimental results is shown in Fig. 19. In the density range of interest the ambipolar diffusion coefficient could be taken to be a constant, $D_a = 17.93\ \text{cm}^2/\text{sec}$. However, because this technique simultaneously measures two quantities, phase and loss, the variation of the plasma density and of the mobility may also be determined simultaneously with respect to time. To calculate the theoretical phase and loss both the real and imaginary parts of the complex permittivity of the plasma,

$$\varepsilon_r = \varepsilon_L - \frac{\omega_p^2}{\omega^2 + \nu^2} - j\frac{\nu}{\omega}\frac{\omega_p^2}{\omega^2 + \nu^2}, \tag{35}$$

must be included. Here ε_L is the permittivity of the host lattice including the contribution from bound charges, ν the collision frequency, and ω_p the plasma frequency, which is given by

$$\omega_p = ne^2/\varepsilon_0 m^*, \tag{36}$$

where n is the density of the photoinduced excess carriers. Also

$$\nu = \frac{1}{\tau} = \frac{e}{\mu_a m^*}, \tag{37}$$

where μ_a is the ambipolar mobility. Thus, in fitting the theory to the experiment, the variations of both the plasma density and the ambipolar mobility are determined with respect to time.

The value of N_0 determined by fitting the experimental data is consistent with the value determined by an independent measurement of the laser intensity. The recombination time τ_r is found to be 25 μsec. In the model a background plasma density of $10^{14}\ \text{cm}^{-3}$ is assumed. This is justifiable because the laser was observed to have a long fluorescent prepulse prior to lasing.

The theoretical and experimental curves agree very well except for the phase shift in the range from 5 to 50 μsec. This discrepancy is probably due to a combination of two factors: first, the fact that the plasma depth and density were assumed to be abrupt and constant, respectively: and second, that the model used to determine the phase shift and attenuation predicts a cutoff of the lowest-order mode that does not actually occur (Marcatili, 1969). Because the condition of the waveguide in this time range is near the "cutoff" condition, the theoretical prediction there may not be accurate.

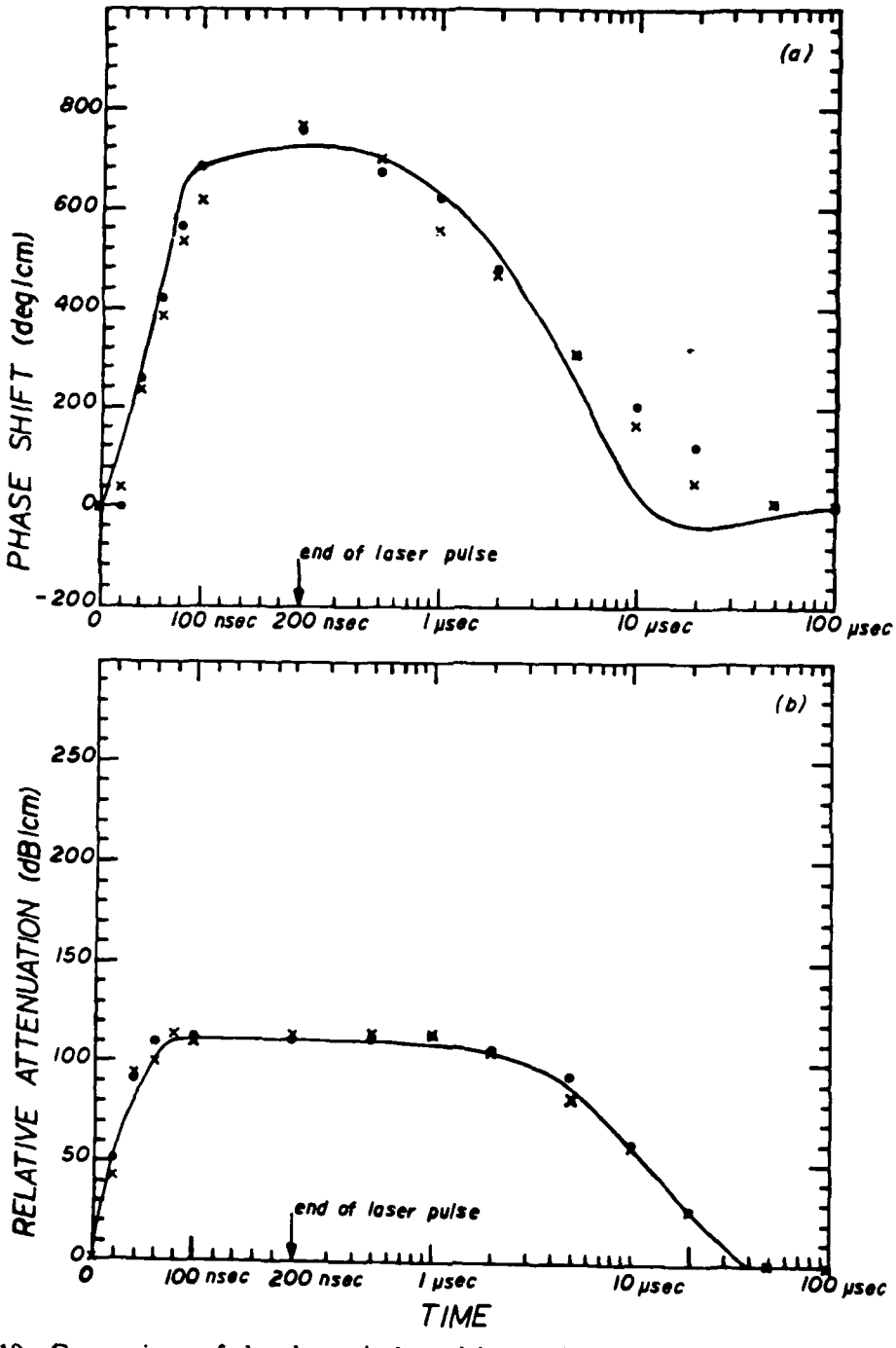

FIG. 19 Comparison of the theoretical model and the experimental results for a 1.0 × 0.5-mm silicon waveguide illuminated by a 900-nm GaAs diode laser: (a) phase shift with respect to time; (b) relative attenuation with respect to time. Note that the time scale is linear for the first 200 nsec; the duration of the laser pulse. ●, Null method; ×, dynamic bridge method; ——, theoretical curve.

B. Frequency-Doubled Mode-Locked Nd:YAG Laser Experiments

The dynamic bridge technique was used to measure the temporal variation of phase and loss in a silicon waveguide after illumination by a frequency-doubled 35 psec single pulse from a mode-locked Nd:YAG laser. The laser illumination was focused by a lens through a rectangular aperture onto the surface of the waveguide. The spot size at the waveguide surface was found by replacing the silicon waveguide with a photodiode detector at the same height, covering the detector except for a small pinhole. The size of the laser spot was determined by moving the pinhole in the direction of the long waveguide dimension and measuring the laser intensity at each place. The spot size was found to be about 0.15 cm.

A comparison of the theoretical model and experimental results in this case is shown in Fig. 20. Here the recombination time was fitted at 20 μsec and the ambipolar diffusion coefficient was held at a constant 17.93 cm^2/sec. The initial plasma density was fitted at 8.5×10^{17} cm^{-3}, an oder of magnitude less than the plasma density inferred from measurements of the laser energy. One reason for this discrepancy is that the complete theoretical model assumes an abrupt junction between the plasma layer and the rest of the silicon waveguide. From the steady-state model of Section III.A it can be seen that the millimeter waves begin to interact with the plasma in the plasma density range from 10^{14} to 10^{16} cm^{-3}, depending on the plasma depth. By choosing the plasma depth and density as in Fig. 18, significant amounts of plasma in the tail region are ignored. These smaller plasma densities at larger plasma depths interact with the millimeter waves, producing larger attenuations than those predicted by the theoretical model. Other reasons for the discrepancy between the theoretically fitted and experimentally inferred initial plasma density could be that fast recombination processes such as Auger and surface recombination are not taken into account in the theory. The large peak in the theoretical attenuation curve is probably due to the fact that the model of the waveguide used (Marcatili, 1969) predicts a cutoff waveguide size for the lowest-order semiconductor waveguide mode. This "cutoff" never really occurs. In the theoretical model, as the plasma is diffusing into the semiconductor waveguide, the waveguide is becoming pinched off. The predicted attenuation in the near-pinched-off case is probably too high due to the model's predicting an actual cutoff condition.

Another way to compare theory and experiment is to use the calculated theoretical phase shift and relative attenuation results to predict a normalized curve corresponding to the output of the detector after the onset of laser illumination. At each instant in time after the onset of laser illumination the theoretical phase shift and attenuation are used to calculate a magnitude for

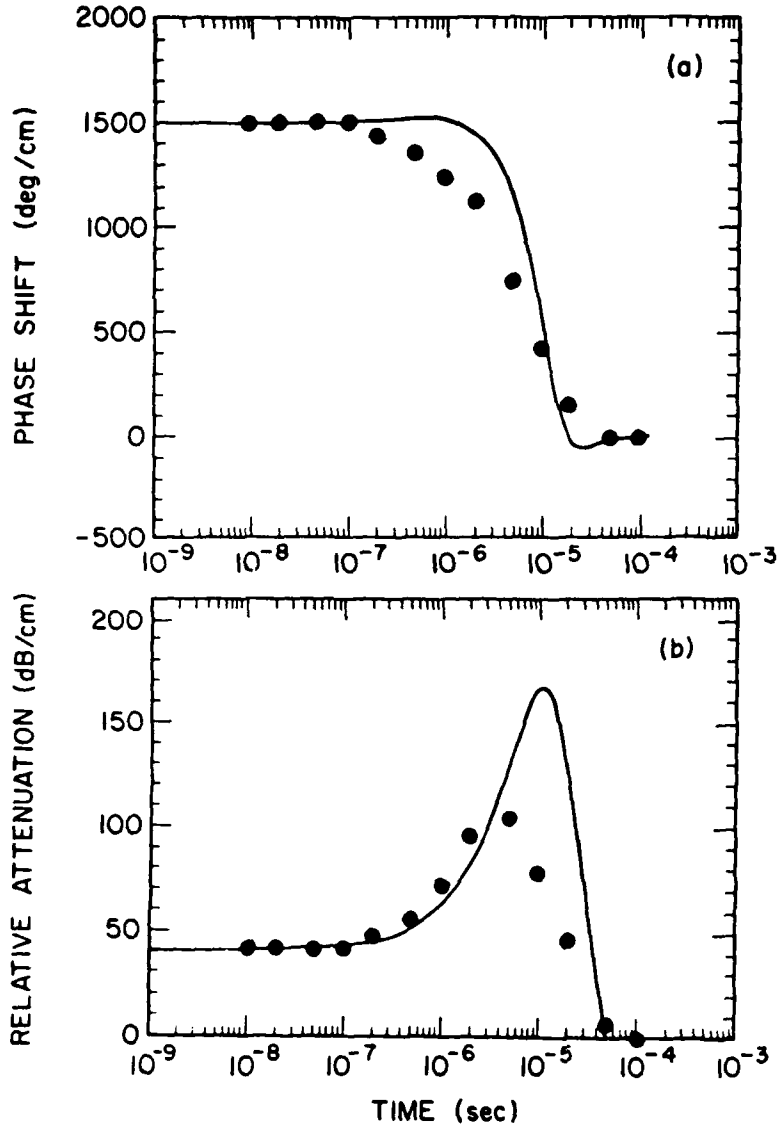

FIG. 20 Comparison of theoretical (——) and experimental (●) results for the situation when the millimeter-wave bridge is illuminated by a single pulse from a frequency-doubled mode-locked Nd:YAG laser: (a) phase shift with respect to time; (b) relative attenuation with respect to time. The experimental technique is the dynamic bridge method.

E_r. Then the detector response is taken into account and a relative magnitude of the millimeter-wave signal is calculated. Repeating this technique for many instants in time after the onset of laser illumination gives a theoretical curve that corresponds to the measured oscilloscope trace. Comparisons of the theoretical curves and the experimental results for several different initial phase offsets are shown in Figs. 21-24. These curves were taken with the laser energy of each shot within a $\pm 1\%$ range. The theoretical fit was done using an average initial plasma density corresponding to an average laser intensity.

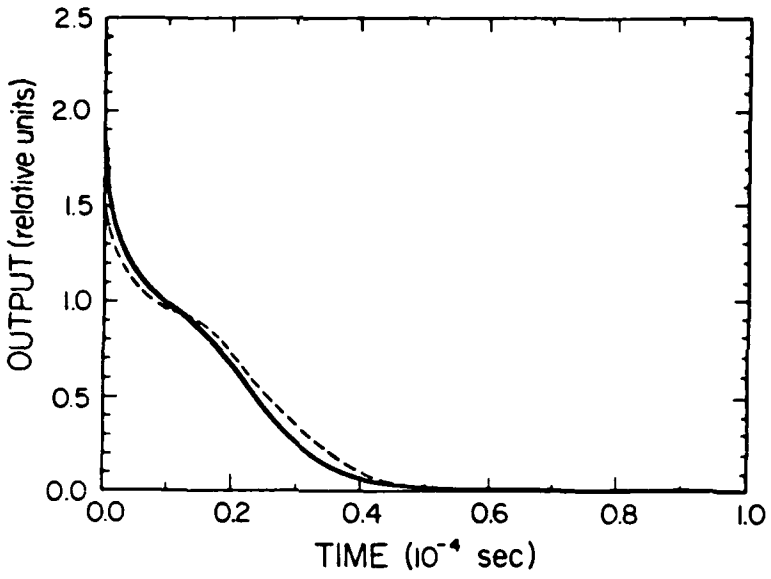

FIG. 21 Comparison of theoretical (——) and experimental (---) results of the normalized output of the millimeter-wave bridge after illumination of the silicon waveguide by a single pulse from a frequency-doubled mode-locked Nd:YAG laser. The initial phase offset is 180 .

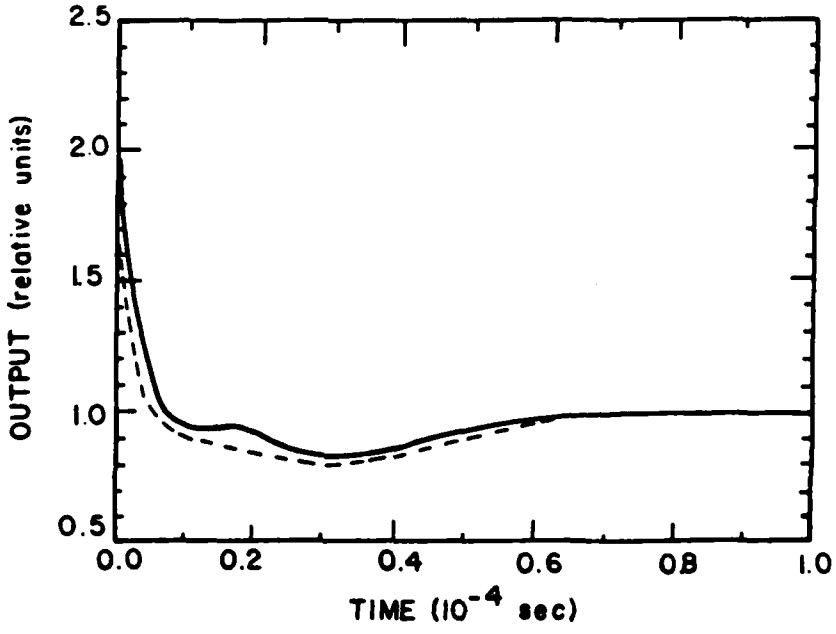

FIG. 22 Comparison of theoretical (——) and experimental (---) results of the normalized output of the millimeter-wave bridge after illumination of the silicon waveguide by a single pulse from a frequency-doubled mode-locked Nd:YAG laser. The initial phase offset is 120 .

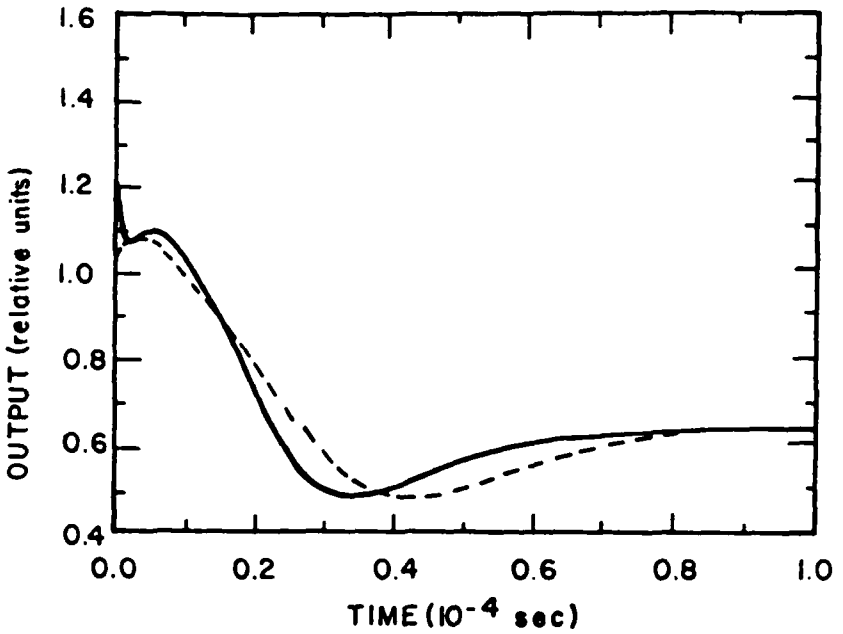

FIG. 23 Comparison of theoretical (——) and experimental (---) results of the normalized output of the millimeter-wave bridge after illumination of the silicon waveguide by a single pulse from a frequency-doubled mode-locked Nd: YAG laser. The initial phase offset is 227°.

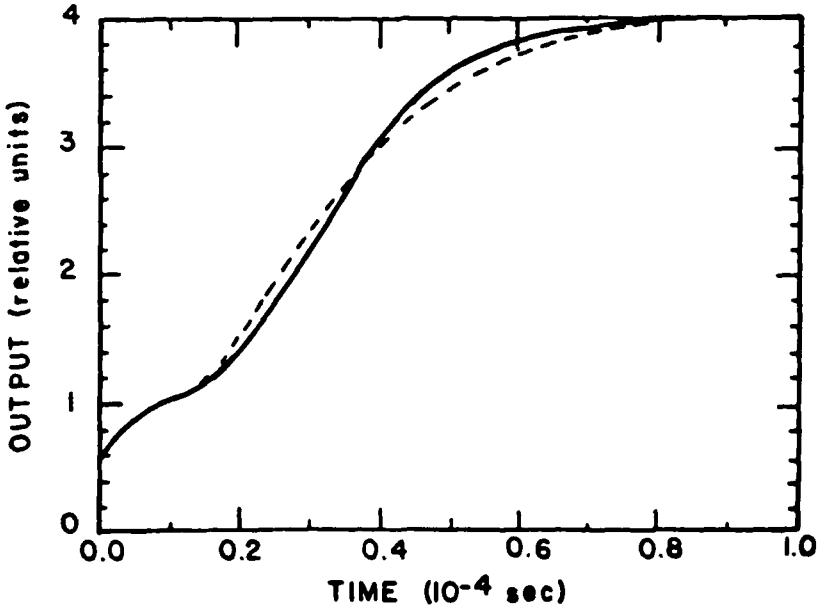

FIG. 24 Comparison of theoretical (— —) and experimental (---) results of the normalized output of the millimeter-wave bridge after illumination of the silicon waveguide by a single pulse from a frequency-doubled mode-locked Nd: YAG laser. The initial phase offset is 0°.

Once again, the fitted initial plasma density was an order of magnitude less than that calculated from the measured laser energy. This discrepancy is probably due to the same factors mentioned earlier.

C. Picosecond Techniques for Modulating and Gating Millimeter-Wave Signals

To produce gated millimeter-wave signals, the experimental arrangement of Fig. 1 is modified to that of Fig. 25. The difference between these two arrangements is that in Fig. 25 an additional silicon waveguide has been inserted in the main transmission line downstream from the bridge. Initially, without laser illumination, the bridge is balanced by adjusting the variable attenuator A and the phase shifter ϕ so that there is no signal at the output. When a single 1.06-μm pulse of 35-psec duration extracted from a mode-locked Nd:YAG laser illuminates the silicon waveguide inside the bridge, a high-density plasma is generated throughout the bulk of the silicon slab. With 50 μJ of laser illumination, the plasma density is so large that the silicon waveguide essentially blocks the transmission of millimeter waves through this arm. The bridge is thus unbalanced and a signal appears at the output. To "turn off" the millimeter-wave signal, a second laser pulse, delayed with respect to the first pulse, is used to illuminate the silicon waveguide outside the bridge. The presence of a high-density plasma in this silicon waveguide then completely terminates the millimeter-wave signal. By adjusting the relative delay between the two laser pulses, a square millimeter-wave pulse of any desired duration can be generated. The oscilloscope traces of some typical square millimeter-wave pulses obtained using this technique are shown in Fig. 26. The pulsewidths in this figure range from 11 nsec to 1 nsec. Pulsewidths shorter than 1 nsec should be readily obtainable, but direct measurement of pulse durations of less than 1 nsec is not possible due to

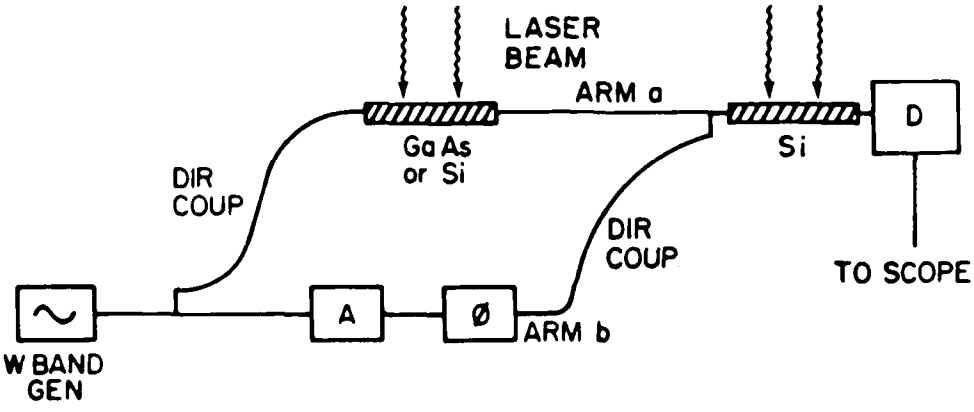

FIG. 25 Experimental arrangements to produce gated millimeter-wave signals.

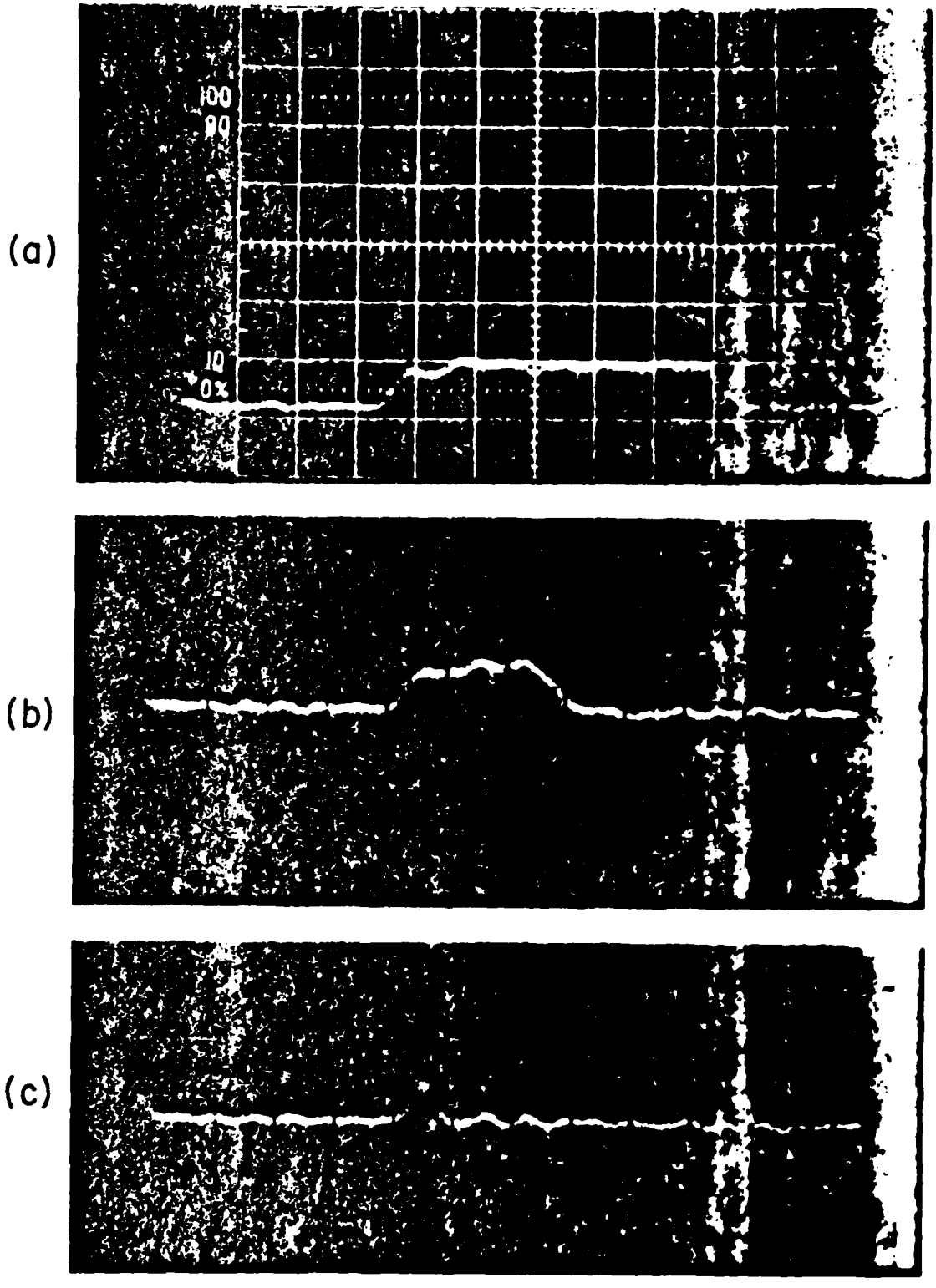

FIG. 26 Square millimeter-wave pulses. Durations: (a) 11 nsec; (b) 5 nsec, (c) 1 nsec Sweep rate was 2 nsec/div in all three cases.

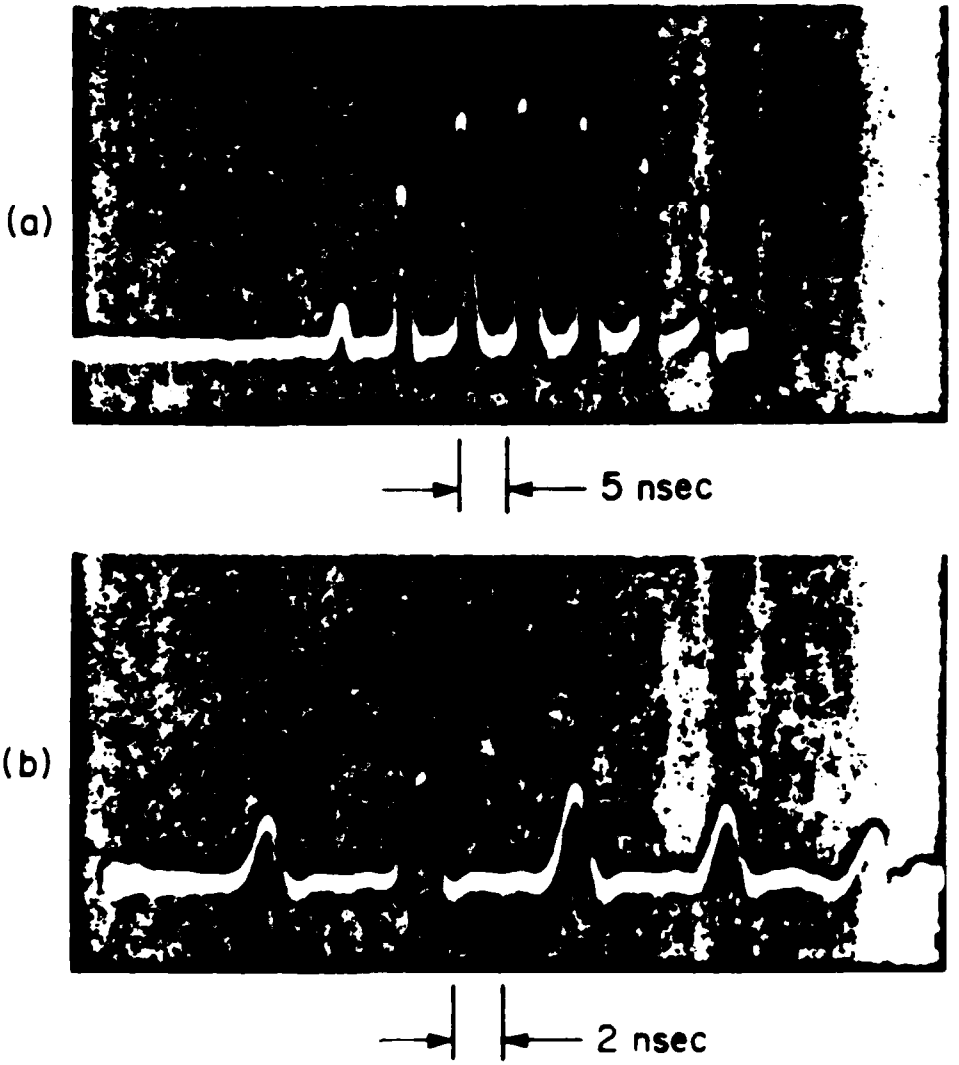

FIG. 27. Millimeter-wave pulse train mimicking the incident optical pulse train. Individual pulse in train is "chirped," and its duration is measured by a correlation technique to be about 700 psec.

oscilloscope bandwidth limitations. One drawback of this method of generating short millimeter-wave pulses is that, because of the long recombination time of the plasma in silicon, fast repetition rates are not possible.

Replacing the silicon waveguide inside the bridge of Fig. 1 with a waveguide made of Cr-doped GaAs increases the generation rate of millimeter-wave pulses to greater than 200 MHz. The rise time of the millimeter-wave pulse corresponds to the duration of the laser pulse, the fall time of the millimeter-wave pulse corresponds to the recombination lifetime of the excess carriers. Because the lifetime of the excess carriers in Cr GaAs is on the order of 100 psec (Lee *et al.*, 1977), it is possible to produce short millimeter-wave pulses without using a silicon waveguide outside the bridge to "turn off" the

millimeter-wave signal. In fact, if a 0.53-μm optical pulse train from a frequency-doubled mode-locked Nd:YAG laser is used to illuminate the Cr:GaAs waveguide, a millimeter-wave pulse train mimicking the incident optical pulse train results. An oscillogram of the millimeter-wave pulse train is shown in Fig. 27. The interpulse spacing of 7 nsec in the millimeter-wave pulse train is the same as that in the optical pulse train. Figure 27 also shows that a modulation approaching 1 GHz is attainable. The pulsewidths of the individual pulses are not resolvable in this figure because the combined response time of the detecting and display system is slower than the expected pulsewidth estimated on the basis of the carrier lifetime data (Lee *et al.*, 1977).

To measure the pulsewidth a correlation technique is used. Referring again to Fig. 25, a 0.53-μm pulse from a frequency-doubled mode locked Nd:YAG laser is used to illuminate the GaAs waveguide inside the bridge, producing a millimeter-wave pulse. A 1.06-μm pulse from the laser is used to illuminate the silicon waveguide outside the bridge and "turn off" the millimeter-wave signal. As the relative delay between the two optical pulses is varied, the integral of the millimeter-wave pulse with respect to time appears at the detector. By taking the derivative, the millimeter-wave pulsewidth could be determined. Plots of the integrated signal and the pulse are given in Fig. 28. The millimeter-wave pulsewidth determined by this technique is 700 psec, wider than the expected pulsewidth by a factor of 3. This discrepancy can be resolved by noting that the "turn off" of the millimeter-wave signal is not instantaneous and by realizing that the millimeter-wave pulse is generated by rapid phase modulation of the signal. The rapid phase modulation of the

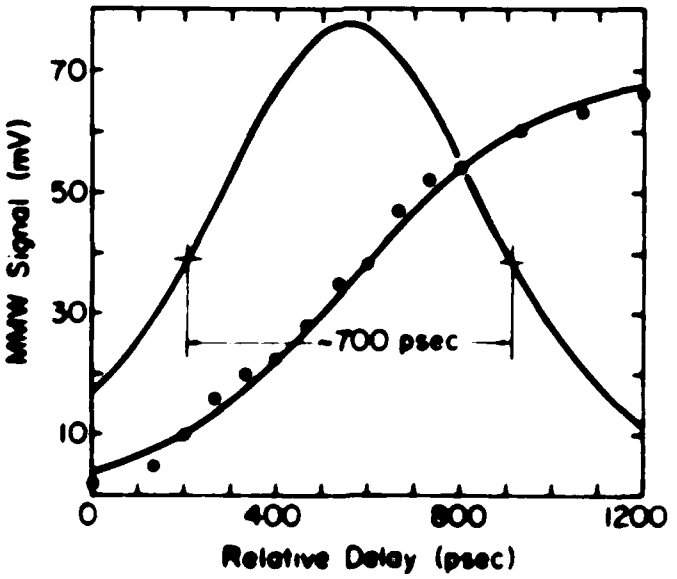

FIG. 28 Plots of the integrated millimeter-wave signal (●) and the millimeter-wave pulse

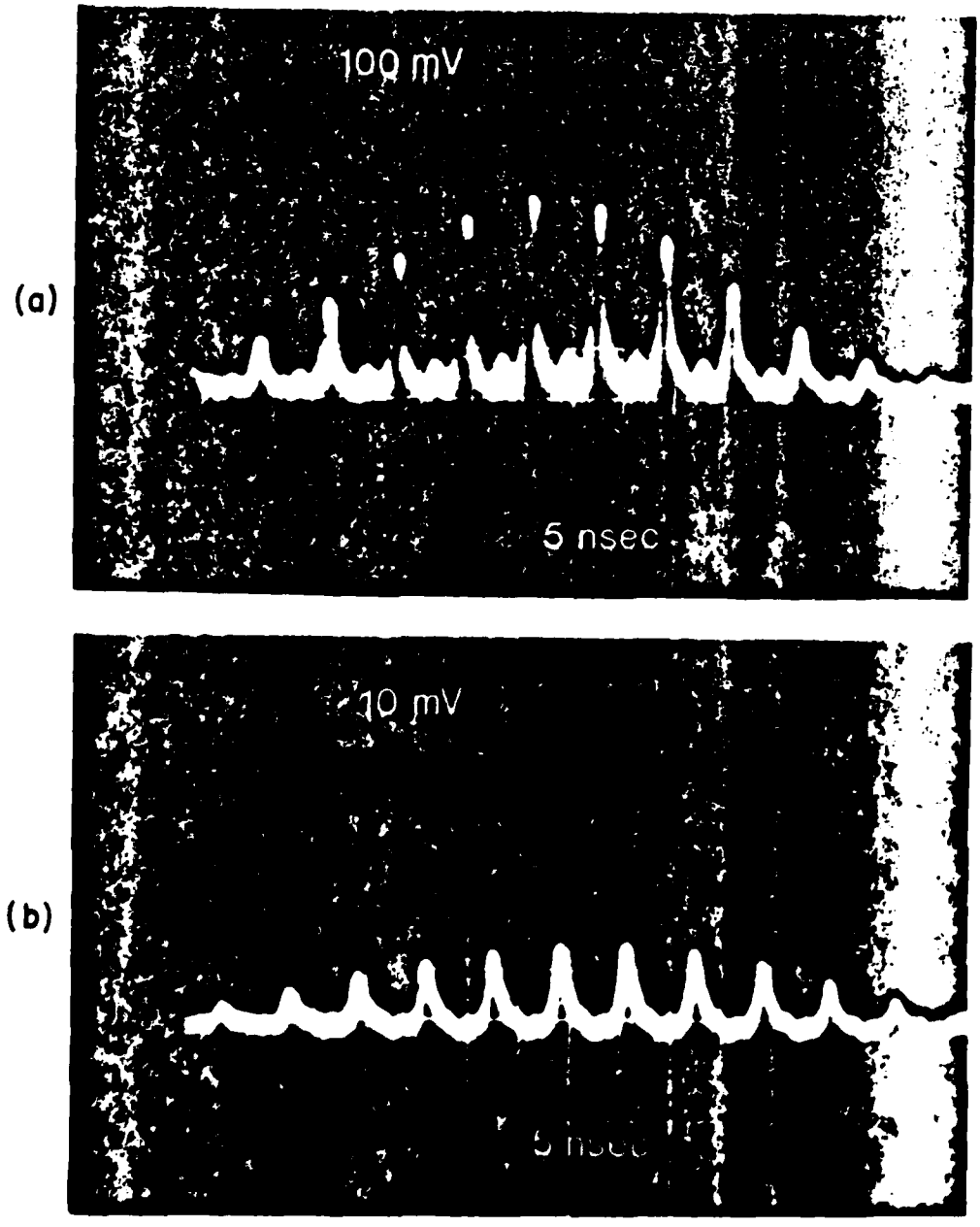

FIG. 29 (a) Optical pulse train from a frequency-double mode-locked Nd:YAG laser. (b) Millimeter-wave pulse train mimicking the incident optical pulse train. The waveguide material is silicon on sapphire, and the oscilloscope sweep speed is 5 sec/div. The traces here are bandwidth limited by the oscilloscope

signal causes the millimeter-wave pulse to be "chirped"; that is, there is a large frequency sweep within the pulse. As the millimeter-wave pulse propagates in a positively dispersive guiding structure, group velocity dispersion will broaden it. Mismatches between the dielectric and metallic waveguides can also contribute to some broadening. Taking these effects into account, the actual pulsewidth of the millimeter-wave pulse is estimated to be 400 psec.

Replacing the silicon waveguide in Fig. 1 with a silicon on sapphire (SOS) waveguide produces results similar to those of Fig. 27. One advantage of the silicon on sapphire waveguide is that it has less static insertion loss than the Cr:GaAs waveguide. Another advantage of a silicon on sapphire waveguide inside the bridge is that the induced plasma is confined to the silicon layer, causing the bridge imbalance to be due primarily to phase shift rather than to loss. Oscillograms of the laser pulse train and the millimeter-wave pulse train for the case of a silicon on sapphire waveguide inside the bridge are shown in Fig. 29.

V. Conclusions

Two measurement techniques and a theoretical model have been developed to characterize the variation of phase shift and attenuation in a bulk semiconductor waveguide due to an optically induced electron-hole plasma. The theoretical model relates the temporal variation of phase and loss in the semiconductor waveguide directly to the transport properties of the induced electron-hole plasma. The two measurement techniques allow simultaneous measurement of the phase and loss in the semiconductor waveguide as a function of time. The null method requires a repeatable laser pulse energy and profile and a relatively fast pulse repetition rate; the dynamic bridge method may be applied to a laser that has slower repetition rate and is less repeatable in pulse energy.

Comparison of the theoretical model and the experimental results indicates that the theoretical model is adequate to explain the temporal variation of the phase and loss in a silicon waveguide after a low-density electron-hole plasma is generated in it by a GaAs diode laser. In the case of larger injected plasma densities, such as those generated by a single pulse from a frequency-doubled mode-locked Nd:YAG laser, the theoretical model should be modified to take into account the actual variation of plasma density with depth in the silicon waveguide.

Gating and modulation of millimeter waves has been demonstrated. Millimeter waves have been gated by using one laser pulse to "turn on" the millimeter-wave signal and another laser pulse, after a suitable delay, to "turn off" the millimeter-wave signal. Modulated millimeter waves have been produced using Cr:GaAs and silicon on sapphire as semiconductor waveguiding materials.

Acknowledgments

The authors would like to thank Mr M G Li for many helpful discussions. This work is supported by the National Science Foundation, The Army Research Office, the Minta Martin Fund for Engineering Research, University of Maryland, and the University of Maryland Computer Facility

REFERENCES

Auston, D. H. (1975). *Appl. Phys. Lett.* **26**, 101-103.

Garver, R. V. (1976). "Microwave Diode Control Devices," Chap. 10. Artech House, Dedham, MA.

Gerlach, H. W. A., and Wellman, R. (1983). *Proc. IEEE MTT-S Int. Microwave Symp.* 70-72.

Glance, B. (1979). *IEEE Trans. Microwave Theory Tech.* **27**, 14-16.

Horn, R. E., Jacobs, H., Klohn, K. L., and Friebergs, E. (1982). *IEEE Trans. Microwave Theory Tech.* **30**, 816-820.

Jacobs, H., and Chrepta, M. M. (1974). *IEEE Trans. Microwave Theory Tech.* **22**, 411-417.

Kaminow, I. P., Carruthers, J. R., Turner, E. H., and Stulz, L. W. (1973). *Appl. Phys. Lett.* **22**, 540-542.

Kiehl, R. A. (1980). *IEEE Trans. Microwave Theory Tech.* **28**, 409-413.

Klein, M. B. (1983). *In* "Infrared and Millimeter Waves" (K. J. Button, ed.), Vol. 9, pp. 133-175. Academic Press, New York.

Klohn, K. L., Horn, R. E., Jacobs, H., and Friebergs, E. (1978). *IEEE Trans. Microwave Theory Tech.* **26**, 751-754.

Kobayashi, M., and Herui, H. (1978). *Appl. Opt.* **17**, 3253.

Kortz, H. P. (1983). *IEEE J. Quantum Electron.* **19**, 578-584.

Lee, C. H., and Mathur, V. K. (1981). *IEEE J. Quantum Electron.* **17**, 2098-2112.

Lee, C. H., Antonetti, A., and Mourou, G. (1977). *Opt. Commun.* **21**, 158-161.

Lee, C. H., Mak, P. S., and DeFonzo, A. P. (1978). *Electron Lett.* **14**, 733-734.

Lee, C. H., Mak, P. S., and DeFonzo, A. P. (1980). *IEEE J. Quantum Electron.* **16**, 277-288.

Levin, B. J., and Wiedener, G. G. (1973). *RCA Rev.* **34**, 489-505.

Li, M. G., Cao, W. L., Mathur, V. K., and Lee, C. H. (1982). *Electron Lett.* **18**, 454-456.

Mak, P. S. (1979). Applications of picosecond photoconductivity in semiconductors. Doctoral dissertation, University of Maryland.

Marcatili, E. A. J. (1969). *Bell Syst. Tech. J.* **48**, 2103.

Minowa, J., Aoyama, K., and Fujii, Y. (1979). *Digest Tech. Pap., IEEE OSA Conf. Laser Eng.* 54-55.

Mortenson, K. E., Armstrong, A. L., Borrego, J. M., and White, J. F. (1971). *Proc. IEEE* **59**, 1191-1200.

Mourou, G., and Knox, W. (1979). *Appl. Phys. Lett.* **35**, 492-495.

Novick, G., Jacobs, H., Locasio, C. M., and Londono, J. (1982). *IEEE Trans. Microwave Theory Tech.* **30**, 2034-2036.

Ogusu, K. (1983). *Electron Lett.* **19**, 253-254.

Paul, J. A., and Chang, Y. W. (1978). *IEEE Trans. Microwave Theory Tech.* **26**, 751-754.

Platte, W. (1981). *IEEE Trans. Microwave Theory Tech.* **29**, 1010.

Sze, S. M. (1981). "Physics of Semiconductor Devices," p. 87. Wiley, New York.

Tomlinson, W. J. (1977). *Appl. Opt.* **16**, 2180-2194.

Vaucher, A. M., Li, M. G., Striffler, C. D., and Lee, C. H. (1982). *Electron Lett.* **18**, 1066-1067.

Vaucher, A. M., Li, M. G., Striffler, C. D., and Lee, C. H. (1983). *IEEE Trans. Microwave Theory Tech.* **31**, 209-216.

Yurek, A. M. (1984). Millimeter wave technique for characterizing the behavior of optically induced plasmas in semiconductor waveguides. Doctoral dissertation, University of Maryland.

END

7-87

DTIC